DOCTOR OF PHILOSOPHY
IN CIVIL ENGINEERING

CYCLE XXX

VULNERABILITY ASSESSMENT OF STEEL LIQUID STORAGE TANKS IN INDUSTRIAL PLANTS

Hoang Nam Phan

PhD student

signature

Prof. Fabrizio Paolacci

Supervisor

signature

Prof. Gianmarco de Felice

Coordinator

signature

Thesis of Doctor of Philosophy
In Civil Engineering
Roma Tre University
Thesis No.: 72

Acknowledgements

I would like to express my deepest gratitude to my advisor, Professor Fabrizio Paolacci, who has offered the knowledge, support, opportunity, and encouragement. Without his supervision and constant help, this dissertation would not have been possible.

I would also like to acknowledge my colleagues at the Da Nang University of Technology for their advice and encouragement of my academic career. Also, I would also like to show my gratitude to professors and colleagues in Trento University and Saclay Nuclear Research Centre who provided expertise and advice that greatly assisted the research.

I have been fortunate to be surrounded by an excellent group of research fellows and graduate students who have offered technical knowledge, lively discussions, and friendship. Great thanks to my research group mates Dr Silvia Alessandri, Dr Daniele Corritore, Mr Yuichi Yoshida, and Mr Mohammad Mohinuddin Ahmed.

Finally, I dedicate this dissertation to my wife, Phuong Mai Le, my boy, Le Huy Phan, my parents, and my in-laws who have been very supportive of my decision to pursue PhD at the Roma Tre University and have always encouraged me. I wish to express my gratitude to them for their all supports that always encouraged me.

Abstract

Industrial plants, especially chemical, petrochemical, and oil processing industries, are complex systems of numerous integrated components and processes, which can make them particularly vulnerable to natural hazard events, in particular earthquakes. The interaction of the earthquakes with industrial equipment may trigger relevant accidents resulting in the release of hazardous materials and thus the increase of overall damage to nearby areas. Therefore, each component in the industrial site requires mandatory risk assessment and development of preventive and protective actions.

Steel liquid storage tanks are more vulnerable to earthquakes than other equipment in industrial plants because they often handle a large amount of toxic and flammable materials that can ignite and burn easily. Catastrophic failure of tanks observed during past earthquakes caused serious economic and environmental consequences. Many of them were designed with outdated analysis methods and with underestimated seismic loads. Therefore, the evaluation of the seismic vulnerability of existing steel liquid storage tanks located in seismic prone areas is extremely important.

The seismic vulnerability of tanks is expressed using fragility curves. These curves are conditional probability statements of potential levels of damage over a range of earthquake intensities. There are a variety of approaches to derive the fragility curves for tanks, e.g., empirical, expert-based, and analytical approaches. Among them, the analytical methods have been widely accepted in recent decades. The development of analytical fragility curves for tanks, in particular existing tanks, faces the challenge of many sources of uncertainty. Therefore, a primary objective of this work is to develop an appropriate methodology to analytically derive fragility curves for existing steel liquid storage tanks with the treatment of uncertainties.

At first, an overview of earthquake damage to steel liquid storage tanks in industrial plants is introduced, together with the definition of critical damage states observed during past earthquakes. Possible numerical models for both above ground and elevated tanks subjected to earthquakes, such as spring-mass models and more refined models, are then presented. Consequently, an efficient procedure for the model calibration of unanchored tanks is proposed. The procedure is mainly based on a static pushover analysis, which is performed using a nonlinear finite element

modelling of the steel tank. The model is then validated through a shaking table campaign and a full nonlinear finite element model.

An overview of seismic fragility methodologies for tanks is next presented. The attention is paid to analytical methods, e.g., cloud and incremental dynamic analysis methods, which are conducted by using probabilistic seismic demand models and nonlinear time history analyses. The sources of uncertainty, classified into ground motion and modelling parameter uncertainties, are incorporated into the probabilistic seismic demand models. A sensitivity study, based on a screening experiment and an analysis of variance, is performed. This study reveals how different levels of modelling parameters, in turn, affect the seismic response of the tanks. Knowledge of the significance of each modelling parameter will provide insight as to whether its variation should be treated explicitly or may perhaps be neglected. Therefore, results of the sensitivity analysis could be used to reduce the number of parameters considered in the fragility analysis.

Subsequently, optimal intensity measures for the probabilistic seismic demand analysis of above ground tanks are presented. Best performance intensity measures are selected based on their efficiency and sufficiency. The applications of the proposed procedure to two case studies of existing above ground and elevated tanks, which are located in seismic prone areas of Italy and Turkey, are finally presented, resulting in fragility curves for different limit states of the tanks. A vulnerability-based design approach of a concave sliding bearing system for the elevated tank is also introduced at the end.

Table of contents

List of figures

List of tables

List of symbols

A_c	Convective acceleration
$A_c(t)$	Convective acceleration time history
A_{cn}	nth convective acceleration
$A_{cn}(t)$	nth convective acceleration time history
A_i	Impulsive acceleration
$A_i(t)$	Impulsive acceleration time history
A_g	Ground acceleration
$A_g(t)$	Ground acceleration time history
c	Equivalent damping coefficient
c_c	Convective damping coefficient
c_i	Impulsive damping coefficient
c_s	Damping coefficient of the support structure
C_c	Coefficient for determining the convective period
C_i	Coefficient for determining the impulsive period
CAV	Cumulative absolute velocity
CAD	Cumulative absolute displacement
D	Tank diameter
D_{EDP}	Engineering demand parameter
D_{iso}	Isolator diameter
D_m	Estimate of the median demand
E	Young’s modulus of the steel tank
g	Acceleration due to gravity
G	Specific gravity
h	Equivalent centroid height
h_c	Centroid height of the convective wall pressure
h_{cn}	Centroid height of the nth mode convective wall pressure
h'_c	Centroid height of the convective wall and base pressures
h'_{cn}	Centroid height of the nth mode convective wall and base pressures
h_i	Centroid height of the impulsive wall pressure
h'_i	Centroid height of the impulsive wall and base pressures
h_{iso}	Isolator height
h_s	Height of the support structure

h_r	Distance of the tank roof centroid to the base
h_w	Distance of the tank wall centroid to the base
H	Maximum design product level
H_t	Tank height
I_1	Modified Bessel function of the first order
I_A	Arias intensity
I_{NP}	Spectral-shape-based intensity measure
IM	Intensity measure
IM_i	Intensity measure associated with the onset of failure for the ith ground motion
J_1	Bessel function of the first order
k_c	Convective stiffness
k_i	Impulsive stiffness
k_{iso}	Stiffness of the isolation system
k_s	Stiffness of the support structure
k	Equivalent stiffness
L	Uplift length
LS	Limit state
m	Equivalent mass
m_c	Convective mass
m_{cn}	nth mode convective mass
m_i	Impulsive mass
m_{iso}	Isolator mass
m_l	Mass of the liquid
m_r	Mass of the tank roof
m_s	Mass of the support structure
m_{tot}	Total mass on the isolation system
m_w	Mass of the tank wall
M	Overturning moment immediately above the base plate
M_c	Overturning moment immediately above the base plate caused by the convective component
M_i	Overturning moment immediately above the base plate caused by the impulsive component
M'	Overturning moment immediately below the base plate
M'_c	Overturning moment immediately below the base plate caused by the convective component
M'_i	Overturning moment immediately below the base plate caused by the impulsive component

M_{OT}	Overturning moment illustrated in the uplift resistance spring
M_W	Moment magnitude
n_A	Number of equally-spaced anchors around the tank circumference
N	Axial force per unit circumferential length
N_{iso}	Isolator vertical load carry capacity
p	Maximum interior pressure
p_c	Convective pressure
p_i	Impulsive pressure
P_A	Anchorage attachment design load
Q	Total base shear
Q_1	Reaction force at the end of the bottom plate
Q_c	Base shear caused by the convective component
Q_i	Base shear caused by the impulsive component
R	Tank radius
R_{iso}	Radius of the concave sliding surface
ψ	Base rotation
S_a	5% damped elastic spectral acceleration at any period
$S_a(T_1)$	5% damped elastic spectral acceleration at the first mode
$S_a(T_2)$	5% damped elastic spectral acceleration at the second mode
$S_a(T_i)$	5% damped elastic spectral acceleration at the impulsive mode
PGA	Peak ground acceleration
PGV	Peak ground velocity
PGD	Peak ground displacement
S^*	Spectral-shape-based intensity measure
R_{jb}	Joyner-Boore distance
$V_{s,30}$	Shear wave velocity of the top 30 m of the subsurface profile
t/t_0	Time scale using in the experimental test
t_s	Thickness of the shell ring under consideration
t_b	Thickness of the bottom plate
t_{eq}	Equivalent uniform thickness of the shell
T	Time period
T_1	First mode period
T_2	Second mode period
T_c	Natural period of the convective mode
T_i	Natural period of the impulsive mode
T_{iso}	Isolator time period
T_r	Return period

V_p	Plastic shear demand
V_n	Shear strength
w	Uplift displacement
$\ddot{x}_g(t)$	Ground acceleration
X_{iso}	Isolator maximum displacement
z	Distance from the liquid surface to the analysis point
α/α_0	Excitation amplitude scaling using in the experimental test
$\beta_{d\|IM}$	Dispersion of the demand
γ	Tank aspect ratio
ζ	Nondimensional r-coordinate
η	Nondimensional z-coordinate
η_{max}	Maximum sloshing wave height
θ	Plastic rotation of the shell-to-bottom plate joint
θ_c	Column drift ratio
θ_{sf}	Drift ratio at the onset of shear failure
λ	Geometrical scaling factor
μ	Friction coefficient
ξ_c	Convective damping ratio, ξ_c = 0.5%
ξ_i	Impulsive damping ratio, ξ_c = 2%
ρ	Liquid density
ρ''	Transverse reinforcement ratio for reinforced concrete columns
σ_{eb}	Critical stress for the elastic buckling
σ_{efb}	Critical stress for the elastic-plastic or elephant's foot buckling
σ_h	Total combined hoop stress in the shell
σ_{hc}	Convective hoop stress in the shell
σ_{hi}	Impulsive hoop stress in the shell
σ_{hs}	Hydrostatic hoop stress in the shell
σ_{cl}	Ideal critical buckling stress
σ_p	Increase in buckling stress due to the internal pressure
σ_y	Steel yield strength
σ_z	Compressive meridional stress in the shell
ω_c	Angular frequency of the convective response
ω_{cn}	nth mode angular frequency of the convective response
ω_i	Angular frequency of the impulsive response

Chapter 1. Introduction

1.1 Problem description

Industrial plants are complex systems of numerous integrated components and processes that can make them particularly vulnerable to natural hazard events. As a result of the interaction between the natural events and the industrial risk, several effects take place in industrial plants, in particular, storage sites, causing damage to pipelines, process equipment, storage tanks and consequently the release of hazardous materials. Since a large amount of toxic and flammable materials are often handled by storage equipment, e.g., piping, vessels, and tanks, consequences of failures can affect wide surrounding areas.

There are different types of natural events triggering industrial accidents, e.g., landslides, hurricanes, high winds, tsunamis, floods, earthquakes, etc. However, in the present study, the attention is paid only to the seismic event; this is because several industrial accidents occurred in the last decades demonstrated that the typology of natural phenomena might cause severe damage to storage equipment items, resulting in losses of contents, thus in multiple and extended releases of hazardous substances. Therefore, cascading events are more likely to occur during a natural disaster than during a normal plant operation.

Earthquake damage in recent decades (e.g., 1995 Hyogoken-Nanbu Japan, 1999 İzmit Turkey, 2003 Tokachi-oki Japan, 2008 Wenchuan China, 2011 Great East Japan, 2012 Emilia Italy, etc.) has revealed that storage tanks are one of the most vulnerable components in an industrial plant. Damage to tanks can cause significant disruption to the facility operation. Seriously, the extensive seismic-induced uncontrolled fires, when flammable materials or hazardous chemicals leak, naturally increase the overall damage to nearby areas.

Prediction and prevention of possible accidental scenarios depend upon the reliability of available tools for the structural design and assessment. Unfortunately, despite the continuous evolution of the knowledge on this matter, there is a lack of standard and established procedures to evaluate the effects of the seismic action on equipment. An emerging tool, i.e., seismic fragility curves, provides valuable support for seismic risk assessment of equipment used in industrial installations (Salzano et al. 2003, Fabbrocino et al. 2005, Alessandri et al. 2017). These curves are conditional probability statements of potential levels of damage over a range of earthquake intensities and can be used as initial fragility-based damage scenarios in the seismic risk assessment procedure (Alessandri et al. 2017). The availability of reliable fragility curves would allow for assessment of the effects of various failure conditions, which are associated with the loss of contents, on the performance of equipment. Such curves are essential tools for decision-support frameworks such as performance-based and cost-benefit analyses.

1.2 Objectives and scope

This research aims to provide an enhanced understanding of the impact of natural disasters, especially earthquakes, on the performance of steel liquid storage tanks in industrial plants. A primary objective is to develop a reliable procedure for vulnerability assessment of existing tanks in seismic prone areas. The intention is to provide support for seismic risk assessment and mitigation efforts of industrial facility components. The associated research tasks include the following:

- Evaluation of seismic damage to steel liquid storage tanks in industrial plants under past earthquakes, identification of potential failure modes to be incorporated in the study.
- Development of detailed simplified and refined models for both above ground and elevated tanks, validation of the proposed model by a shaking table test.
- Proposal of optimal ground motion intensity measures for probabilistic seismic demand model of above ground and elevated tanks.
- Identification and probabilistic modelling of potentially uncertain modelling parameters, screening of the most significant modelling parameters by a sensitivity analysis for enhancing fragility curve evaluation.
- Determination of damage states and limit state capacities for tanks, development of component fragility curves based on different analytical approaches with the treatment of uncertainties for specific case studies of existing tanks.
- Illustration of the use of seismic fragility curves for risk assessment and mitigation activities.

1.3 Dissertation outline

The content of the dissertation is organised into the following chapters:

- Chapter 2 provides an overview of seismic damage to steel liquid storage tanks in industrial plants during past earthquakes and an identification of damage states for tanks based on past field observations.
- Chapter 3 presents possible numerical models of steel liquid storage tanks including both above ground and elevated tanks. A spring-mass model of unanchored tanks calibrated from a nonlinear static pushover analysis is proposed.
- Chapter 4 presents a shaking table test campaign on an unanchored steel liquid storage tank. A nonlinear finite element modelling of the tank is also developed to validate the accuracy of the above spring-mass model.
- Chapter 5 provides methodologies for fragility curve development of steel liquid storage tanks. The attention is paid to analytical fragility curves. The analytical approaches that include probabilistic seismic demand models, capacity estimates, and fragility curve fitting models are discussed in detail in this chapter. A sensitivity analysis of the seismic response and fragility to parameter uncertainties is also presented.
- Chapter 6 presents a study to select optimal ground motion intensity measures for tanks. The characteristics of intensity measures are assessed based on their efficiency and sufficiency.
- Chapter 7 presents a study to evaluate the sensitivity of the seismic response and fragility of an unanchored steel storage tank to parameter uncertainties. The tank is ideally located in a refinery in Sicily (Italy), defined as Case study #1.
- Chapter 8 presents a study to evaluate the vulnerability of elevated steel liquid storage tanks supported by reinforced concrete columns, defined as Case study #2. The nonlinear behaviour of the columns considering both flexure and shear behaviours is taken into account in the model. The uncertainty in ground motion concerning near-source and far-field records is assessed and discussed in detail. A vulnerability-based design of a concave sliding bearing system for the tank is also introduced at the end.
- Chapter 9 summarises the research and concludes, as well as discusses anticipated impacts of the work and suggestions for future research.

Chapter 2. Seismic damage to steel liquid storage tanks: A historical overview and identification of damage states

2.1 Na-Tech events

An increasing concern is present worldwide for the impact of cascading effects triggered by natural events. Severe accidents may occur because of the impact of natural events on industrial plants where relevant quantities of hazardous substances are stored or processed. Loss of containment (LOC) of hazardous materials may be expected, leading to direct impact on the population and possible mid- and long-term effects on the environment due to the release of chemical materials. These events are usually defined as “natural disasters triggering technological accidents” (Na-Tech) (Young et al. 2004).

There are different types of natural events triggering industrial accidents, e.g., landslides, hurricanes, high winds, tsunamis, floods, earthquakes, etc. Past decade accidents in industrial sites evidenced that typology of natural phenomena may cause severe damage to equipment items, resulting in losses of containment, thus in multiple and extended releases of hazardous substances. These multiple and simultaneous failures are more likely to occur during a natural disaster than during normal plant operation. Some examples of Na-tech events like the 2002 flood in the Samir refinery in Mohammedia, Morocco or the 1999 earthquake in the Tupras refinery, in İzmit, Turkey are available in the literature or the accident databases. In both cases, the natural events generated fires and explosions in several storage equipment items.

The occurrence of technological accidents triggered by natural events has been presented in several databases. For example, past industrial accidents have been reported in MHIDAS (SRD) and FACTS (TNO). However, there is a lack of information available on the interactions between natural disasters and simultaneous technological accidents. Past accidents evidence that structural damage to the equipment directly struck by lightning is more frequent; however, in general, seismic event produces severe consequences. This event may cause simultaneous failures of industrial components. In the following, past earthquake damage to industrial plants, and in particular to storage tank equipment, is presented. Damage states of tanks during past earthquakes are also revealed.

2.2 Historical overview of seismic damage to storage tanks

In the past, several major earthquakes have caused significant damage to major industrial facilities. A careful examination of their impact on these facilities can be extremely valuable as one attempts to assess the probable risks to an industrial facility in a future earthquake. The performance of structures and equipment in past earthquakes can serve as a guide to identify potential problems and weaknesses in components and systems. Possible and likely failure modes of components and the effects of these failure modes on the overall system can be identified through such a survey. In 1964, the Niigata earthquake (M_W 7.6) caused major destruction to industrial plants (Suzuki 2008). Niigata City, which had just recovered from the Great Niigata Fire of 1955, sustained considerable damage from fire and liquefaction that resulted from the earthquake. Most devastatingly, the pipes of a gasoline tank owned by Showa Shell Sekiyu, located between the airport and the harbour, were damaged by the shaking. Gasoline from the tank was brought to the sea surface by the tsunami and underground water released by the liquefaction and ignited 5 hours after the earthquake. The fire spread to nearby tanks and induced explosions that fed the fire, allowing it to continue for 12 days, as shown in Figure 2.1.

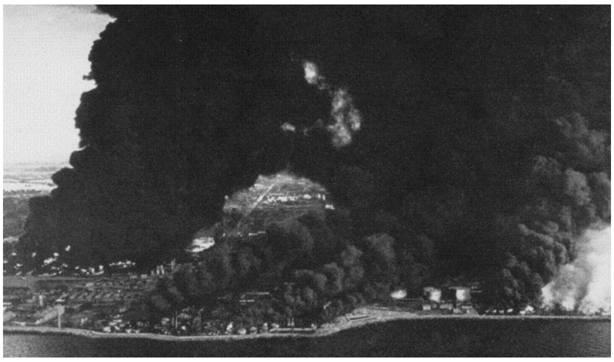

Figure 2.1. Petroleum complex conflagration after the 1964 Niigata earthquake (Suzuki 2008)

This fire is said to be the worst industrial complex fire in the country's history. At the time, the fire was said to be caused by the liquefaction, but later research into large earthquakes revealed that long period ground motion also played a role. The great Hanshin-Awaji earthquake or Kobe earthquake (M_W 6.9) on January 17, 1995 caused destructive damage to a tremendous number of manufacturing facilities (Suzuki 2008). The quake ravaged many of the facilities of what was then the world's sixth-largest container port and the source of nearly 40% of Kobe's industrial output.

The 2003 Tokachi-oki earthquake (M_W 8.0) that occurred in the subduction zone southeast Hokkaido, Japan, generated large-amplitude long-period ground motions with periods of several seconds to around 10 s in sedimentary basins in Hokkaido. These long-period strong ground motions excited sloshing of liquid in large oil storage tanks, causing damage to many storage structures (Hatayama et al. 2008). The most severe damage occurred at a refinery in the city of Tomakomai, which lies in the Yufutsu sedimentary basin, southwestern Hokkaido. Seven oil storage tanks with floating roofs suffered fire damage and/or sinking of the roof (Figure 2.2). The liquid sloshing in those tanks that suffered severe damage had a fundamental-mode natural period of 5-12 s, comparable to the period of ground motions caused by the earthquake.

The 2004 Chūetsu earthquake (M_w 6.6) occurred in Niigata Prefecture in October 2004, 40 years after the earlier Niigata earthquake, causing great damage to factory facilities in Ojiya and other locations (Suzuki 2008).

Figure 2.2. Full-surface fire of naphtha tanks occurred after two days of the 2003 Tokachi-oki earthquake (Hatayama et al. 2008)

The 2011 Tōhoku earthquake (M_W 9.0) and tsunami which hit Japan with an unprecedented height of water. Production and storage facilities located along the coast were directly impacted and the extraordinary disaster (Ibata et al. 2013). The Cosmo oil refinery located in Chiba prefecture was subjected to only low levels of earthquake forces. At the site of refinery, PGA values of 0.114 were measured during the main shock. The earthquake shock damaged the brace on a liquefied petroleum gas (LPG) tank and caused the weakened braces of the tank to buckle and subsequently collapse; this ruptured the pipes connected to the tank and led to the release of flammable gases that eventually ignited (Figure 2.3).

Figure 2.3. LPG tanks burned at the Cosmo oil refinery in Ichihara city, Chiba Prefecture after the 2011 Tōhoku earthquake (Reuter 2011)

The accident resulted in significant damage on-site, destroying all 17 storage tanks (Figure 2.4).

Figure 2.4. LPG tank farm in the Cosmo oil refinery was destroyed after the 2011 Tōhoku earthquake (USGS 2011)

The Tangshan earthquake (M_W 7.9) close to Beijing in 1976 seriously damaged or destroyed the heavy-industry zone and coal mines in its vicinity. On May 12, 2008, a major earthquake devastated the Wenchuan area in Sichuan province in the heartland of China. A significant proportion of Chinese chemical production and industrial plants were affected by the earthquake (Krausmann 2010). Tanks and vessels suffered damage caused by debris impact, foundation damage, or toppling under the influence of the earthquake loads, as examples in Figure 2.5. The damage severity correlated well with the age of the plant. Older facilities had suffered more extensive and severe damage than those built more recently according to the latest design codes. The main cause of worker death and injury was the collapse of warehouses, office, and manufacturing buildings; this concerned mostly concrete structures with insufficient confinement or poor reinforcement. The falling debris resulted in equipment damage and loss as well as pipe severing and crushing. Pipes were also severed or bent when connected tanks were displaced or buildings collapsed. Numerous hazardous-materials releases occurred with spills being the dominant accident scenario.

Figure 2.5. Observed damage in a chemical facility after the 2008 Wenchuan earthquake (Krausmann 2010)

In Europe, there are many vulnerable installations located in seismic prone areas. Among different types of industrial installations, except nuclear plants, the petrochemical industry is one of the most vulnerable ones, which has to be treated with particular attention because of the large number of installations in the European territories, the important allied industries, and the seismic vulnerability demonstrated on several occasions. For example, the 1999 İzmit earthquake (M_w 7.4) is considered the largest event which damaged to an industrialised area since the 1906 San Francisco and the 1923 Tokyo earthquakes. The İzmit earthquake caused significant structural damage to the Tupras refinery itself and associated tank farm with crude oil and product jetties, triggered multiple fires in the naphtha tank farms, as shown in Figure 2.6 (Sezen and Whittaker 2006). The multiple fires burned for four days, necessitated the evacuation of thousands of residents living near the plant. The fire in the refinery and associated tank farms caused extensive damage. There was damage to cooling towers and the port area. Collapse of a 150-m-high heater stack on the boiler and crude oil processing unit caused significant damage and started a second fire. Fault rupture and soil failure caused extensive damage to pump station and pipelines at about 20 locations. The failure of the water supply caused problems in controlling the fire. There were at least 15 gas firms with spherical storage tanks in the area. On May 20 and 29, 2012, two earthquakes of magnitude 6.11 and 5.96 hit the Emilia region in the Po Valley, one of the most industrialised zones of northern Italy. The majority of structures severely damaged by the seismic events were industrial facilities. The large amount of industrial facilities in the stricken area, in combination with their intrinsic deficiencies, made several industries disproportionately vulnerable to these events, compared to their moderate seismic intensity (Brunesi et al. 2014).

Figure 2.6. Damage to the tank farm in the Tupras refinery after the 1999 İzmit earthquake (Sezen and Whittaker 2006)

Other observations were also carried out by researchers in US and Taiwan during past earthquakes. The San Fernando earthquake in the vicinity of Los Angeles in 1971 extensively damaged lifeline systems including power, gas, and water lines. Substation equipment, piping, and tanks of these lifelines were seriously damaged. The 1989 Loma Prieta earthquake striking San Francisco and the 1994 Northridge earthquake striking Los Angeles area damaged factories and energy supply facilities. The 1999 Chi-chi earthquake in Taiwan seriously damaged petroleum complexes and thermal power stations.

2.3 Identification of damage states

Typical damage to ground supported steel liquid storage tanks during past earthquakes is in the form of:

- Buckling in the shell plate,

- Failure of the tank roof,
- Base sliding and uplift,
- Failure of anchor bolts,
- Local fracture of the annular plate,
- Plastic rotation of the shell-to-bottom plate joint,
- Failure of the support system,
- Failure of the piping system.

2.3.1 Shell buckling

The shell buckling modes include shear buckling and bending buckling that are associated with geometry parameters of tanks such as height to radius ratio and radius to thickness ratio. Shear buckling occurs for small ratios of height to radius (i.e., broad configuration) while bending buckling predominantly occurs for large ratios (i.e., slender configuration). Two distinct bending buckling phenomena have been observed during past seismic events including diamond shape buckling and elephant's foot buckling. The diamond shape buckling became widely known after it occurred in many wine storage tanks in the 1980 Greenville/Mt. Diablo earthquake, and recently, in the 2014 Napa Valley earthquake (Figure 2.7).

Figure 2.7. Diamond shape buckling in wine storage tanks after the 2014 Napa Valley earthquake (Fischer et al. 2016)

Figure 2.8. Elephant's foot buckling (left) and diamond shape buckling (right) observed after the 2012 Emilia earthquake (Brunesi et al. 2014)

The elephant’s foot buckling mode was widely seen in the 1964 Alaska earthquake, the 1971 San Fernando earthquake, the 1994 Northridge earthquake, and the 2012 Emilia earthquake. This type of buckling can cause spill incidents of liquid through crack penetration. A typical example of the buckling phenomena is illustrated in Figure 2.8, as the field observation from the 2012 Emilia earthquake.

The characteristic outward bulge above the tank base results from the combination of the large circumferential tensile stresses induced by the internal hydrostatic and hydrodynamic pressures and the axial compression due to the overturning moment caused by the horizontal seismic load. The resisting mechanism, developed by the axial compressive and hoop tensile stresses, cannot survive further vertical load increments, since the annular strips at the base yield in tension (Brunesi et al. 2014). The elephant’s foot buckling is a major failure mode in steel tanks and explicitly or implicitly mentioned in current codes, e.g., EN 1998-4 (2006), NZSEE (2009), and API 650 (2007), where the compressive design buckling stress can be expressed in terms of the yield strength and an appropriate reduction factor that depends on the shell slenderness.

2.3.2 Roof damage

The failure of tank roofs is mainly caused by sloshing; this occurred in the 1964 earthquakes in Niigata and Alaska. More recently, the roofs of some petroleum tanks failed in the 1999 İzmit earthquake in Turkey and the 2003 Tokachi-oki earthquake in Japan.

Figure 2.9. Deformation of cylindrical tank with fixed roof at the Tupras refinery after the 1999 İzmit earthquake (Sezen and Whittaker 2006)

For example, sloshing actions of combustible liquid inside the tanks deformed the tank roofs and upper tank walls under the İzmit earthquake, as shown in Figure 2.9. Insufficient freeboard in fixed-roof tanks may result in a plate buckling type of damage at the roof level. A few oil storage tanks also failed in the 2003 Tokachi-Oki earthquake in Japan. The long period strong ground motions excited sloshing of liquid in the tanks, causing fire damage and sinking to the floating roofs (Figure 2.10). It is thought that these floating roofs sank into the storage tanks as a result of damage to the roof pontoons because of large-amplitude sloshing. The severely damaged tanks have capacities of 30000-110000 m^3 with maximum sloshing wave heights of 1.3-3 m and natural fundamental-mode sloshing periods of 7-12 s, comparable to the period of ground motions caused by the earthquake (Hatayama 2007).

Figure 2.10. Sinking of floating roofs in two kerosene tanks at a refinery in the city of Tomakomai after the 2003 Tokachi-oki earthquake (Hatayama 2007)

The condition that renders a storage tank susceptible to fire or sinking of the roof can be determined by comparing the maximum sloshing wave height with the freeboard of the tank. Sloshing response in cylindrical storage tanks can be computed based on the velocity potential theory. It has been introduced into many seismic design codes for the tanks, e.g., EN 1998-4 (2006), NZSEE (2009), and API 650 (2007).

2.3.3 Anchor bolt failure

In case self-anchoring is not adequate, tanks are anchored with bolts. The rocking motion in the tanks caused by the overturning moment induces pulling forces in anchor bolts. The observed tank damage from the 1977 San Juan earthquake included anchorage failure at the junction of the tanks to their concrete bases. Rehabilitation efforts occurred after the earthquake for these anchorage failures, and this included strengthening of the existing anchorage system in addition to reducing the amount of liquid in each tank.

In addition to the tank shell bulging, some of the tanks exhibited weld rupture at the joint of the bottom course with the angular plate used as part of the anchorage system; this caused loss of liquid inside of the tank.

The tank damage observed during the 1977 San Juan earthquake is the same as the damage documented through the 2014 Napa Valley earthquake as well as the 2010 Maule earthquake. Anchorage failure is a common type of damage observed in all of the previous. The anchor bolts are not meant to dissipate the energy from the earthquake, but rather prevent the tank from rocking off the foundation. Anchorage failures occurred after the 2014 Napa Valley earthquake, mainly in tanks that were full. Figure 2.11 shows some examples of anchorage failures observed after the Napa Valley earthquake.

Figure 2.11. Examples of anchorage failures observed after the 2014 Napa Valley earthquake (Fischer et al. 2016)

Anchorage failures in flat-bottomed tanks are collected in Figure 2.12, after the 2012 Emilia earthquake. In particular, these mechanisms are usually associated with the elastic diamond-shaped buckling of the tank wall, as presented in Figure 2.8. In many cases, excessive inelastic strain demands took place in the anchor bolts causing their fracture or pull-out from the concrete pads.

Figure 2.12 shows two anchoring system-related modes. The former depicts the spalling of concrete, induced by the insufficient distance between the anchor bolt and the edge of the foundation and low resistance of the concrete, while the latter presents a flexural failure occurred in the anchor plates. Hence, these systems, poorly anchored and detailed to sustain earthquake-induced demand, collapsed because of lack of proper steel reinforcement around the anchor and inadequate resistance of the foundation concrete. Failures were induced by sliding and rocking of the tank, and they were observed to occur in the weakest link of the anchoring system (Brunesi et al. 2014).

Figure 2.12. Examples of anchorage failures observed after the 2012 Emilia earthquake (Brunesi et al. 2014)

The type and extent of this damage show the importance of seismic design for storage tanks. Especially, the rocking motion which lifts up the annular plate and pulls out the anchor bolts from their foundations. In this case, the stretch of the anchor bolts should be the subject of careful design.

2.3.4 Bottom plate failure

This form of failure may occur in unanchored tanks. The rocking and uplift of the tank base can lead to a large inelastic rotation demand at the welded shell-to-bottom plate joint and large multi-axial membrane stress in the base plate of tanks. The shell-to-bottom plate joint is susceptible to low-cycle fatigue failure under repeated cycles of the uplift.

In past earthquakes like the one in Nigata in 1964, the liquefaction of materials under the tanks, coupled with imposed seismic moments on the tank base from lateral accelerations, resulted in the base rotation and gross settlements on the order of several meters. In other cases on firm foundations, fracture of the base plate welds occurred in tanks not restrained or inadequately restrained against uplift. In these cases, seismic accelerations resulted in uplift displacements on the tension side of the tank, up to 0.35 m recorded in the 1971 San Fernando earthquake. Since the base plate is held down by the hydrostatic pressure of the tank contents, the base weld is subject to high stresses and fracture may result. In some cases, the resulting loss of liquid has resulted in scouring the foundation materials in the vicinity, reducing support to the tank in the damaged area and exacerbating the damage. Figure 2.13 shows an unanchored tank on a concrete pedestal which was slid around 100 mm and lifted about 200 mm in one edge after the 2010 Maule Earthquake. The lateral displacement at the roof was about 1000 mm.

Figure 2.13. Damage caused by sliding and overturning and subsequent impact of tanks after the 2010 Maule Earthquake (González et al. 2013)

Current codes, e.g., EN 1998-4 (2006), NZSEE (2009), and API 650 (2007), limit the plastic rotation of the shell-to-bottom plate joint. In EN 1998-4 and NZSEE, the rotation capacity of the joint is limited to 0.2 rad. This limit comes from the assumption that a plastic hinge with a length of twice the thickness of the base plate forms at the base plate, next to the shell-to-bottom plate joint, and the maximum strain should be limited to 5%. However, Cortes et al. (2011) suggested that this rotation limit is overly conservative and proposed an increase of the limit of 0.4 rad.

2.3.5 Support system failure

Steel liquid storage tanks supported above grade by columns or frames have failed because of the inadequacy of the support system under lateral seismic forces; this occurred to a steel cement silo in Alaska in 1964. Many elevated water tanks failed or were severely damaged in the 1960 Chilean earthquake. In most of the cases, the collapse of the tanks was mainly due to the insufficient shear strength of concrete support members.

Observed damage to support structures has also been found in a group of elevated tanks in the Habas plant after the 1999 İzmit earthquake, Turkey. Two of the three liquid gas storage tanks collapsed due to the collapse of support columns, as shown in Figure 2.14. Column failures and impact of the tanks to the ground led to buckling of the outer shells of the collapsed tanks. It is estimated that approximately 1200 tons of cryogenic liquefied oxygen were released as a result of the collapse of the two oxygen storage tanks. The liquefied nitrogen tank next to the collapsed tanks was undamaged except for some hairline cracks in the columns. The two damaged tanks on the left in Figure 2.14 contained liquefied oxygen, while the undamaged tank on the right had liquefied nitrogen. Habas representatives on site reported that the liquefied oxygen tanks were 85% full and the liquefied nitrogen tank was about 25% full immediately before the earthquake.

Figure 2.14. Support columns of a group of liquefied oxygen tanks collapsed after the 1999 İzmit earthquake (Sezen and Whittaker 2006)

Other failures of support structures can be observed after the 2011 Bhuj earthquake in India when many elevated water tank stagings suffered damage and a few collapsed. These water tanks are located in the area of a radius of approximately 125 km from the epicentre. The majority of these tanks are supported by cylindrical shaft type staging which developed circumferential flexural cracks near the base. Two of such tanks located in regions of the highest intensity of shaking collapsed, while a few developed cracking near brace-column joint regions. Observed damage to support structures during past earthquakes illustrates that their seismic design is very important to ensure efficient functioning of the rested tanks and need careful treatment.

2.3.6 Piping system failure

One of the most common causes of loss of tank contents in earthquakes has been the fracture of piping at connections to the tank wall, which is due to large vertical displacements of the tank caused by the buckling, uplift, sliding or foundation failure; this happened to steel tanks in the 1992 Landers earthquake. Failure of rigid piping that connects to adjacent tanks has also been caused by relative horizontal displacements of the tanks. Piping failure has also resulted in extensive scour in the foundation materials. Another failure mode has been the breaking of pipe that enters the tank from underground, due to the relative movement of the tank and the pipe; this occurred several times during the 1985 Chilean earthquake. Rigid overflow pipes attached to steel tanks have exerted large forces on the tank wall supports due to the relative movement of the tank to the ground. The wall supports of one such pipe tore out of the shell of an oil tank in Richmond in the 1989 Loma Prieta earthquake. The pipe support failure left a small hole in the shell around mid-height of the tank. A failure example of the pipe attached to the tank wall is shown in Figure 2.15, together with a diamond shape buckling of the tank wall.

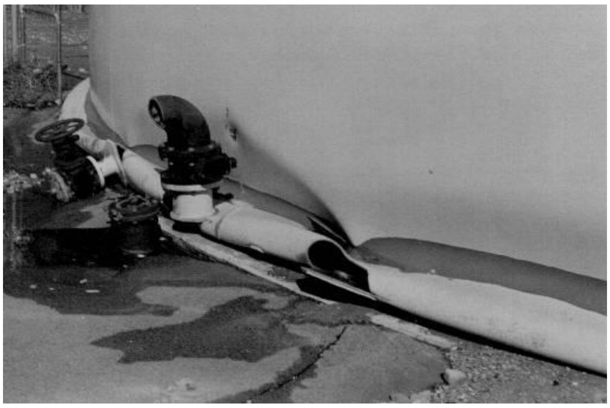

Figure 2.15. Failure of pipes attached to the tank wall (Manos Clough 1982)

Current design codes (e.g., EN 1998-4 2006, NZSEE 2009, and API 650 2007) adopt an empirical procedure for determining actions on nozzles, whereas flexibility of the attached is suggested. In general, local loads on the tank nozzle depend primarily on the seismic response of the attached piping system, rather than the response of the liquid storage tank.

2.4 Closure

A historical overview of earthquake damage to steel liquid storage tanks in industrial plants is presented in this chapter. Field observations of the damage confirm the devastating impact that natural disasters can cause on industrial facilities. The release of numerous hazardous materials was triggered by the earthquakes with spills being the dominant accident scenario. In some cases, fires and explosions occurred when flammable and explosive materials were released and found an ignition source or reacted with other materials. The impact of earthquakes on industrial plants demonstrates that there is a need for a realistic assessment of the expected earthquake severity and the resultant loading on structures, and a reliable tool for seismic risk assessment of the plants. The observed earthquake damage to storage tanks in industrial plants, which are one of the most vulnerable components, is also introduced. The damage ranges from failures of fixed or floating roofs, support system, piping system attached to the tank wall, anchor bolts, shell and bottom plate, and their connections. The finding of critical failure modes of the tank is an important step in their seismic vulnerability assessment.

Chapter 3. Numerical modelling of cylindrical liquid storage tanks

3.1 Literature overview

A large number of studies have been conducted on the dynamic response of liquid storage tanks. The earliest study was due to Jacobsen (1949) who reported an analytical result on the hydrodynamic pressure developed in rigid tanks subjected to the horizontal base motion and anchored to the rigid foundation. The irrotational motion of a compressible inviscid fluid was represented by Laplace equation which satisfies specified boundary conditions. Housner (1963) used an approximate simplified approach, in which the total hydrodynamic pressure was decomposed into impulsive and convective parts. This approach, which easily identifies the base shear and overturning moment, found widespread application in practice and comprise the basis of today's seismic design codes for liquid containers. Wozniak and Mitchell (1978) generalised the Housner's model for short and slender tanks. Veletsos and Yang (1977) used a different approach to arrive at a similar type of mechanical model for rigid circular tanks. They found that the pressure distributions due to the liquid motion for rigid and flexible anchored tanks were similar; however, the magnitude was highly dependent on the flexibility of the wall. It was concluded that the flexibility effects might be important depending on the system characteristics and the seismic excitation. Haroun and Housner (1981) developed a reliable method for analysing the dynamic behaviour of deformable cylindrical tanks, which was based on a finite element model of the tank-liquid system. Veletsos (1984) improved Housner's mechanical analogue to take into account the effects of tank wall flexibility. Veletsos and Tang (1987) analysed the dynamic response of cylindrical liquid storage tanks to a rocking base motion. Fische and Rammerstorfer (1999) presented an analytical procedure which allows one to study explicitly the influence of the wall deformations on both the liquid pressure and the surface elevation for typical wall deformation shapes. Malhotra et al. (2000) simplified the flexible tank model of Veletsos (1984); the procedure has been adopted in EN 1998-4 (2006).

Due to practical and economic reasons, many liquid storage tanks have been directly constructed on the compacted soil without anchoring. The dynamic behaviour of unanchored tanks is considerably different than that of rigidly anchored ones. Malhotra and Veletsos (1994a) studied extensively the uplift behaviour of the bottom plate of unanchored tanks by idealising the base plate as uniformly loaded semi-infinite, prismatic beams that rest on a rigid foundation. The effect of elastic end constraints, the influence of the axial forces associated with large deflections, and the effect of plastic yielding in the beam were considered. In a sequel to their work, the uplift analysis of the base plate in cylindrical liquid storage tanks and the uplift response of unanchored liquid storage tanks were thoroughly investigated (Malhotra and Veletsos 1994b, Malhotra and Veletsos 1994c, Malhotra 1995).

The numerical technique, e.g., the finite element method (FEM), has become a highly useful tool; it has possibly been used for the numerical analysis not only of the tank itself but also the contained liquid with more reliable analysis results. However, because of the complex nonlinear behaviour of the coupled tank-liquid-foundation system, the modelling of this type of structure is a very challenging topic, and many studies are still being performed in this field.

Barton and Parker (1987) first investigated the seismic response of liquid-filled cylindrical storage tanks using the FEM implemented in the structural analysis computer code ANSYS. Both added mass concepts and displacement-based fluid finite elements were employed to allow for the effects of the liquid. Virella et al. (2006) presented dynamic buckling analyses of anchored steel tanks subjected to horizontal earthquake excitations using nonlinear three-dimensional finite element models. The added mass in lumped form was attached to the shell nodes of the finite element models using massless spring elements. Recently, an application of nonlinear fluid-structure interaction methods to the seismic analysis of anchored and unanchored tanks has been presented by Ozdemir et al. (2010). In their numerical models, Arbitrary Lagrangian-Eulerian (ALE) description of the liquid-structure interface was employed, and the fluid motion was governed by the Navier-Stokes equations. Later, a nonlinear static pushover analysis of unanchored steel liquid storage tanks was proposed by Vathi and Karamanos (2015), where the hydrodynamic pressure distributions on the tank wall were calculated and applied to the steel tank model by a load subroutine in the ABAQUS software. The uplift mechanism of the base plate was captured through the relationship between the base uplift and the overturning moment caused by the liquid motion. Phan et al. (2017b) proposed a full nonlinear finite element model of an unanchored tank using the ABAQUS software. The steel tank was modelled based on a Lagrangian formulation, while an ALE adaptive mesh was used in the liquid domain to permit large deformations of the free surface sloshing. Their analysis results were in good agreement with those of experimental data.

Several laboratory measurements were conducted on storage tanks to verify analytical and numerical techniques developed for the seismic analysis of such structures. Kana (1979) investigated the influence of wall flexural vibrations on induced stresses using a laboratory testing. A series of experiments of reduced scale model was conducted, and preliminary observations were evaluated. These evaluations allowed formulation of an approximate analytical model for prediction of seismically induced stress. Clough (1977) studied experimentally in broad cylindrical tanks to evaluate seismic design procedures. As the continuation of this study, Manos and Clough (1982) carried out shaking table tests as well as static tilt tests on scaled tank models. They focused on the higher order out of round response of unanchored tanks which induced in addition to rocking cantilever type response. Manos (1986) carried out experiments to determine impulsive mode frequencies and base-overturning moments of broad and tall tanks. Tanaka et al. (2000) conducted dynamic tests on small and large-scale models under earthquake loading to investigate elephant’s foot buckling and side slipping behaviour of cylindrical tanks. De Angelis et al. (2010) investigated the effectiveness of the base isolation on steel liquid storage tanks through numerical models and shaking table tests that were conducted on a reduced scale model of a real steel tank, typically used in petrochemical plants.

3.2 Background theory

3.2.1 System considered and assumptions

The hydrodynamic pressures and forces acting on a cylindrical tank can be expressed by the sum of two components: (i) an impulsive component, which represents the effect of the part of the liquid that may be considered to move in synchronism with the tank wall as a rigid mass, and (ii) a convective component, which represents the effect of the part of contained liquid undergoing a sloshing motion. The impulsive effects turn out to be proportional to the acceleration of the ground motion, whereas the convective effects depend on the sloshing frequencies of the fluid.

The system considered is shown in Figure 3.1. It is a rigid circular cylinder fixed to a rigid base. The tank is filled with a fluid density ρ to a filling level H. The total mass of the fluid is denoted by m_l. The fluid is assumed to be incompressible and nonviscous. The fluid-tank system is presumed to be subjected to a horizontal ground acceleration $\ddot{x}_g(t)$ directed along the x-axis.

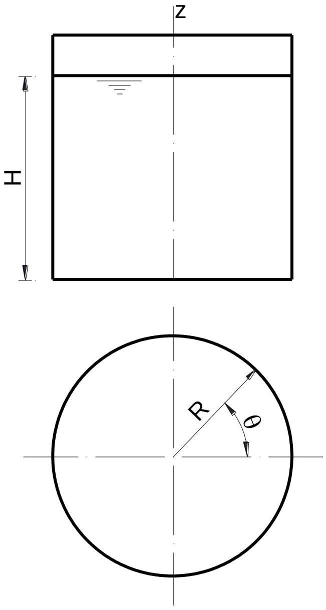

Figure 3.1. System considered

3.2.2 Governing equation of fluid motion

The equation of motion for the fluid referred to the cylindrical coordinate system (r, z, θ) shown in Figure 3.1, is:

$$\frac{\partial^2 \phi}{\partial r^2} + \frac{1}{r}\frac{\partial \phi}{\partial r} + \frac{1}{r^2}\frac{\partial^2 \phi}{\partial \theta^2} + \frac{\partial^2 \phi}{\partial z^2} = 0 \tag{3.1}$$

where ϕ is the velocity potential function. The velocity components of the fluid in the radial, tangential and vertical directions are given by:

$$v_r = -\frac{\partial \phi}{\partial r},\ v_\theta = -\frac{\partial \phi}{r\partial \theta},\ v_z = -\frac{\partial \phi}{\partial z} \tag{3.2}$$

The hydrodynamic pressure is related to ϕ by the equation:

$$p = \rho\frac{\partial \phi}{\partial t} \tag{3.3}$$

The boundary conditions of the problem are as follows:

$$\left.\frac{\partial\phi}{\partial z}\right|_{z=0} = 0, -\left.\frac{\partial\phi}{\partial r}\right|_{z=R} = \dot{x}_g(t)\cos\theta,\ \left.p\right|_{z=H} = \rho g\delta(t) \tag{3.4}$$

where $\delta(t)$ is the instantaneous value of the vertical displacement of the fluid at the surface. This expression neglects the contribution of the inertia force associated with $\delta(t)$. Using equations (3.3) and (3.4) and differentiating with respect to time, one obtains:

$$\frac{\partial^2\phi}{\partial t^2} + g\frac{\partial\phi}{\partial z} = 0 \tag{3.5}$$

It is convenient to express the solution of Eq. (3.1) as the sum of the two partial solutions:

$$\phi = \phi_i + \phi_c \tag{3.6}$$

with ϕ_1 subject to the following boundary conditions:

$$\begin{array}{llll} z=0 & \dfrac{\partial\phi_i}{\partial z} = 0 & \quad r=R & \dfrac{\partial\phi_i}{\partial r} = -\dot{x}_g(t)\cos\theta \\ z=H & \dfrac{\partial\phi_i}{\partial t} = 0 & & \end{array} \tag{3.7}$$

with ϕ_2 subject to the following boundary conditions:

$$\begin{array}{ll} z=0 & \dfrac{\partial\phi_c}{\partial z} = 0 \\ r=R & \dfrac{\partial\phi_c}{\partial r} = 0 \\ z=H & \dfrac{\partial^2\phi_c}{\partial t^2} + g\dfrac{\partial\phi_c}{\partial z} = -g\dfrac{\partial\phi_i}{\partial z} \end{array} \tag{3.8}$$

Thus, ϕ_i represents the solution for the so-called impulsive effects. The solution ϕ_c, which effectively corrects for the difference between the correct boundary condition in Eq. (3.5) and the one defined by Eq. (3.7), represents the so-called convective effects.

3.2.3 Impulsive solution

The solution for this case is given by:

$$\phi_i = -\dot{x}_g\left(t\right)H\cos\theta\sum_{n=1}^{\infty}\frac{8\left(-1\right)^{n+1}}{\left[\left(2n-1\right)\pi\right]^2}\frac{I_1\left[\left(2n-1\right)\frac{\pi}{2}\frac{r}{H}\right]}{I_1'\left[\left(2n-1\right)\frac{\pi}{2}\frac{R}{H}\right]}\cos\left[\left(2n-1\right)\frac{\pi}{2}\frac{z}{H}\right] \tag{3.9}$$

where I_1 is the modified Bessel function of the first kind, and I'_1 is its derivative (Appendix A). The pressure induced by the impulsive effects is obtained by application of Eq. (3.9) into Eq. (3.3):

$$p_i = -\ddot{x}_g\left(t\right)\rho H\cos\theta\sum_{n=1}^{\infty}\frac{8\left(-1\right)^{n+1}}{\left[\left(2n-1\right)\pi\right]^2}\frac{I_1\left[\left(2n-1\right)\frac{\pi}{2}\frac{r}{H}\right]}{I_1'\left[\left(2n-1\right)\frac{\pi}{2}\frac{R}{H}\right]}\cos\left[\left(2n-1\right)\frac{\pi}{2}\frac{z}{H}\right] \tag{3.10}$$

The total hydrodynamic force exerted by the liquid on the tank, which is also equal to the total base shear, is obtained from:

$$Q_i = \int_0^H\int_0^{2\pi} p_i\big|_{r=R}\cos\theta R\,d\theta\,dz \tag{3.11}$$

with the following result:

$$Q_i = -\ddot{x}_g\left(t\right)m_l\frac{H}{R}\sum_{n=1}^{\infty}\frac{16}{\left[\left(2n-1\right)\pi\right]^3}\frac{I_1\left[\left(2n-1\right)\frac{\pi}{2}\frac{R}{H}\right]}{I_1'\left[\left(2n-1\right)\frac{\pi}{2}\frac{R}{H}\right]} \tag{3.12}$$

The corresponding overturning moment about the base of the tank is determined from:

$$M_i = \int_0^H\int_0^{2\pi} p_i\big|_{r=R}\cos\theta zR\,d\theta\,dz \tag{3.13}$$

with the following result:

$$M_i = -\ddot{x}_g(t) m_l H \frac{H}{R} \sum_{n=1}^{\infty} \frac{16}{\left[(2n-1)\pi\right]^3} \frac{I_1\left[(2n-1)\frac{\pi}{2}\frac{R}{H}\right]}{I_1'\left[(2n-1)\frac{\pi}{2}\frac{R}{H}\right]} \left[1-\frac{2(-1)^{n+1}}{(2n-1)\pi}\right] \tag{3.14}$$

The hydrodynamic pressure on the base of the tank is obtained from Eq. (3.10) by setting $z = 0$, and the corresponding overturning moment is obtained from:

$$M_i' = \int_0^{2\pi}\int_0^{2\pi} p_i\big|_{z=0} \cos\theta r^2 dr d\theta \tag{3.15}$$

with the following result:

$$M_i' = -\ddot{x}_g(t) m_l H \sum_{n=1}^{\infty} \frac{16(-1)^{n+1}}{\left[(2n-1)\pi\right]^3} \frac{I_2\left[(2n-1)\frac{\pi}{2}\frac{R}{H}\right]}{I_1'\left[(2n-1)\frac{\pi}{2}\frac{R}{H}\right]} \tag{3.16}$$

3.2.4 *Convective solution*

The convective solution for an arbitrary ground motion is derived from the convective solution for a harmonic ground acceleration using the inverse Fourier transform and the convolution (Duhamel's integral). In this section, only the main steps of the procedure are reported. The reader is referred to Yang (1976) for all the mathematical manipulations. Considering a harmonic ground acceleration $\ddot{x}_g(t) = x_0 e^{i\omega t}$, the function ϕ_c which satisfies Eq. (3.1) and boundary conditions is given by:

$$\phi_c = -\frac{1}{i\omega}\ddot{x}_0 e^{i\omega t} H \frac{R}{H}\cos\theta \sum_{n=1}^{\infty} \frac{1}{1-(\omega/\omega_{cn})^2} \frac{2}{\lambda_n^2-1} \frac{J_1\left(\lambda_n \frac{r}{R}\right)}{J_1(\lambda_n)} \frac{\cosh\left(\lambda_n \frac{z}{R}\right)}{\cosh\left(\lambda_n \frac{H}{R}\right)} \tag{3.17}$$

where J_1 is the Bessel function of the first kind (Appendix A) and ω_{cn} are the natural frequencies of sloshing fluid, given by:

$$\omega_{cn} = \sqrt{\frac{\lambda_n g}{R} \tanh\left(\lambda_n \frac{H}{r} \right)} \tag{3.18}$$

The harmonic convective pressure for the tank is obtained by application of Eq. (3.17) into Eq. (3.3):

$$p_c = \ddot{x}_0 e^{i\omega t} \rho H \frac{R}{H} \cos\theta \sum_{n=1}^{\infty} \frac{1}{1-\left(\omega / \omega_{cn}\right)^2} \frac{2}{\lambda_n^2 - 1} \frac{J_1\left(\lambda_n \frac{r}{R} \right)}{J_1\left(\lambda_n\right)} \frac{\cosh\left(\lambda_n \frac{z}{R} \right)}{\cosh\left(\lambda_n \frac{H}{R} \right)} \tag{3.19}$$

The frequency response function of the convective pressure, defined by Eq. (3.17), is of the form:

$$p_c\left(\omega\right) = \sum_{n=1}^{\infty} \frac{f\left(r,\theta,z\right)}{1-\left(\omega / \omega_{cn}\right)^2} \tag{3.20}$$

The pressure $p_c(t)$ for an arbitrary acceleration input $\ddot{x}_g(t)$ is given by:

$$p_c = \sum_{n=1}^{\infty} f\left(r,\theta,z\right) \int_0^t \omega_{cn} \ddot{x}(t) \sin\left[\omega_{cn}\left(t-\tau\right) d\tau \right] \tag{3.21}$$

where the integral is the Duhamel’s integral which represents the instantaneous value of the pseudo-acceleration, $A_{cn}(t)$, of a single-degree-of freedom system having a circular natural frequency ω_{cn} and subjected to the prescribed ground acceleration $\ddot{x}_g(t)$. Thus, the counterpart of Eq. (3.19) for transient response may be written as:

$$P_c = \rho H \cos\theta \sum_{n=1}^{\infty} \frac{2}{\lambda_n^2 - 1} \frac{R}{H} \frac{J_1\left(\lambda_n \frac{r}{R} \right)}{J_1\left(\lambda_n\right)} \frac{\cosh\left(\lambda_n \frac{z}{R} \right)}{\cosh\left(\lambda_n \frac{H}{R} \right)} A_{cn}\left(t\right) \tag{3.22}$$

Proceeding similarly, one finds the following expressions for the other response quantities:

$$Q_c = m_l \sum_{n=1}^{\infty} \frac{2}{\lambda_n \left(\lambda_n^2 - 1\right)} \frac{R}{H} \tanh\left(\lambda_n \frac{H}{R} \right) A_{cn}\left(t\right) \tag{3.23}$$

$$M_c = m_l H \sum_{n=1}^{\infty} \frac{2}{\lambda_n\left(\lambda_n^2 - 1\right)} \frac{R}{H} \tanh\left(\lambda_n \frac{H}{R}\right)\left[1 - \frac{R}{\lambda_n H} \tanh\left(\frac{\lambda_n H}{2R}\right)\right] A_{cn}(t)$$

(3.24)

$$M'_c = m_l H \sum_{n=1}^{\infty} \frac{2}{\lambda_n\left(\lambda_n^2 - 1\right)} \left(\frac{R}{H}\right)^2 \frac{J_2(\lambda_n)}{J_1(\lambda_n)} \frac{1}{\cosh\left(\lambda_n \frac{H}{R}\right)} A_{cn}(t) \qquad (3.25)$$

3.2.5 *Recast expressions*

The spatial-temporal variation of the rigid impulsive pressure acting on the tank wall can be conveniently rewritten by the expression:

$$p_i(\zeta, \eta, \theta, t) = C_i(\zeta, \eta) \rho H \cos\theta A_g(t) \qquad (3.26)$$

$$\text{with } C_i(\zeta, \eta) = 2 \sum_{n=0}^{\infty} \frac{(-1)^n}{I'_1(v_n/\gamma) v_n^2} \cos(v_n \eta) I_1\left(\frac{v_n}{\gamma} \zeta\right), \; v_n = \frac{2n+1}{2}\pi \qquad (3.27)$$

where $\zeta = r/R$ and $\eta = z/H$ is the nondimensional coordinate, and $A_g(t)$ is the ground acceleration time history in the free-field. Figure 3.2 shows the distributions along the height and the bottom of the impulsive pressure for different values of the tank aspect ratio, $\gamma = H/R$. The values are calculated for $\zeta = 1.0$ (i.e, at the wall of the tank) and $\cos\theta = 1.0$ (i.e., in the plane of the horizontal seismic action), and normalised to $\rho R A_g$. As illustrated in the right figure, the pressure distribution on the bottom plate becomes linear for large values of the aspect ratio, and the pressure distributions are almost the same for the aspect ratios $\gamma = 2$, 2.5, and 3.

The impulsive mass, m_i, denotes the mass of the contained fluid which moves together with the walls and can be determined from Eq. (3.12) as the fraction of the impulsive base shear and the ground acceleration:

$$m_i = m_l 2\gamma \sum_{n=0}^{\infty} \frac{I_1(v_n/\gamma)}{v_n^3 I'_1(v_n/\gamma)} \qquad (3.28)$$

The heights of the impulsive mass measured from the bottom, h_i and h'_i, which correspond to M_i and M'_i, can also be calculated from equations (3.14) and (3.16), given as:

$$h_i = H\frac{\displaystyle\sum_{n=0}^{\infty}\frac{(-1)^n I_1(\nu_n/\gamma)}{\nu_n^4 I_1'(\nu_n/\gamma)}\left[\nu_n(-1)^n - 1\right]}{\displaystyle\sum_{n=0}^{\infty}\frac{I_1(\nu_n/\gamma)}{\nu_n^3 I_1'(\nu_n/\gamma)}} \tag{3.29}$$

$$h_i' = H\frac{\displaystyle\frac{1}{2}+2\gamma\sum_{n=0}^{\infty}\frac{\nu_n + 2(-1)^{n+1}}{\nu_n^4}\frac{I_1(\nu_n/\gamma)}{I_1'(\nu_n/\gamma)}}{\displaystyle 2\gamma\sum_{n=0}^{\infty}\frac{I_1(\nu_n/\gamma)}{\nu_n^3 I_1'(\nu_n/\gamma)}} \tag{3.30}$$

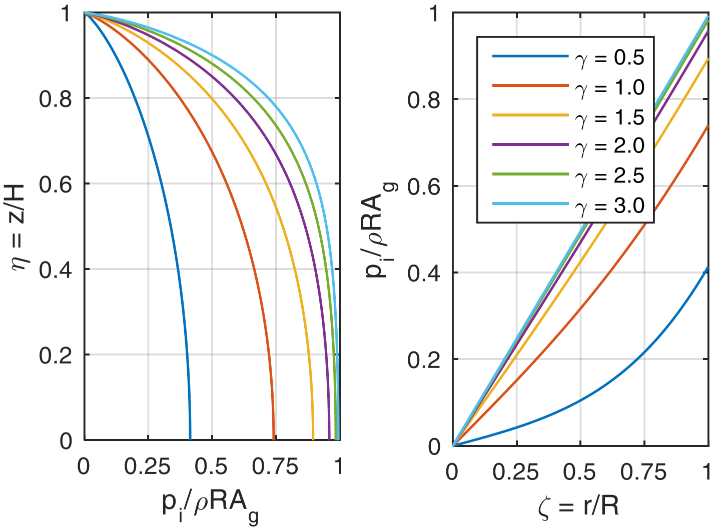

Figure 3.2. Impulsive pressure distributions along the height (left) and the bottom (right) for different values of the aspect ratio

The spatial-temporal variation of the convective pressure component is rewritten as follows:

$$p_c(\zeta,\eta,\theta,t) = \rho\sum_{n=1}^{\infty}\psi_n \cosh(\lambda_n\gamma\eta) J_1(\lambda_n\zeta)\cos\theta A_{cn}(t) \tag{3.31}$$

with

$$\psi_n = \frac{2R}{\left(\lambda_n^2 - 1\right) J_1\left(\lambda_n\right)\cosh\left(\lambda_n \gamma\right)} \tag{3.32}$$

Similarly, the nth modal convective mass is calculated based on Eq. (3.23):

$$m_{cn} = m_l \frac{2\tanh\left(\lambda_n \gamma\right)}{\gamma\lambda_n\left(\lambda_n^2 - 1\right)} \tag{3.33}$$

moreover, their corresponding heights are obtained using equations (3.24) and (3.25):

$$h_c = H\left[1 + \frac{1 - \cosh\left(\lambda_n \gamma\right)}{\lambda_n \gamma \sinh\left(\lambda_n \gamma\right)}\right] \tag{3.34}$$

$$h'_{cn} = H\left[1 + \frac{2 - \cosh\left(\lambda_n \gamma\right)}{\lambda_n \gamma \sinh\left(\lambda_n \gamma\right)}\right] \tag{3.35}$$

The first mode sloshing pressure distributions along the height and the bottom for different values of the aspect ratios are shown Figure 3.3.

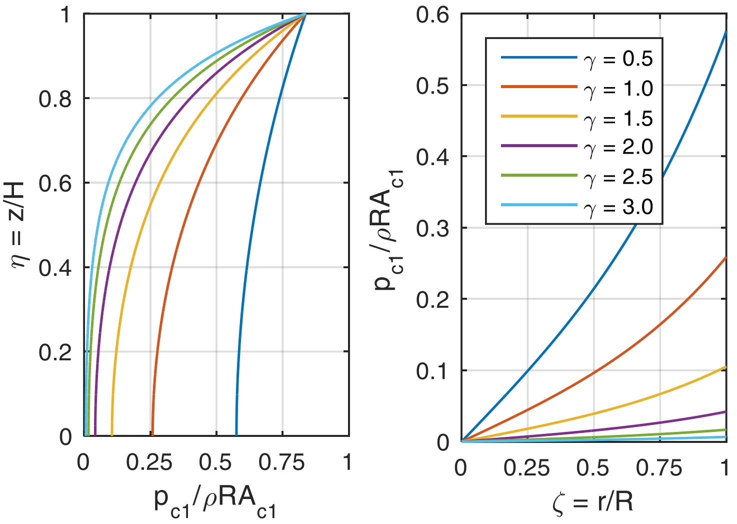

Figure 3.3. First mode convective pressure distributions along the height (left) and the bottom (right) for different values of the aspect ratio

In broad tanks, the sloshing pressures maintain relatively high values down to the bottom, while in slender tanks the sloshing effect is limited to the vicinity of the surface of the liquid. Figure 3.4 presents the pressure distributions of three different convective modes for two values of the aspect ratio, γ = 1.0 and 2.0. It can be observed that the effects of the higher convective modes are very limited and can be neglected in the analysis.

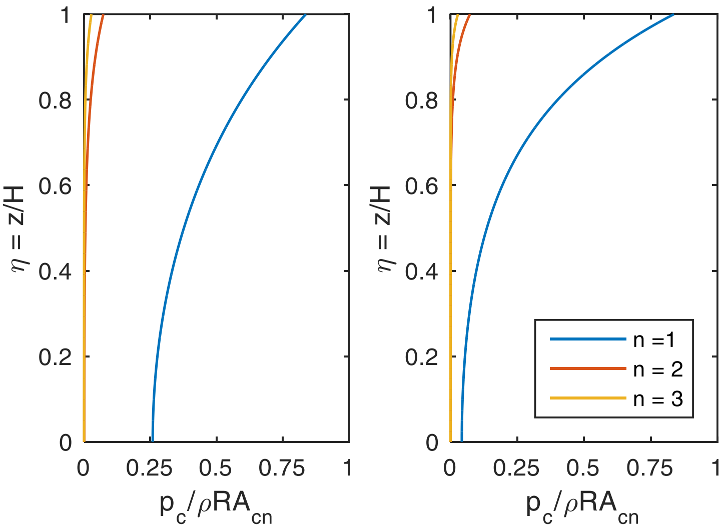

Figure 3.4. Convective pressure distributions of the three modes for aspect ratios 1.0 (left) and 2.0 (right)

Figure 3.5 shows the quantities m_i, h_i and h'_i as functions of γ. It can be seen that m_i increases with the increase of γ and tends asymptotically to the total liquid mass, while both h_i and h'_i tend to stabilise to values around $0.5H$. For broad tanks, h_i is a little less than $0.5H$, while h'_i is significantly larger than H; this is due to the predominant contribution to M'_i of the impulsive pressure acting on the bottom.

The variations of the convective masses m_{c1} and m_{c2} and their corresponding heights h_{c1}, h_{c2}, h'_{c1}, and h'_{c2} in terms of γ are shown in Figure 3.6. In most of the cases, the amount of convective mass contributed by the second mode is very limited. The values of h_{c1}, h_{c2}, h'_{c1}, and h'_{c2} are small than H in most ranges of the aspect ratio, except there is a significant increase of h'_{c1} for very broad tanks with values of the aspect ratio around 0.5.

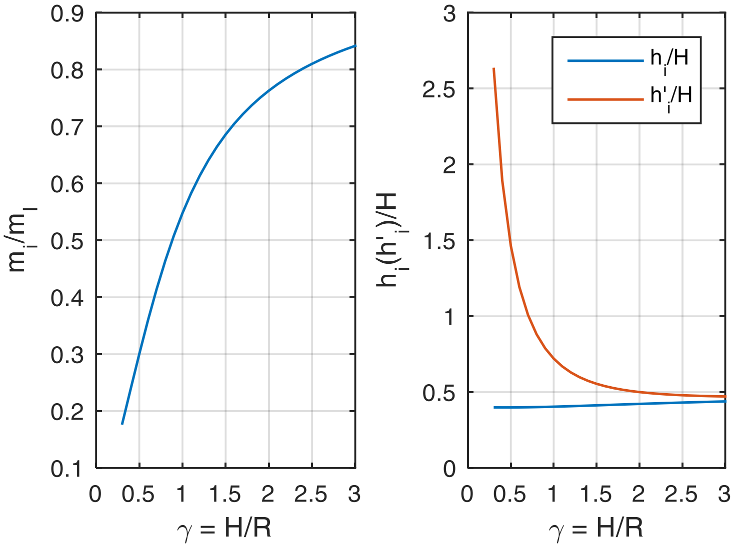

Figure 3.5. Impulsive mass (left) and heights (right) as functions of the aspect ratio

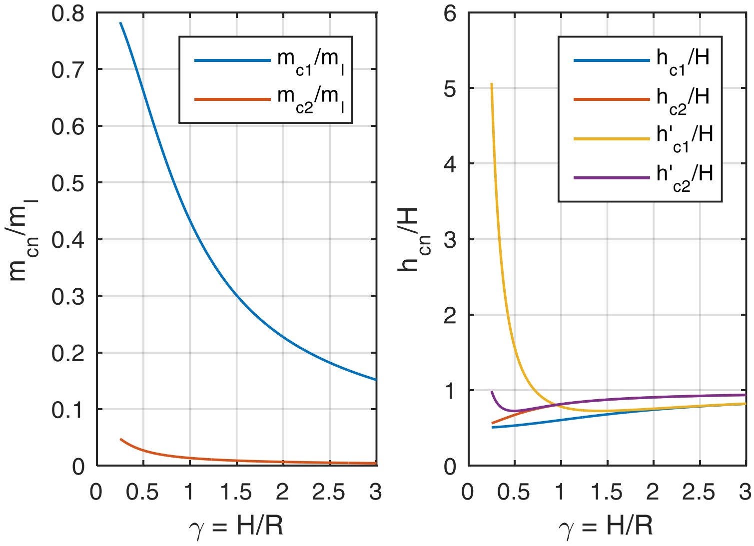

Figure 3.6. First two sloshing modal masses (left) and heights (right) as functions of the aspect ratio

3.3 Spring-mass models of tanks

The seismic analysis guidelines of tanks, e.g., EN 1998-4 (2006), NZSEE (2009), and API 650 (2007), are based mainly on the spring-mounted masses analogy first proposed by Housner (1963). This analogy is derived from the solution of the hydrodynamic equations that describe the behaviour of liquid inside a rigid container. EN 1998-4 (2006) mentions the mechanical model of Veletsos and Yang (1977) as an acceptable procedure for rigid circular tanks. For flexible circular tanks, models of Veletsos (1984) and Haroun and Housner (1981) are described along with the simplified procedure of Malhotra et al. (2000). NZSEE (2009) uses the mechanical model of Veletsos and Yang (1977) for rigid circular tanks and that of Haroun and Housner (1981) for flexible tanks. API 650 (2007) uses the mechanical model of Housner (1963) with modifications of Wozniak and Mitchell (1978). API 650 (2007) deals with circular steel tanks, which are flexible tanks. However, since there is no appreciable difference in the parameters of mechanical models of rigid and flexible tank models, these codes evaluate parameters of impulsive and convective modes from rigid tank models. The spring-mass models, presented in the following, for anchored and unanchored circular steel tanks, are mainly based on the suggestions of Malhotra and Veletsos (1994c) and Malhotra et al. (2000).

3.3.1 Above ground tanks

3.3.1.1 Anchored tank model

The possible numerical model of the anchored tank represented by two viscoelastic oscillators is shown in Figure 3.7. In particular, the impulsive and convective masses (m_i and m_c, respectively) are connected to the tank wall by equivalent one-dimensional spring-dashpot systems. The calculations of mass, height, and natural period for each system can be obtained by the method first presented by Velesos and Yang (1977) and later modified by Malhotra et al. (2000) to be simple, yet accurate, and more generally applicable. Specifically, these modifications include: (i) representing the tank-liquid system by the first impulsive and first convective modes by combining the higher impulsive modal mass with the first impulsive mode and the higher convective modal mass with the first convective mode, (ii) adjusting the impulsive and convective heights to account for the overturning effect of the higher modes, and (iii) generalising the impulsive period formula so that it can be applied to steel as well as concrete tanks of various wall thicknesses. For a given ground motion, the impulsive and convective responses are calculated independently and combined by the absolute-sum rule. This procedure has been adopted by EN 1998-4 (2006). The natural periods of the impulsive, T_i, and the convective, T_c, responses are calculated, as follows:

$$T_i = C_i \frac{H\sqrt{\rho}}{\sqrt{t_{eq}/R} \times \sqrt{E}} \tag{3.36}$$

$$T_c = C_c \sqrt{R} \tag{3.37}$$

where t_{eq} is the equivalent uniform thickness of the tank wall, ρ is the mass density of liquid, and E the modulus of elasticity of the tank material. The coefficients C_i and C_c are obtained from Table 3.1. For tanks with non-uniform wall thickness, t_{eq} is calculated by taking a weighted average over the wetted height of the tank wall, assigning the highest weight near the base of the tank where the strain is maximal.

Table 3.1. Recommended design values for the first impulsive and convective modes of vibration as a function of the tank height-to-radius ratio (Malhotra et al. 2000)

H/R	C_i	C_c	m_i/m_l	m_c/m_l	h_i/H	h_c/H	h_i'/H	h_c'/H
0.3	9.28	2.09	0.176	0.824	0.400	0.521	2.640	3.414
0.5	7.74	1.74	0.300	0.700	0.400	0.543	1.460	1.517
0.7	6.97	1.60	0.414	0.586	0.401	0.571	1.009	1.011
1.0	6.36	1.52	0.548	0.452	0.419	0.616	0.721	0.785
1.5	6.06	1.48	0.686	0.314	0.439	0.690	0.555	0.734
2.0	6.21	1.48	0.763	0.237	0.448	0.751	0.500	0.764
2.5	6.56	1.48	0.810	0.190	0.452	0.794	0.480	0.796
3.0	7.03	1.48	0.842	0.158	0.453	0.825	0.472	0.825

The corresponding stiffness and damping coefficient of each response are:

$$k_i = \omega_i^2 m_c \text{ and } c_i = 2\xi_i m_i \omega_i \quad \text{with } \omega_i = 2\pi / T_i \tag{3.38}$$

$$k_c = \omega_c^2 m_c \text{ and } c_c = 2\xi_c m_c \omega_c \quad \text{with } \omega_c = 2\pi / T_c \tag{3.39}$$

where ω_i and ω_c are the angular frequency of the impulsive and convective responses, respectively.

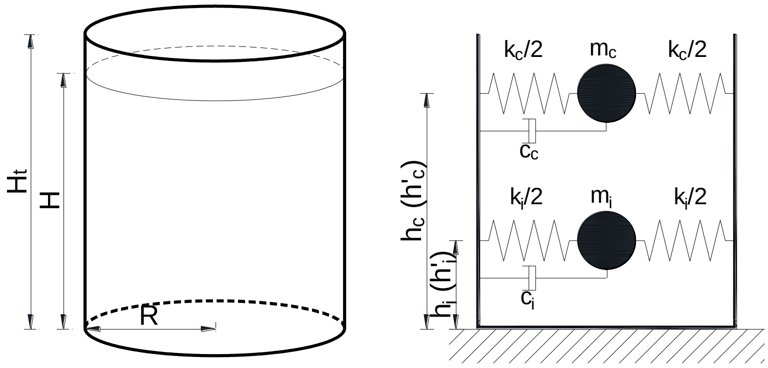

Figure 3.7. Spring-mass model for the anchored tank

The impulsive and convective responses are combined by taking their numerical sum rather than their root-mean-square value. The total base shear is given by Eq. (3.40):

$$Q = \left(m_i + m_w + m_r\right) \times A_i + m_c A_c \tag{3.40}$$

$$M = \left(m_i h_i + m_w h_w + m_r h_r\right) \times A_i + m_c h_c A_c \tag{3.41}$$

$$M' = \left(m_i h_i' + m_w h_w + m_r h_r\right) \times A_i + m_c h_c' A_c \tag{3.42}$$

where m_w is the mass of tank wall, m_r is the mass of tank roof, A_i is the impulsive acceleration response, and A_c is the convective acceleration response.

The overturning moment above the base plate, in combination with ordinary beam theory, leads to the axial stress at the base of the tank wall. The net overturning moment immediately above the base plate, M, is given by Eq. (3.41), where h_i and h_c are the heights of the centroids of the impulsive and convective hydrodynamic wall pressures, and h_w and h_r are the heights of the centres of gravity of the tank wall and roof, respectively. The overturning moment immediately below the base plate, M', is dependent on the hydrodynamic pressure on the tank wall as well as that on the base plate. It is given by Eq. (3.42), where the heights h_i' and h_c' are obtained from Table 3.1.

3.3.1.2 Unanchored tank model

In the case of unanchored tanks, the partial uplift of the bottom plate occurs when the tanks are subjected to strong seismic excitations. The seismic response of the tanks is highly influenced by the uplift mechanism. The uplift response of the base plate is nonlinear, which is due to continuous variation of the base contact area, plastic yielding of the plate material, and the effects of membrane forces associated with large displacements in the plate.

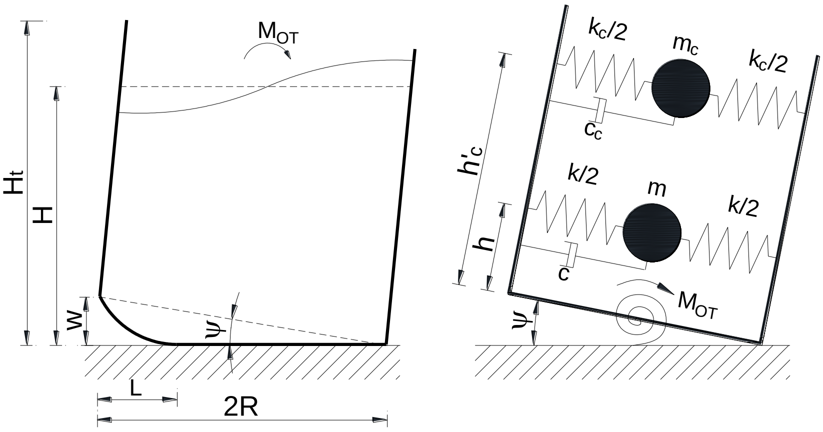

Figure 3.8. Spring-mass model for the unanchored tank

A simplified model of unanchored tanks has been proposed by Malhotra and Veletsos (1994c). The uplift mechanism of the tanks is simulated by a rotation spring that represents the rocking resistance of the base, as shown in Figure 3.8. In this model, the masses of the tank wall, m_w, and tank roof, m_r, are lumped with the impulsive mass. The total impulsive mass, $m = m_i + m_w + m_r$, is attached to the tank wall at an equivalent height, $h = (m_i h_i' + m_w h_w + m_r h_r)/m$, by a viscoelastic oscillator with a stiffness, $k = \omega_i^2 m$, and a damping coefficient, $c = 2\xi_i m\omega_i$.

The relationship between the overturning moment, M_{OT}, and the base rotation, ψ, can established by the method reported by Malhotra and Veletsos (1994a). In this approach, the tank base plate is modelled using uniformly loaded, semi-infinite, prismatic beams that are connected at their ends to the cylindrical tank wall. This model of the anchored tanks has been recently used by many researchers (Vathi and Karamanos 2015, Ormeño et al. 2015, Bakalis et al. 2016, Cortes and Prinz 2017, etc.).

3.3.2 Elevated tanks

When a tank rests upon on a support structure, its dynamic response is additionally influenced by the lateral flexibility of the support structure that is usually beneficial given by an increase of the fundamental period (Karamanos et al. 2006).

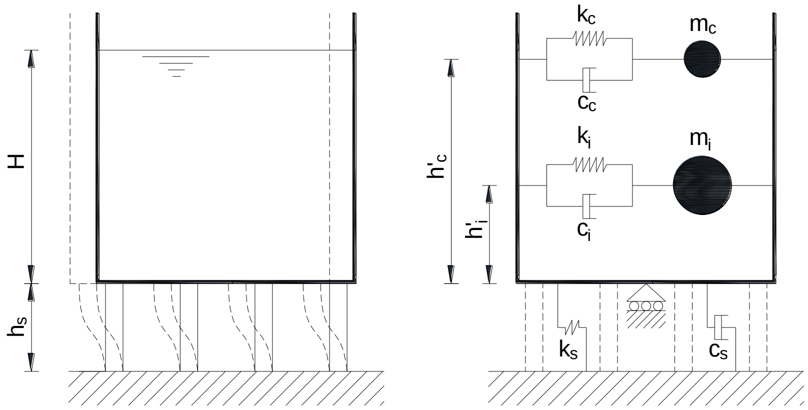

Figure 3.9. Spring-mass model of elevated tanks

In some instances, the support structure can be considered axially rigid, assuming a shear-type deformation. Accordingly, a possible numerical model can be represented as shown in Figure 3.9, where the impulsive and convective masses m_i and m_c are connected to the tank wall by two elastic springs of stiffness k_i and k_c and damping coefficients c_i and c_c. The support structure can also be represented by an equivalent elastic spring with stiffness k_s and damping coefficient c_s.

However, for strong seismic actions, the axial load in the support structure may vary because of the seismic overturning moment. The variation of the axial compression significantly affects the nonlinear behaviour of the support structure. On this point, it is necessary to build a three-dimensional model in which the structural behaviour of the support structure is correctly simulated, as shown in Figure 3.10. In this three-dimensional model, the motion of the masses is reproduced using two elastic cantilever beams with lateral stiffness k_i and k_c. The masses m_i and m_c are lumped at the free end of the elements, and the lengths h_i and h_c are chosen to reproduce the overturning effect at the tank base. For each mass m_i or m_c, only the translational horizontal degree of freedom is activated in this model. In order to correctly simulate the effect of the overturning moment, which includes also the hydrodynamic pressure acting at the tank base, an additional rotational inertia mass lumped with the impulsive mass should also be considered.

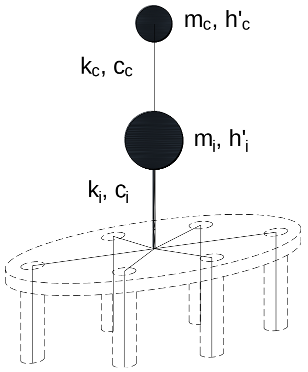

Figure 3.10. Three-dimensional stick model of elevated tanks

However, given that in most of the cases, the rotation angle of the tank base is small and can be negligible; this effect may not need to be accounted for. The detail on this three-dimensional model will be presented in Chapter 8 with the application to an elevated tank.

3.4 Calibration of spring-mass model for unanchored tanks

3.4.1 Discussion of previous models

The unanchored tank model, presented in Section 3.3, is mainly based on the proposal of Malhotra and Veletsos (1994c), where the uplift mechanism of the base plate is treated by a moment-rotation spring, added at the tank base. Previously, Clough (1977) first derived the relation between the uplift length and overturning moment, neglecting the geometrical and material properties of the shell and bottom plate. The uplift area with a crescent shape was assumed in his work. Cambra (1982, 1983) experimentally investigated a broad tank and derived a relationship between overturning moment and base uplift. Lau and Clough (1989) investigated the static tilt behaviour of unanchored cylindrical tanks, using the finite element method. They used a beam model, with equal vertical forces at ends, to model the asymmetric uplift of the tanks. Peek and Jennings (1988) used the finite difference energy method to solve the partially uplifted base plate and its interaction with the shell wall. The nonlinearities of the base plate due to contact, material yielding, and membrane actions were all included in their approach.

Previous studies confirmed that the response of unanchored tanks is highly influenced by the uplift mechanism, and the nonlinearities associated with the base uplift have great effects on the uplift response. Hence, simplified procedures may not adequately capture this complex mechanism, and some aspects need to be clarified as follows:

- The above beam model is a one-dimensional problem; this means that it does not take into account the two-dimensional nature of the problem.
- The effects of the hoop stress, which develops in the bottom plate close to the joint of the shell and bottom plate, has been neglected.
- The interaction between the base uplift and the shell wall has been neglected.
- In the beam model, it is assumed that the tank base does not experience any sliding.

In the next section, an efficient procedure for the spring-mass model calibration of unanchored tanks is proposed. The procedure is mainly based on a static pushover analysis, which is performed using a nonlinear finite element modelling of the tank system.

3.4.2 Nonlinear static pushover analysis

A static pushover analysis procedure for the tank system is first proposed. The procedure is based on a three-dimensional finite element model using the ABAQUS software, where both geometric and material nonlinearities are considered (SIMULIA 2014). The shell and bottom plate are modelled using four-node shell elements with reduced integration. The system is assumed resting on a rigid foundation that is modelled using solid elements. However, an elastic foundation can be considered with the use of soil elements. The successive contact and separation between the bottom plate and its rigid foundation are taken into account by a surface-based contact modelling algorithm. The penalty-based method with a friction coefficient is used for simulating the frictional contact between the bottom plate and the foundation. The elastic-plasticity of the steel tank is modelled based on the stress-strain relationship of the material. Because of the structural symmetry, only half of the tank system is modelled, and symmetry plane boundary conditions are employed to reduce the computational time. For example, Figure 3.11 shows the finite element modelling of an unanchored tank.

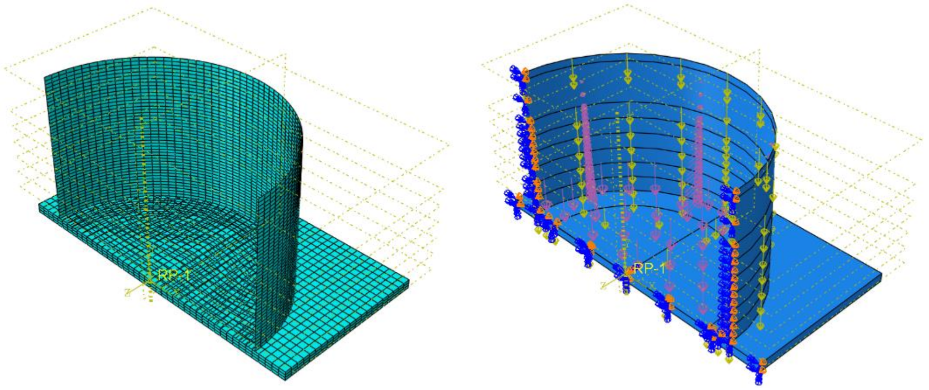

(a) (b)

Figure 3.11. An example of the finite element modelling of an unanchored tank: (a) finite element meshes and (b) boundary conditions and load cases

Due to the slight effect of the convective component to the response of the tank, only the impulsive component is considered in the analysis. The impulsive hydrodynamic pressures acting on the shell and bottom plate are calculated using Eq. (3.26), which is normalised to the liquid density and the acceleration magnitude. The loading is applied as a distributed surface load (i.e., pressure) to the shell and bottom plate, as shown in Figure 3.11(b), using the DLOAD subroutine. Three loading steps of the static pushover analysis, including gravity load of the steel tank, hydrostatic pressure of the contained liquid, and hydrodynamic pressure caused by the impulsive component, are shown in Figure 3.12.

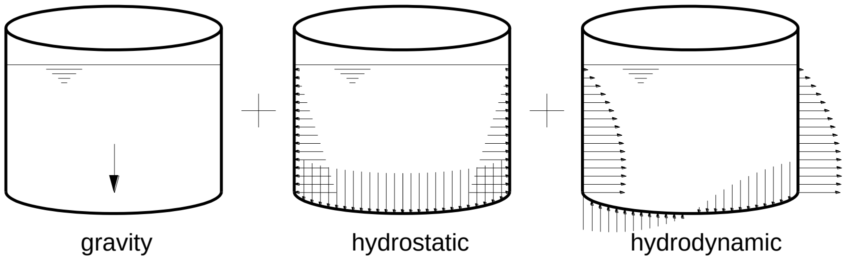

(a) (b) (c)

Figure 3.12. Three loading steps on tank shell and bottom plate: (a) gravity load, (b) hydrostatic pressure, and (c) impulsive hydrodynamic pressure

3.4.3 Calibration of spring-mass model

Similarly to the previous unanchored tank model, the hydrodynamic pressures caused by the liquid motion can be expressed by sum of two components: (i) an impulsive component which represents the effect of the part of the liquid that moves unison with the shell plate, and (ii) a convective component which represents the effect of the part of liquid undergoing a sloshing motion. The sloshing effects are characterised by long period oscillations, whereas the impulsive ones are dominated by oscillations of a shorter period. The contribution of the convective component to the response is small and can be neglected. Furthermore, for broad tanks with the height-to-radius ratio (H/R) less than 1.5, the contribution of higher impulsive modes to the response can also be ignored (Veletsos et al. 1992). Therefore, the tank-liquid system may be considered to respond as a single degree-of-freedom (SDOF) system, as shown in Figure 3.13.

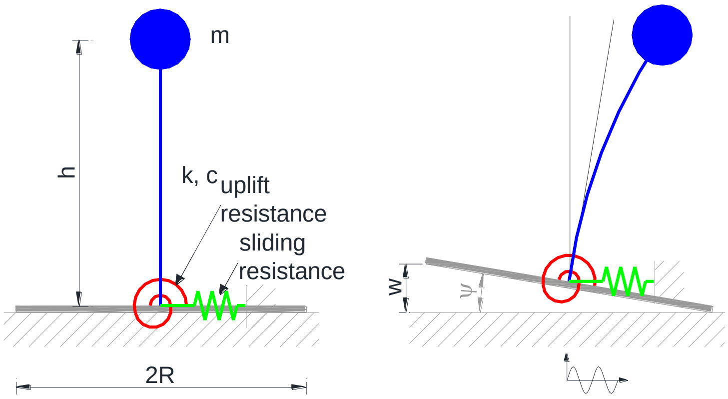

Figure 3.13. Lumped mass model of unanchored tanks

The equivalent mass of the system can be calculated based on the total base shear response, Q, obtained from the pushover analysis, $m = Q/A_g$, where A_g is the ground acceleration applied to the model pushover. The mass are connected with the base by a cantilever column with characteristics: stiffness $k = \omega_i^2 m$, damping coefficient $c = 2\xi_i m\omega_i$, and length $h = M_{OT}/(mA_g)$. It is noticed that the values of m and h are calculated at the state that the uplift and sliding have not yet occurred, and the system still remains linear. In these formulas, ω_i is the natural frequency of the impulsive motion that is calculated using the formula in EN 1998-4 (2006), ξ_i is the impulsive damping ratio assumed to be 2%, and h equals to the height of the lateral seismic force related to the equivalent mass for the slab moment (or overturning moment), M_{OT}. The uplift mechanism of the bottom plate may be modelled by adding a rotational spring that represents the rocking resistance of the bottom plate. The $M_{OT} - \psi$ relationship is obtained from the static pushover analysis of the three-dimensional finite element model.

3.5 Seismic response calculations

The critical responses of above ground tanks under the seismic load are the maximum hoop tensile and meridional stresses in the tank wall, the maximum displacement of the liquid free surface, and the rotation demand of the shell-to-bottom plate joint in the case of unanchored tanks.

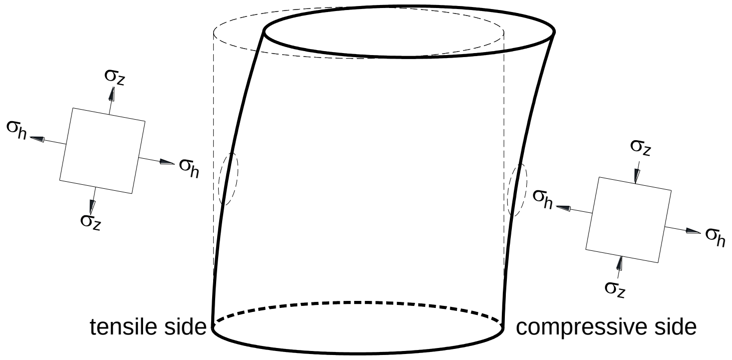

Figure 3.14. Tensile hoop and meridional stresses in the tank wall

The hoop hydrodynamic stresses for the impulsive and convective components of the liquid motion (denoted as σ_{hi} and σ_{hc}, respectively) can be calculated based on explicit equations stated in API 650 (2007), as follows:

For tanks with $D/H \geq 1.333$:

$$\sigma_{hi} = \frac{8.48 A_i G D H}{t_s} \left(\frac{z}{H} - 0.5 \left(\frac{z}{H} \right)^2 \right) \tanh\left(0.866 \frac{D}{H} \right) \tag{3.43}$$

For tanks with $D/H < 1.333$ and $z < 0.75D$:

$$\sigma_{hi} = \frac{5.22 A_i G D^2}{t_s} \left(\frac{z}{0.75D} - 0.5 \left(\frac{z}{0.75D} \right)^2 \right) \tag{3.44}$$

For tanks with $D/H < 1.333$ and $z \geq 0.75D$:

$$\sigma_{hi} = \frac{2.6A_i GD^2}{t_s} \tag{3.45}$$

For all proportions of D/H:

$$\sigma_{hc} = \frac{1.85A_c GD^2 \cosh\left(3.68\left(H - z\right)/D\right)}{t_s \cosh\left(3.68H/D\right)} \tag{3.46}$$

where t_s is the thickness of the shell ring under consideration (mm), z is the distance from the liquid surface to the analysis point (positive down) (m), and G the specific gravity.
The total hoop stress in the tank wall is a sum of the hydrostatic hoop stress (σ_{hs}) and the hydrodynamic hoop stress:

$$\sigma_h = \sigma_{hs} + \sigma_{hi} + \sigma_{hc} \tag{3.47}$$

The meridional stress, σ_z, in mechanically anchored tanks is related to meridional membrane force, N, per unit circumferential length:

$$\sigma_z = \frac{N}{t_s} \tag{3.48}$$

The axial force per unit circumferential length is given by the following equations:
On the compressive side of the tank:

$$N = -\frac{1.273M}{D^2} - w_t \tag{3.49}$$

On the tensile side of the tank:

$$N = \frac{1.273M}{D^2} - w_t \tag{3.50}$$

where M is the ringwall moment and w_t is the load per unit circumferential length caused by the shell and roof weight.
The anchor seismic design load, P_A, is defined:

$$P_A = N\left(\frac{\pi D}{n_A}\right) \tag{3.51}$$

where N is the maximum tensile force per unit circumferential length given in Eq. (3.50) and n_A is the number of anchors around the tank circumference.

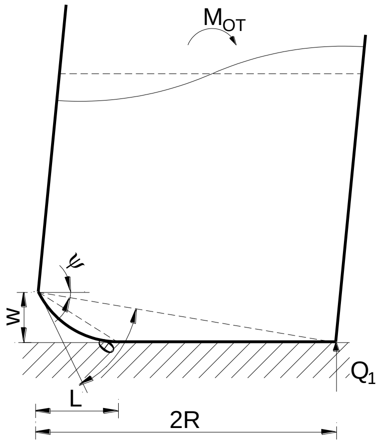

Figure 3.15. Plastic rotation of the bottom plate

In unanchored tanks, the maximum compressive meridional stress in the tank wall is evaluated approximately, following the suggestion of Cambra (1982). If Q_1 is the reaction at the right end when the tank base is rocking about that point (Figure 3.15), then the maximum compressive stress computed by this approach is given by:

$$\sigma_z = \frac{9}{\pi}\frac{Q_1}{Rt_s} \tag{3.52}$$

The rotation demand of the shell-to-bottom plate joint associated with an uplift at the edge w and a base separation of L is given:

$$\theta = \left(\frac{2w}{L} - \frac{w}{2R}\right) \tag{3.53}$$

The sloshing wave height is provided mainly by the first convective mode, the expression for the maximum sloshing wave height is:

$$\eta_{\max} = 0.84RA_c / g \tag{3.54}$$

3.6 Limit state capacity calculations

As mentioned in Section 2.3, the commonly observed failure modes of steel liquid storage tanks during past earthquakes involve buckling in the membrane compression or near the base of the tank wall, material yielding under the extreme hoop tensile stress, failure of the anchor bolts (i.e., in the case of anchored tanks), plastic rotation of the shell-to-bottom plate joint (i.e., in the case of unanchored tanks), and failure of the support system (i.e., in the case of elevated tanks).

Buckling of the tank wall is the most common type of failure in unanchored storage tanks because of the concentration and high magnitude of the compressive force developed in the tank wall when the tank base is uplifted from the ground support. The instability of the tank wall near the base and above the base should be verified for two possible failure modes, i.e., elastic buckling (or diamond-shaped buckling) and elastic-plastic buckling (or elephant’s foot buckling). The critical buckling stresses for elastic and elastic-plastic buckling are calculated using the formulas developed by Rotter (1985a, b); these formulas are later adopted in EN 1998-4 (2006) and NZSEE (2009), given as:

$$\sigma_{eb} = \sigma_{c1}\left(0.19 + 0.81\frac{\sigma_p}{\sigma_{cl}}\right) \tag{3.55}$$

$$\sigma_{efb} = \sigma_{cl}\left[1-\left(\frac{pR}{t_s f_y}\right)^2\right]\left(1-\frac{1}{1.12+\left(\dfrac{R}{400t_s}\right)^{1.5}}\right)\left(\frac{\dfrac{R}{400t_s}+\sigma_y/250}{\dfrac{R}{400t_s}+1}\right) \tag{3.56}$$

where $\sigma_{cl} = 0.6E_t t_s/R$ is the ideal critical buckling stress, σ_p is the increase in buckling stress due to the internal pressure. In Eq. (3.56), p is the maximum interior pressure. The other common failure mode concerns to material yielding of the tank wall due to the extreme hoop tensile stress. As described in API 650 (2007), the maximum allowable hoop tension membrane stress is the lesser of the basic allowable membrane for the shell plate material increased by 33% or $0.9\sigma_y$. The performance of the anchor bolts can be evaluated through the maximum allowable stress. The maximum allowable stress for the anchorage parts shall not exceed 80% of the minimum yield stress. In the case of unanchored tanks, the rotation demand caused by the base uplift should be less than the estimated rotation capacity of 0.2 rad as mentioned in EN 1998-4 (2006).

3.7 Example of seismic response analysis

3.7.1 Description of case study

An example of the above ground tank is presented. The tank is a moderately-broad tank. It is a 27.77-m-diameter tank with a total height of 16.51 m. The tank is filled with the water having a density of 1000 kg/m^3, and the filling level of the tank is equal to 15.7 m, which corresponds to an aspect ratio of the tank, $\gamma = H/R$, equal to 1.131. The shell plate thickness varies from 6.4 mm at its top course to 17.7 mm at its bottom course. An equivalent shell plate thickness of 13.1 mm is calculated using the weighted average method. The bottom plate has a thickness of 8 mm. The material of the tank shell, the bottom plate and the roof is structural steel S235 (equivalent to A36 steel) with yield stress σ_y = 235 MPa. For the purposes of the present study, the tank are simulated as both anchored and unanchored conditions.

3.7.2 Spring-mass model parameters

The dynamic parameters of the spring-mass model described in Section 3.3 for the sample tank are shown in Table 3.2. Both anchored and unanchored conditions of the tank are considered.

Table 3.2. Parameters of the spring-mass model for the sample tank

Parameter	Anchored	Unanchored
Impulsive mass, m_i (T)	5639	5639
Convective mass, m_c (T)	3870	3870
Equivalent mass, m (T)	-	6815
Impulsive natural period, T_i (s)	0.22	0.22
Convective natural period, T_c (s)	5.60	5.60
Impulsive mass height, h_i (m)	6.69	6.69
Impulsive mass height with base pressure, h_i' (m)	10.25	10.25
Convective mass height,h_c (m)	9.99	9.99
Convective mass height with base pressure, h'_c (m)	11.71	11.71
Equivalent height, h (m)	-	9.91

When the tank is unanchored, the uplift mechanism of the base plate is taken into account by a resisting spring. The behaviour of the spring can be represented by the $M_{OT} - \psi$ relationship. This relationship can be obtained from the static pushover analysis. This work presents two types of the static pushover analysis, based on the beam model of Malhotra and Veletsos

(1994a) and the proposed nonlinear pushover analysis using the ABAQUS software. The von Mises stress and deformation contours of the tank with the base uplift at a A_g = 0.62 g obtained from the nonlinear static pushover analysis is shown in Figure 3.16.

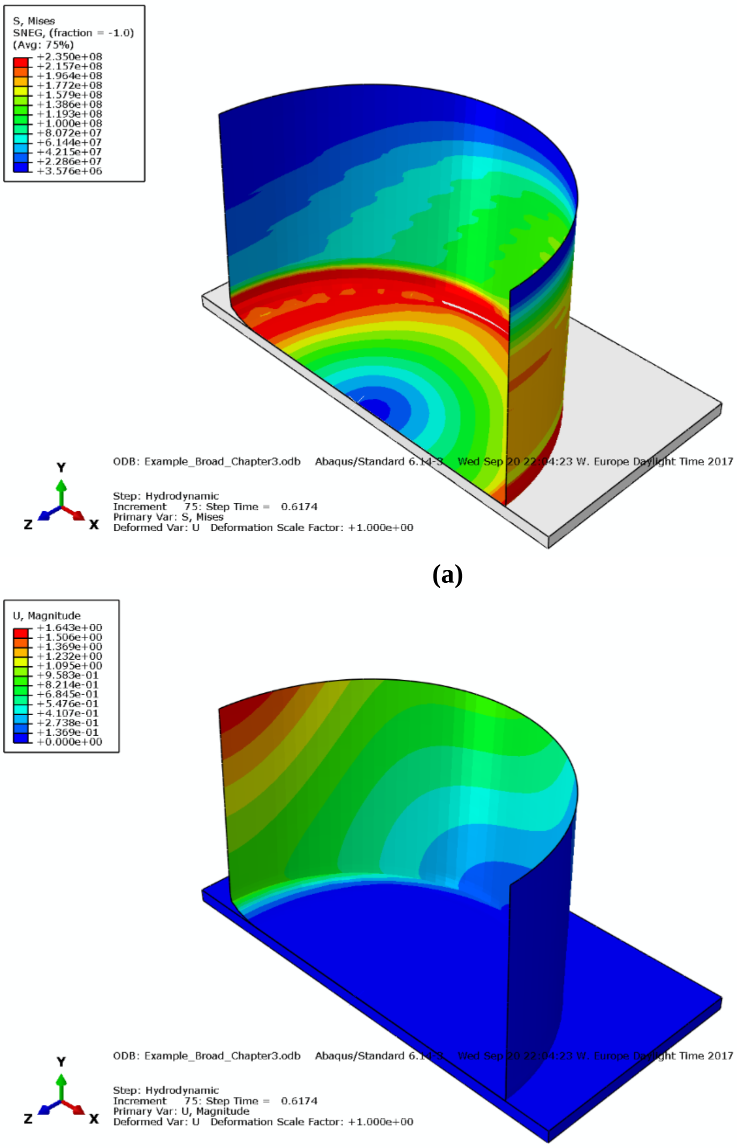

(a)

(b)

Figure 3.16. Contours of the von Mises stress (a) and the vertical displacement (b) of the tank obtained at an acceleration of 0.62 g

A comparison of the $M_{OT} - \psi$ relationship among the two methods is shown in Figure 3.17. A quite good agreement between the two curves is observed, despite the discrepancy found in the post yield zone. The curve obtained by the beam model seems to underestimate the response of the unanchored tank; however, for the very large deformation, i.e., $\psi > 0.02$ rad, the beam model curve is overestimate.

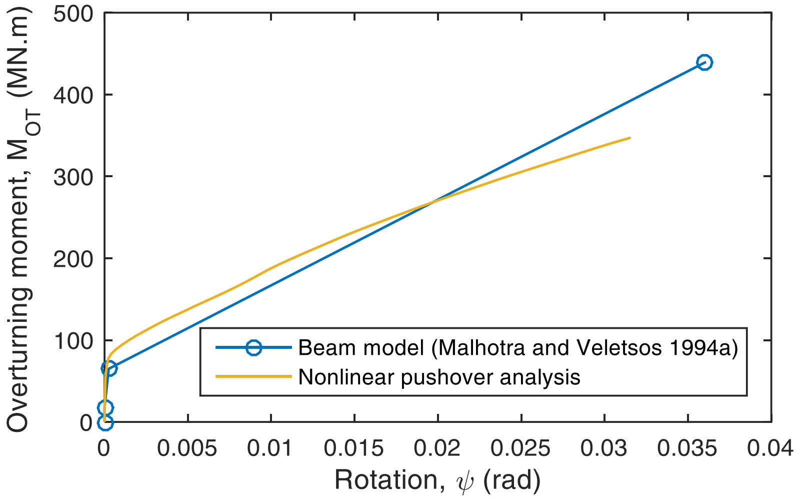

Figure 3.17. Moment-rotation curve of the sample tank

3.7.3 Seismic response analysis

The spring-mass models of the anchored and unanchored conditions of the tank are analysed dynamically using a time history accelerogram. In this example, a horizontal component of the ground motion recorded from the Duzce 1999 earthquake in Turkey is considered; the acceleration traces for which is shown in Figure 3.18, together with the elastic response spectrum with 5% damping shown in Figure 3.19.

The response histories of the convective and impulsive components for both anchored and unanchored conditions of the tank are shown in Figure 3.20. It is observed that the convective responses for both cases are almost the same, as shown in Figure 3.20(a). The uplift may not affect the sloshing mode of the tank. Compared to the impulsive response history of the anchored tank [Figure 3.20(b)], the history of the unanchored tank has longer periods of oscillation and smaller amplitudes, and it exhibits nearly uniform amplitudes for a major part of the response. This finding demonstrates the significant effect of the uplift on the impulsive pressure acting on the tank.

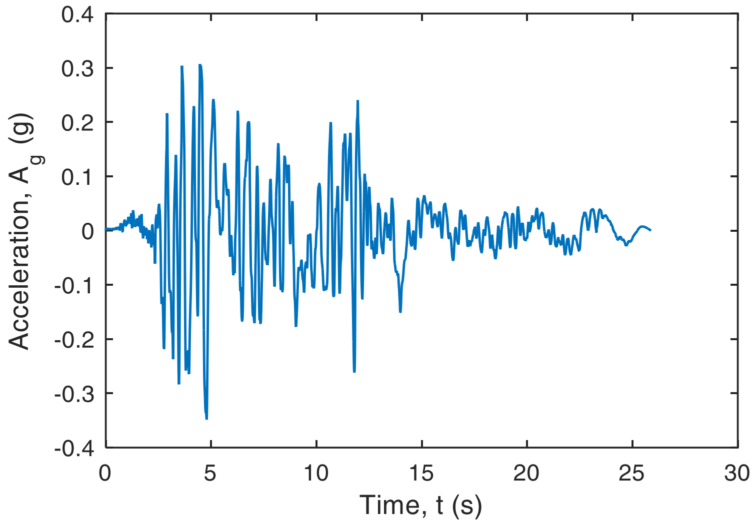

Figure 3.18. Time history data of the accelerogram

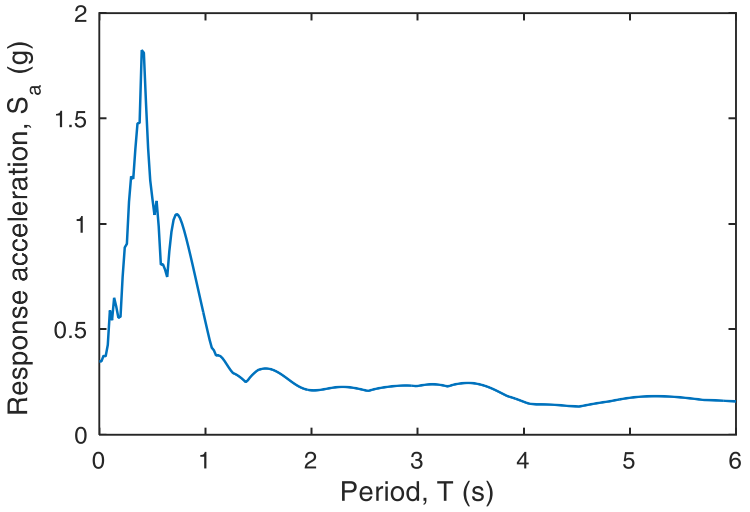

Figure 3.19. 5% damping elastic response spectrum

The history responses of the uplift displacement at the two ends of the base in the unanchored condition are shown in Figure 3.21. The maximum base uplift of 0.3 m calls for appropriate flexibilities in the design of any piping that may be attached to the tank wall.

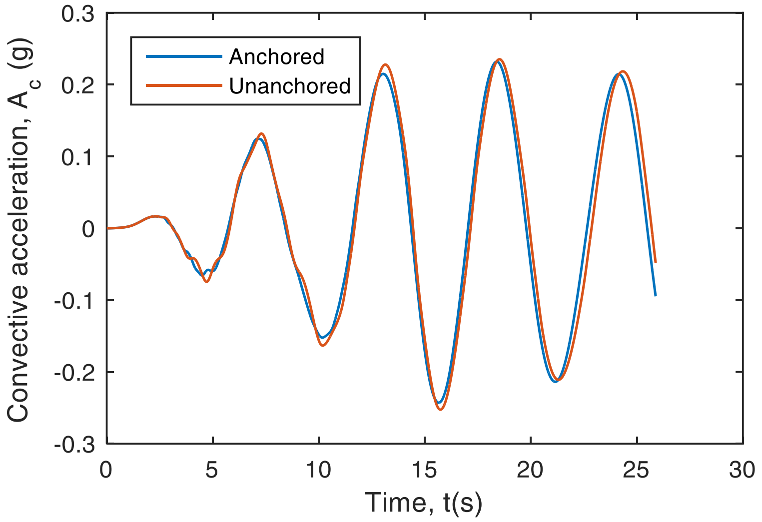

(a)

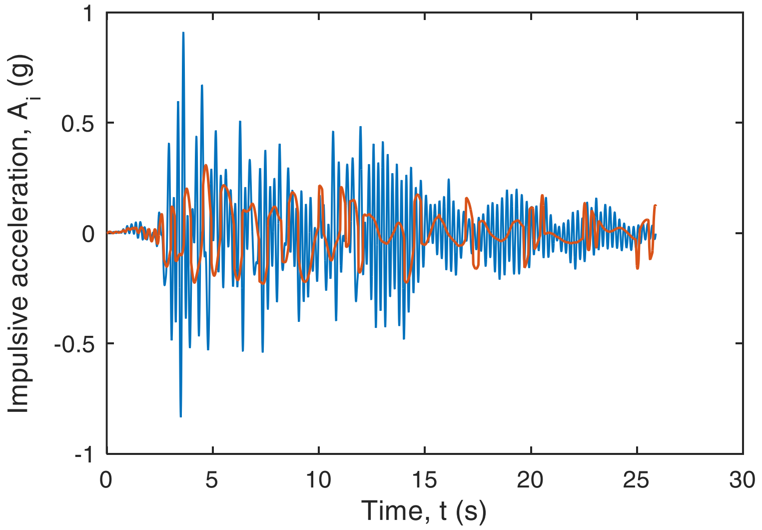

(b)

Figure 3.20. Time history of the acceleration for both anchored and unanchored conditions: (a) convective response and (b) impulsive response

The critical responses of the tank for both conditions, including the maximum sloshing of the liquid free surface, the hoop tensile stress in each shell course, the compressive meridional stress in the bottom shell course, and the plastic rotation of the shell-to-bottom plate joint, are calculated using the above formulas. Their peak responses are summarised in Table

3.3, together with their corresponding limit state capacities. It is shown that the base uplift may significantly reduce the hydrodynamic pressures, resulting a lower tensile hoop stress in the tank wall in the case of the unanchored condition. The reduction of the pressures may be associated with increased axial stresses in the tank wall and large plastic rotations at the joint of the shell and bottom plate.

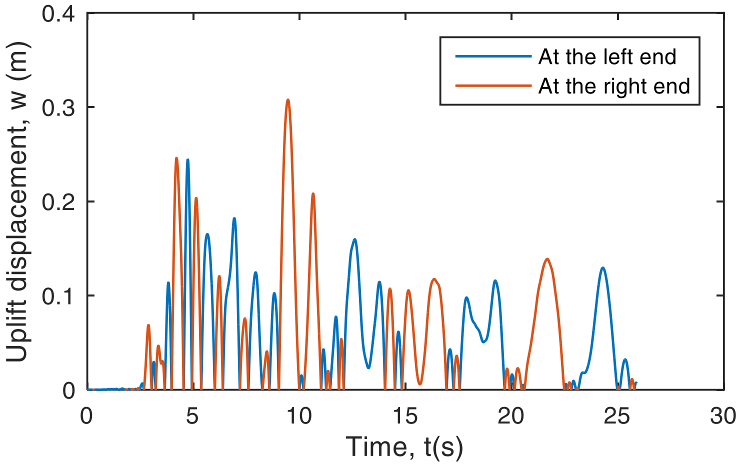

Figure 3.21. Time history of the uplift displacement

Table 3.3. Peak value of the tank responses

Response	Anchored	Unanchored	Limit state capacity
η_{max} (m)	2.83	2.95	0.8
σ_h (MPa) (course 1 - course 8)	212.4, 222.3, 232.5, 243.2, 254.5, 263.9, 252.4	155.1, 158.7, 162.7, 167.3, 173.1, 178.8, 172.7	209.3
σ_z (MPa) (course 1)	55.6	68.0	82.7
θ (rad)	-	0.535	0.2

3.8 Closure

Possible numerical models have been presented for the evaluation of the response to horizontal ground shaking of above ground and elevated steel liquid storage tanks. The tank-liquid system is simplified as a spring-mass model considering the most important parameters of the system. In the case of elevated tanks, the modelling of steel tank is similar to the above ground ones. The support structure is simulated by either a spring-mass model or nonlinear elements considering both flexural and shear behaviours. A more accuracy procedure that is based on a nonlinear static pushover analysis and a calibrated spring-mass model is proposed in this chapter. The validation of the proposed modes for unanchored above ground and elevated tanks will be carried out in next chapters. As shown from the seismic response analysis of a sample tank, the base uplift increases the effective period of vibration of the unanchored system as compared to its fully anchored condition. This effect also reduces the impulsive hydrodynamic pressure and the associated overturning base moment. This reduction is associated with a significant amount of base uplift and plastic yielding at the joint of the shell and bottom plate.

Chapter 4. Shaking table test campaign and nonlinear finite element modelling for validation of spring-mass model

4.1 Introduction

There has been an increasing trend toward the finite element modelling of unanchored steel liquid storage tanks subjected to seismic loading, as mentioned in sections 3.1 and 3.4. The analysis procedure has been based on three possible different models: (i) the simplified spring-mass model in which the impulsive and convective components are modelled as SDOF systems, (ii) the added mass model in which the impulsive and convective forces are converted in equivalent masses along the height of the shell, and (iii) the full nonlinear finite element model in which the real interaction between fluid and structure is considered. Because of many sources of nonlinear behaviour mechanisms of unanchored tanks, the finite element model that includes the fluid-structure interaction has been widely used. However, the analysis procedure is costly in terms of computational time.

With the aim to validate the spring-mass model previously presented, an experimental study is carried out on an unanchored broad tank, and a full nonlinear finite element model of the tank is also developed using the ABAQUS software. A reduced-scale unanchored steel liquid storage tank with the broad configuration is selected for this study. The specimen is built at the CEA EMSI laboratory in Saclay (France) within the framework of the European research project INDUSE-2-SAFETY. A number of tests are carried out with two input signals to obtain significant responses of the tank, e.g., hydrodynamic pressure, sloshing wave height, and uplift displacement. The numerical modelling of the tank is developed using the ABAQUS software with an explicit time integration approach. In particular, the steel tank is modelled based on the Lagrangian formulation, while an acoustic finite element mesh is used in the liquid domain. A comparative study of the seismic response of the tank is presented. The results in terms of the hydrodynamic pressure response, the maximum sloshing of the liquid free surface, and the uplift response of the base plate obtained from the finite element and spring-mass models are evaluated and compared with the experimental data.

4.2 Shaking table test on a broad steel liquid storage tank

4.2.1 Specimen design and instrumentation principle

The test on the broad tank, named as Broad #1 test, was conducted at the Laboratory of Seismic Mechanic Studies at the Saclay Nuclear Research Centre.

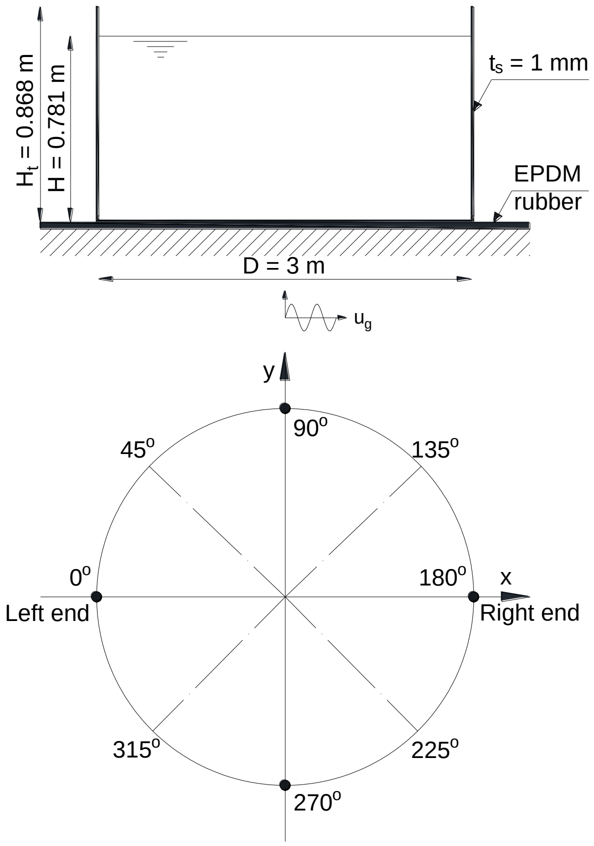

Figure 4.1. Schematic of the specimen

The specimen, having a diameter of 3 m and a total height of 0.868 m, is scaled from an existing broad tank at a refinery in Italy with scale ratio $\lambda = 1/18$. The schematic of the reduced-scale tank, which includes both vertical and horizontal planes, is shown in Figure 4.1. The tank shell is formed by a cylindrical SS304 stainless steel sheet that has 1-mm-thickness. The shell plate is welded to a round-base plate of the same material and thickness. The top of the shell is reinforced with a ring of 20-mm-height × 20-mmwidth × 1-mm-thickness. The stainless steel has Young's modulus of 193 GPa, a Poisson's ratio of 0.3, and a density of 8030 kg/m^3. The yield strength of steel in tension is 290 MPa. The specimen is positioned in the centre of the table plate on an intermediate EPDM sheet. This rubber membrane helps increase friction coefficient between the tank base and the table to decrease the sliding effect and protect the mechanical bearings and electrical circuits in case of water overtopping. The estimated mass of the empty tank is 123 kg. The tank is filled with water at 90% of its height (i.e., 0.781 m), resulting in a total mass of 5.6 tons. Considering the geometry and mass of the specimen, the VESUVE shaking table is used. The main characteristic of the table is shown in Table 4.1. The test model of the tank on the VESUVE shaking table is shown in Figure 4.2.

Table 4.1. Shaking table characteristic

DOF	Control	Dimension (m)	Payload (ton)	Displacement (mm)	Frequency (Hz)
1	Displacement	3.1 × 3.8	20	± 100	0-40

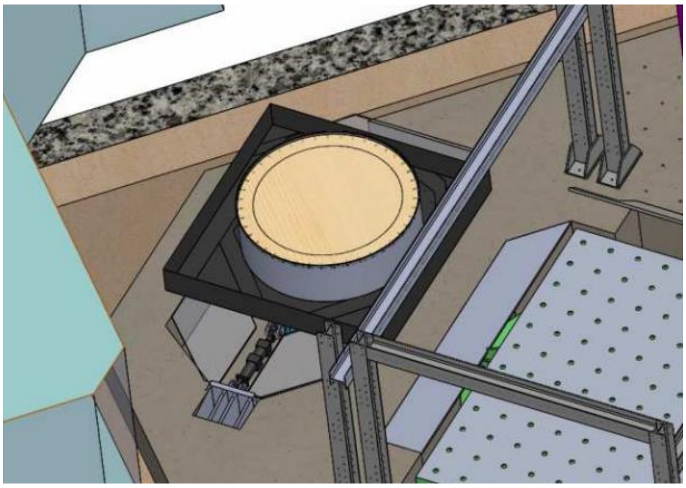

Figure 4.2. Broad tank test model on the shaking table

The instrumentation placed on the tank and the table is to measure the mechanical inputs and outputs of the experimental system. The detail of the instrumentation principle on the inner and outer wall of the tank is described Figure 4.3. The whole test system and some special measure equipment, e.g., strain gauges, wave gauges, and external sensors, are shown in figures 4.4 and 4.5.

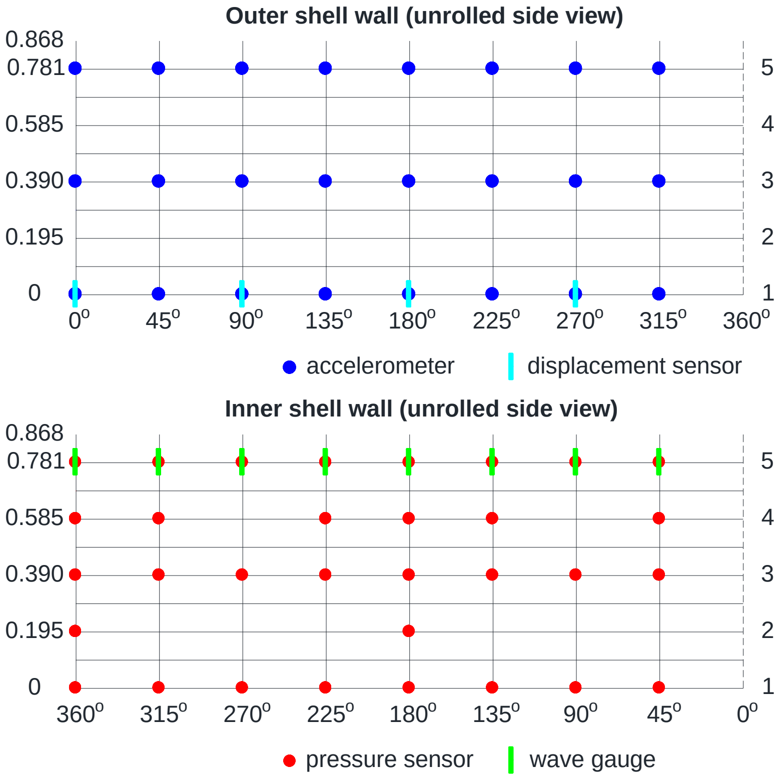

Figure 4.3. The instrumentation principle on the inner and outer wall of the tank (unrolled side view)

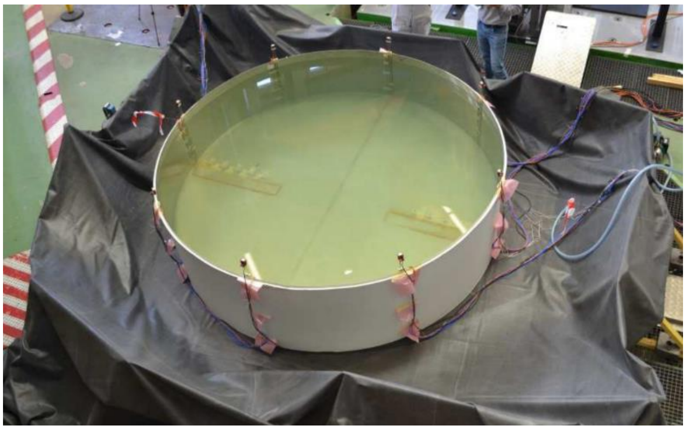

Figure 4.4. Broad test instrumentation

Strain gauges **Wave gauges** **External sensors**

Figure 4.5. Detail of instrumentation

4.2.2 Selection and scaling of input signals

The horizontal components of the Chi-Chi Taiwan 21/09/1999 and Northridge USA 17/01/1994 earthquakes have been used. These two components of the earthquakes are chosen from sets of accelerograms that were selected according to target uniform hazard spectra of an examined site, i.e., Priolo Gargallo in Italy. The horizontal component of the Chi-Chi and Northridge earthquakes resulted in the highest response of the free surface sloshing and the base uplift, respectively, among accelerograms in the sets. Different time scales based on the Froude similarity are defined for each test, depending on the specific response of the tank. Similarity requirements and scaling relationships for the test are detailed in Appendix B. As a conclusion,

- for the sloshing response of the liquid free surface, the time scale $t/t_0 = \sqrt{\lambda}$ is used for the Chi-Chi earthquake at a low frequency,
- for the uplift response of the tank base, the time scale $t/t_0 = \lambda$ is used for the Northridge earthquake at a high frequency.

A number of tests have been conducted with different levels of the peak ground displacement. In this study, only two tests are presented herein. The first test with the Chi-Chi signal to obtain the sloshing response of the liquid free surface, and the second test with Northridge signal to obtain the uplift response of the base plate. The input signals for the two tests are shown in Figure 4.6.

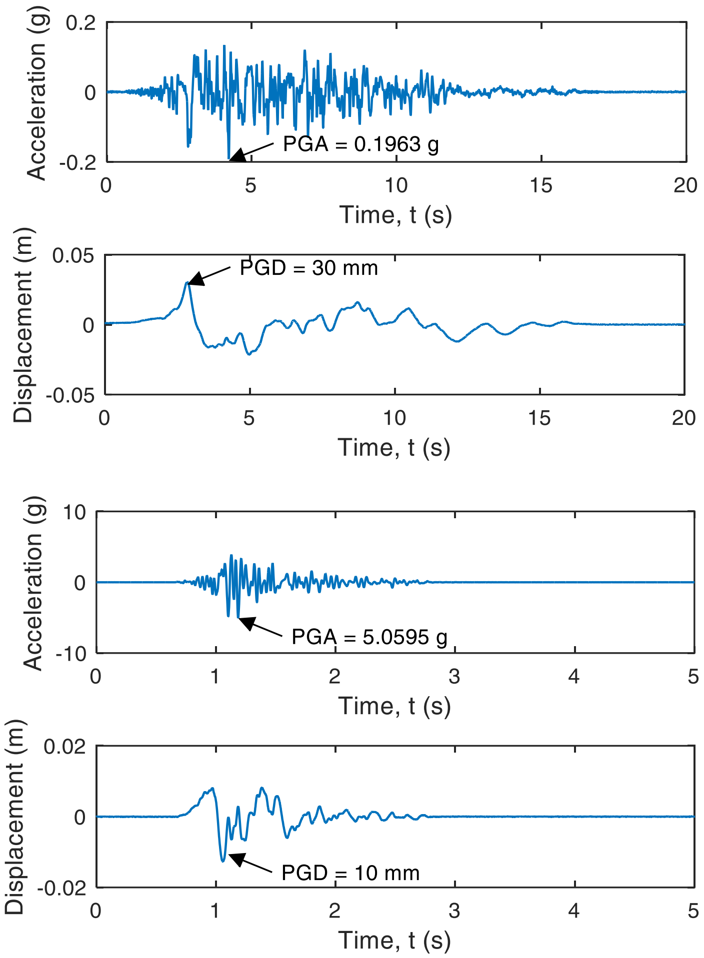

Figure 4.6. Input signals for the tests: (a) Chi-Chi signal and (b) Northridge signal

4.3 Development of nonlinear finite element modelling

The behaviour of the liquid is commonly represented by the Lagrangian approach, where the liquid is assumed to be linearly elastic, inviscid, and irrotational (Bayraktar et al. 2010, Phan et al. 2017b). This approach can be used to model the liquid motion in a rigid or flexible container; however, mesh-based Lagrangian methods have limitations with large deformations. If the liquid undergoes large deformations, the mesh has to be restructured to accommodate the new configuration. In this case, an ALE adaptive mesh may be used in the liquid domain to permit large deformations, especially at the liquid free surface (Phan et al. 2017b). A coupling approach, so-called Eulerian-Lagrangian coupling (CEL), is useful for tank sloshing simulations. The CEL allows for the interaction between the Lagrangian tank domain where the material is fixed to the mesh and the Eulerian fluid domain where the material can flow through the mesh. The use of Eulerian elements eliminates the problem of extreme element deformation associated with Lagrangian fluid meshes (Tippmann et al. 2009). However, this approach faces the challenge in modelling the contact between the fluid domain and the steel tank. When a thin shell plate is considered, the leakage of the material may occur at the interface during the analysis. Moreover, this approach is quite time-consuming because a more refined mesh needs to be used in the interface to avoid any penetration of the fluid. Therefore, a simplification of the finite element model is commonly used through considering the liquid as inviscid, irrotational, and with no mean flow; this leads to using the acoustic wave equations which consider the propagation of the vibrating waves inside the fluid. Thus, this is the simplest formulation to take into account the fluid-structure interaction and thus less computational resources are required. The approach is called as “structural-acoustic coupling” and adopted in the ABAQUS software (SIMULIA 2014).

In this study, the coupled structural-acoustic analysis has been performed based on a coupling model of the tank-liquid system. In particular, the finite element meshes of steel tank consist of four-node, doubly curved quadrilateral shell elements (S4R). Each node of shell element has three translational and three rotational degrees of freedom. The liquid is modelled using eight-node brick acoustic elements (AC3D8). The acoustic finite element model is based on the linear wave theory and considers the dilatational motion of the liquid. To derive the equations for acoustic wave propagation, a number of assumptions have to be made to simplify the equations of fluid dynamics. The acoustic element has only one pressure unknown as the degree of freedom at each node. Hence, no actual flow occurs in an acoustic simulation. The tank-liquid interaction is considered using a surface-based tie constraint between the tank inner and liquid surface. This constraint is formulated based on a master-slave contact method, in which normal force is transmitted using tied normal contact between both surfaces through the simulation. When the system is subjected to large deformations, the ALE framework can be used to prescribe the movement of the acoustic mesh, including interior nodes, to follow and adapt to the movement of the structure. The sloshing waves are considered in the liquid model. Assuming the small-amplitude gravity waves on the free surface of the liquid, the pressure boundary condition specified at the free liquid surface can be presented in the form of Eq. (3.5), given as:

$$\frac{\partial^2 p}{\partial t^2} + g\frac{\partial p}{\partial z} = 0 \tag{4.1}$$

where p is the hydrodynamic pressure at the free liquid surface.
The tank model is unanchored and rested on a rigid slab that is modelled using solid elements. The successive contact and separation between the tank base plate and its rigid foundation are taken into account by a surface-based contact modelling algorithm. The boundary conditions of the model are shown in Figure 4.7.

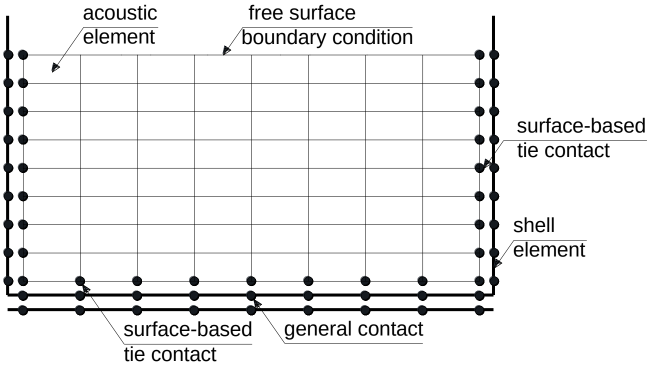

Figure 4.7. Boundary conditions of the liquid-tank model

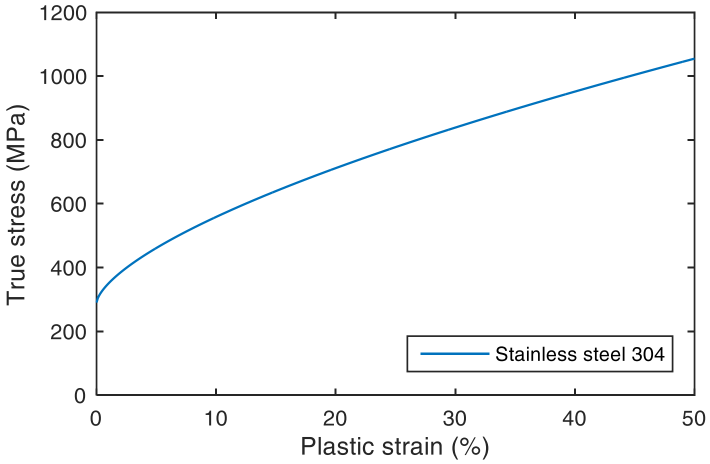

Figure 4.8. True stress-strain curve of the stainless steel 304

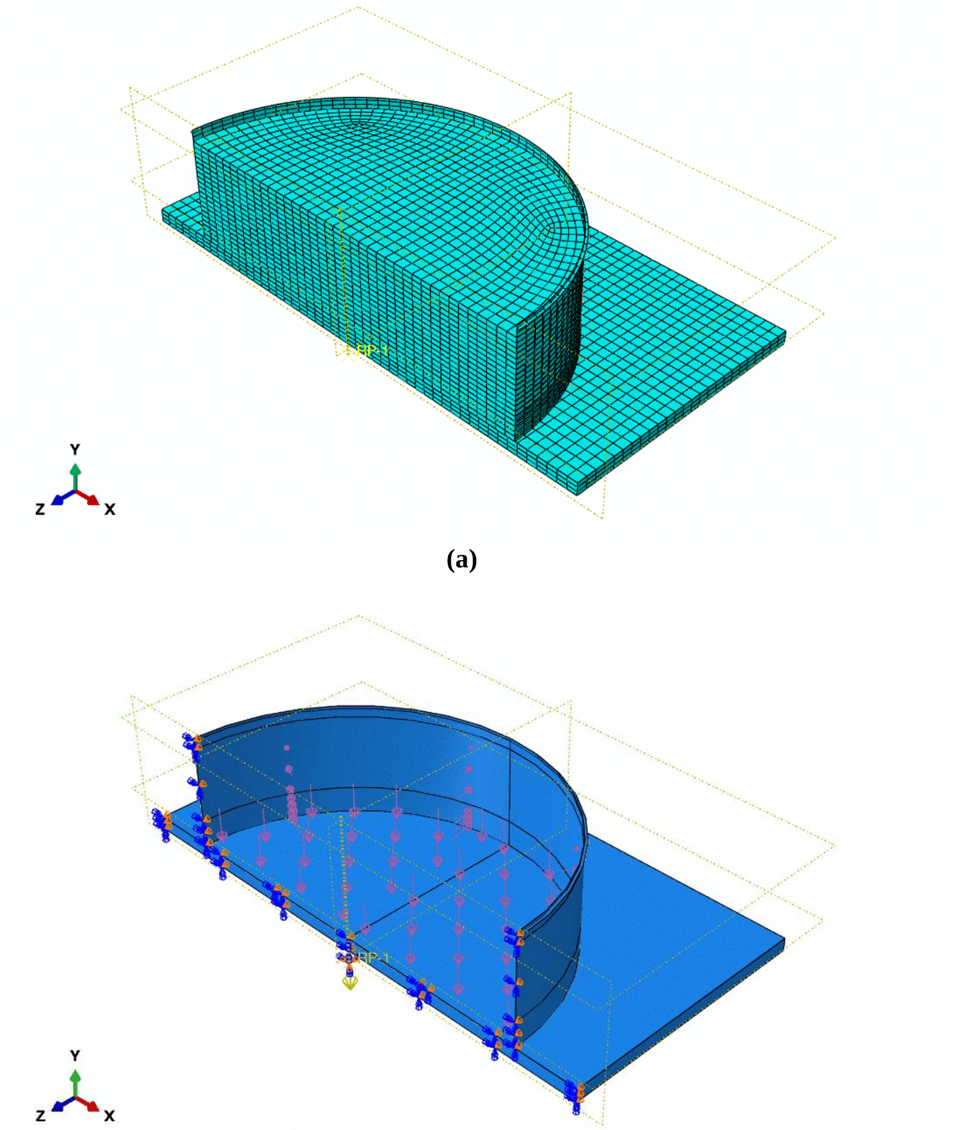

(a)

(b)

Figure 4.9. Numerical model of the tank-liquid system: (a) finite element meshes and (b) gravity and static loadings

Both geometric and material nonlinearities are considered in the analysis. The plasticity of the steel tank is modelled based on the stress-strain curve of the material. The curve obtained from mechanical testing is converted into the true stress and the plastic strain, as shown in Figure 4.8. The water density is considered to be 998.21 kg/m^3, and its bulk modulus is 2150 MPa. The Rayleigh mass proportional damping is employed for the tank model assuming a damping ratio of 2.0%, for the fundamental vibration mode of the tank-liquid system.

Due to the structural symmetry and to reduce the computational cost, only half of the tank-liquid system is modelled, and symmetry plane boundary conditions are employed. The mesh convergence analysis results in an optimal mesh size of 0.04 m and 0.08 m in the longitudinal direction and the circumferential direction, respectively, to achieve acceptable accuracy. The finite element mesh of the tank model is illustrated in Figure 4.9(a).

The acoustic wave equations do not include any terms for body forces, which means that forces such as gravity are not included. Hence, at the first step, the tank is subjected to the gravity load and the hydrostatic pressure acting on the shell and bottom plate, as shown in Figure 4.9(b). The hydrodynamic pressures acting on the shell and bottom plate are measured during the dynamic analysis through the tie contact between the shell and acoustic elements.

The modal analyses of the tank model is first performed. The natural frequency calculation is based on the Lanczos eigensolver method. The acoustic-structural coupling is projected onto the subspace of eigenvectors using SIM-based linear dynamic procedures. The natural periods of the tank computed by the modal analysis are in close agreement with those obtained from EN 1998-4 (2006), as shown in Table 4.2.

Table 4.2. Modal analysis results

Vibration mode	Refined model	EN 1998-4
First impulsive, T_i (s)	0.013	0.016
First convective, T_{c1} (s)	2.100	2.100
Second convective, T_{c2} (s)	1.068	1.068
Third convective, T_{c3} (s)	0.895	0.841

4.4 Development of spring-mass model

The spring-mass model of unanchored tanks, suggested in Section 3.4, will be validated in this study. The seismic responses including the hydrodynamic pressure, sloshing wave height, and the uplift are calculated and compared to the experimental data and those obtained from nonlinear finite element analysis. The nonlinear static pushover analysis of the tank is first conducted resulting in the behaviour of the uplift resistant spring, the equivalent mass of the liquid, and the height of mass. Figure 4.10 shows the uplift response of the tank base at a PGA level of 1.136 g as a result of the pushover analysis. The relationship between the overturning moment and the rotation is presented in Figure 4.11.

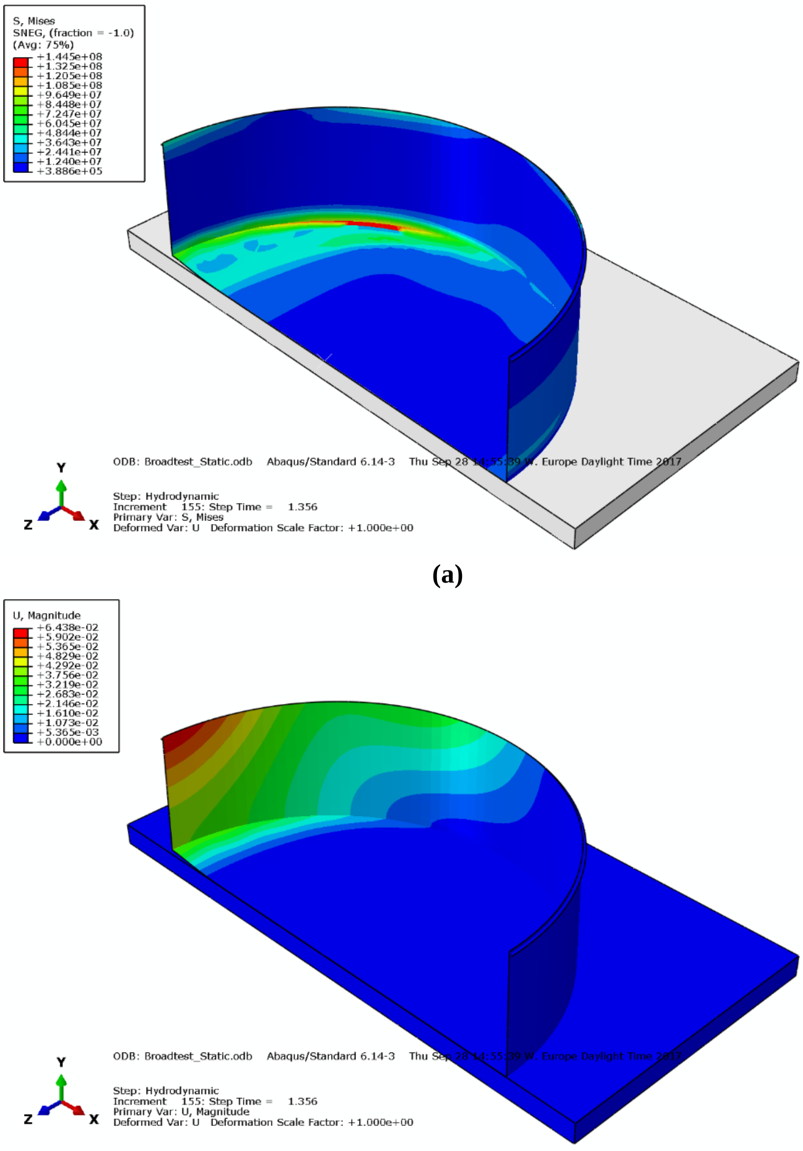

(a)

(b)

Figure 4.10. Contours of the von Mises stress (a) and the vertical displacement (b) of the tank subjected to the Northridge signal at t = 1.36 s

The parameters of the spring-mass model are calculated from the pushover analysis results and shown in Table 4.3. The model assumes that the vibration period of the equivalent mass of the system equals to that of the impulsive component obtained using the formula in EN 1998-4 (2006).

Table 4.3. Dynamic parameters of the spring-mass model

m (T)	h (m)	T_i (s)	T_c (s)	k (kN/m)	c (kN-s/m)
1.705	1.099	0.016	2.104	2.479e+05	26.004

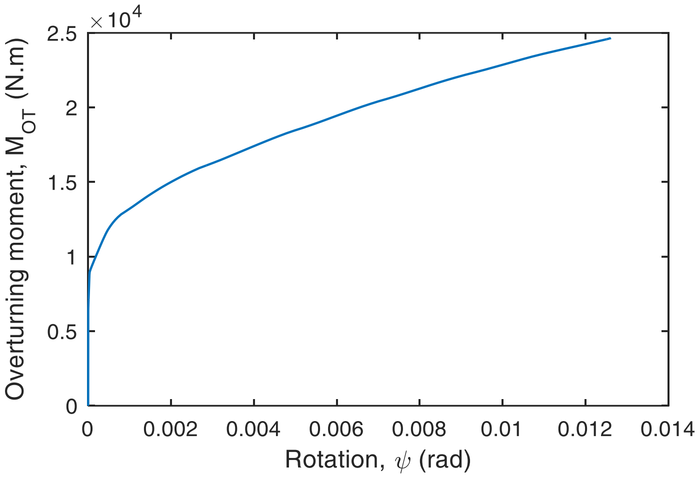

Figure 4.11. Overturning moment-rotation curve of the tank

4.5 Comparative study

4.5.1 Hydrodynamic pressure

The time histories of hydrodynamic pressure observed at two measurement locations (0° and 180° positions at the tank base) for the tank subjected to the Chi-Chi signal are given in Figure 4.12. The pressure measurements of the tank obtained from the spring-mass model, three-dimensional finite element model and experimental test are in good agreement, and all numerical findings match perfectly with the corresponding experimental results. The peak pressure responses are shown in Table 4.4. There are very small differences (i.e., < 10 %) observed for the results of three approaches.

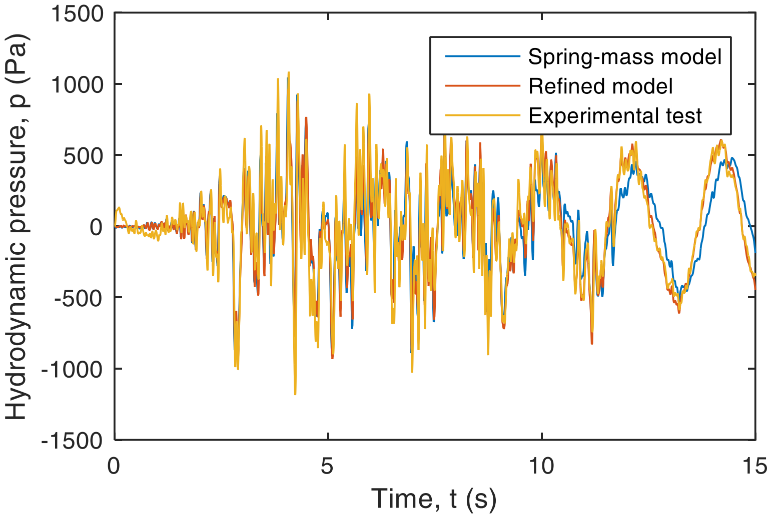

(a)

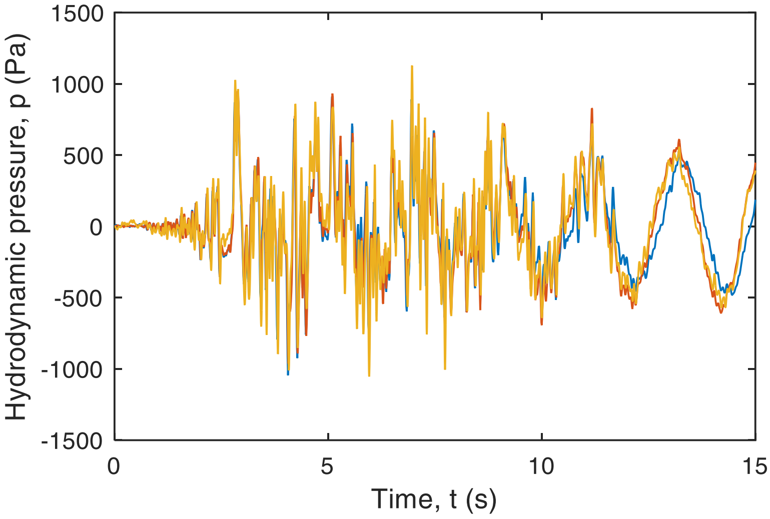

(b)

Figure 4.12. A comparison of time history hydrodynamic pressure acting on the tank base: (a) 0° position and (b) 180° position

Table 4.4. Peak pressure response (positive value)

	Spring-mass model	Refined model	Experimental test
p at 0° (Pa)	1044.5	1063.5	1085.1
p at 180° (Pa)	1024.6	1051.0	1128.5

4.5.2 Sloshing response

The time history responses of the sloshing wave height at two measurement locations, 0° and 180° positions, of the wave gauge in Figure 4.3, are presented in Figure 4.13. The results are obtained from the analysis using the Chi-Chi signal. It can be seen from the figures that the numerical results are highly consistent with those obtained from the experimental test in terms of both frequency and amplitude. The maximum sloshing wave heights measured from the present models and the experimental data are shown in Table 4.5, and the experimental data observed is slightly higher than the numerical ones. It is also noticed from the experimental data that the sloshing wave height measured at the 180° position is higher than the freeboard height of the tank, i.e., 0.087 m. An overtopping of the contained liquid was observed during the test.

4.5.3 Uplift response

Figure 4.14 presents the time history responses of the base uplift of the tank model measured at the left and right ends (0° and 180° positions) of the bottom plate, and their peak values are shown in Table 4.6. The responses are obtained with the Northridge input signal. The uplift displacements of experimental study include negative values because the tank is settled on an EPDM rubber, and the only positive values of the uplift displacements are plotted in the figures. The numerical and experimental models lead to a relatively accurate description of the base uplift displacement at the right end for the input earthquake motion; however, there are some parts of the history response at the left end showing slight differences among three obtained results. In general, it can be concluded from the comparative study that the mass-spring model is capable of capturing the peak responses compared with the detailed finite element analysis and the test, along with the relative trends during the entire dynamic loading.

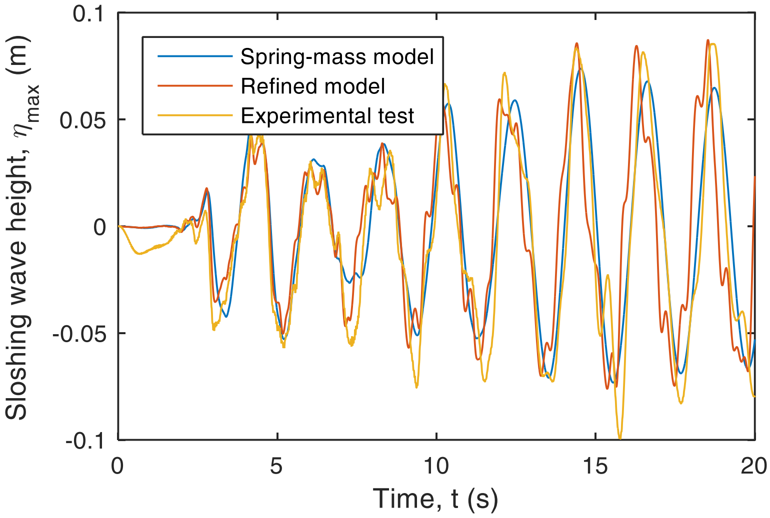

(a)

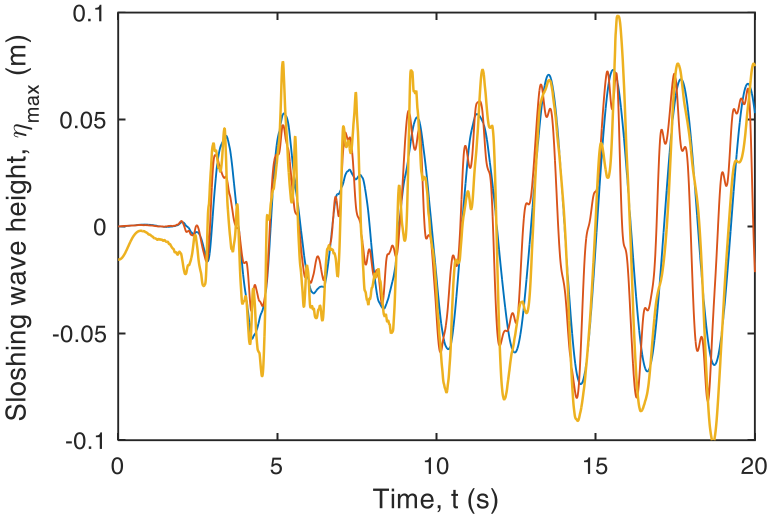

(b)

Figure 4.13. A comparison of time history sloshing wave height response: (a) 0° position and (b) 180° position

Table 4.5. Peak sloshing response

	Spring-mass model	Refined model	Experimental test
η_{max} at 0° (m)	0.074	0.081	0.086
η_{max} at 180° (m)	0.073	0.073	0.089

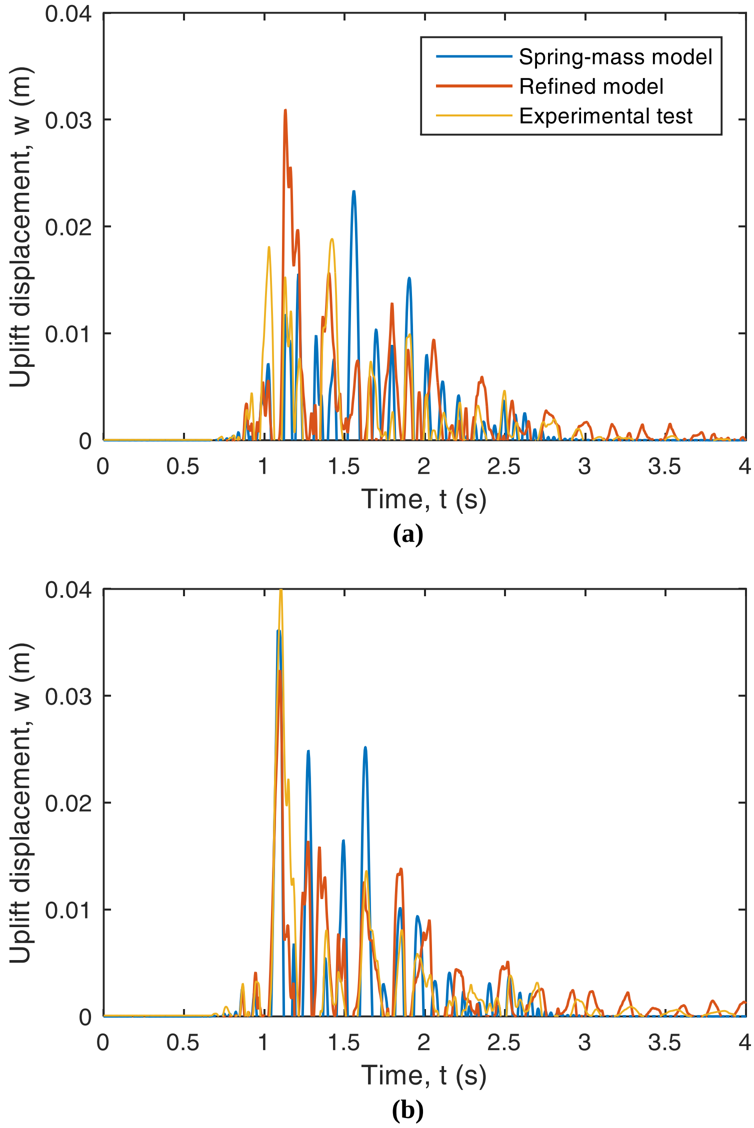

Figure 4.14. A comparison of time history uplift response: (a) 0° position and (b) 180° position

Table 4.6. Peak uplift response

	Spring-mass model	Refined model	Experimental test
w at 0° (m)	0.023	0.031	0.019
w at 180° (m)	0.036	0.032	0.041

4.6 Closure

In this chapter, the validation of the spring-mass model of unanchored tanks using a refined three-dimensional finite element model and a shaking table test is presented. The test is conducted at the CEA EMSI laboratory within the framework of the INDUSE-2-SAFETY project. The specimen is a reduced-scale of a large broad tank located in a refinery in Italy. A nonlinear finite element model of the tank is developed using the ABAQUS software. The analysis results from both spring-mass and refined models in terms of the hydrodynamic pressure, the sloshing wave height and the base uplift are obtained and compared well with those observed from the experimental test. It can be concluded from the compatible results between the numerical and experimental studies that the proposed spring-mass models is a reliable tool for the seismic analysis of steel liquid storage tanks. An application of this proposed model will be presented in Chapter 7, where the vulnerability of an existing unanchored tank is assessed.

Chapter 5. Seismic fragility analysis methods for liquid storage tanks

5.1 Introduction

Seismic fragility curve is one of the key aspects of seismic risk assessment of industrial plants; it is defined as the probability of exceeding a certain limit state conditioned to the selected seismic intensity measure. This conditional probability can be expressed as:

$$\text{Fragility} = P\left[LS \mid IM\right] \tag{5.1}$$

where LS is the limit state or level of damage to the engineered system or component, IM is the ground motion intensity measure, often expressed in terms of peak ground acceleration or spectral acceleration at the fundamental period. Figure 5.1 shows an example of the continuous form of fragility curve and interpretation at a particular ground motion intensity.

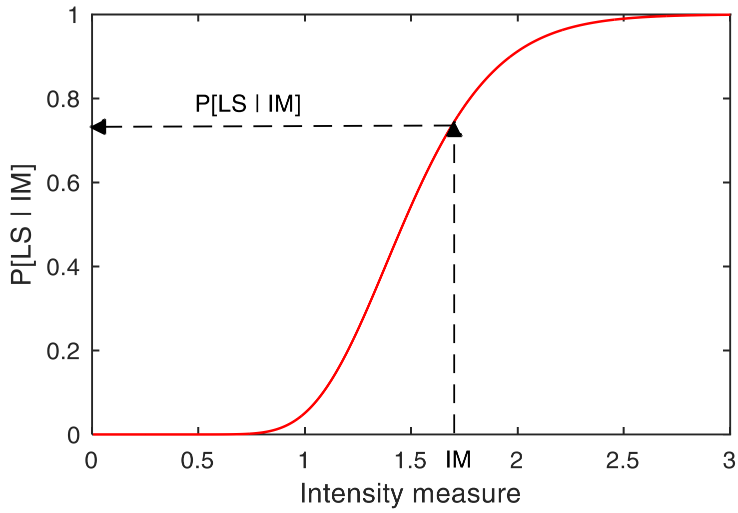

Figure 5.1. Fragility curve example

A number of approaches for the fragility curve evaluation of the structural damage have been investigated since the 1980s and early 1990s. They are classified in empirical, expert judgment-based, and analytical approaches. Empirical methods are based on post-earthquake surveys and observations of actual damage. They are specific to particular sites, geological, and geotechnical conditions as well as the properties of the damaged structures. Consequently, the use of these functions in different regions is always questionable. Expert judgment fragility curves are based on expert opinion and experience. Therefore, they are versatile and relatively fast to establish, but their reliability is questionable because of their dependence on the experiences of the experts. Analytical fragility curves represent damage distributions simulated from the analyses of structural models, and thus they are becoming ever more attractive in terms of the ease and efficiency by which data can be generated.

There are a few of contributions focusing on the seismic fragility analysis of tanks. An observational method for the development of seismic fragility relationships can be found in Salzano et al. (2003), where damage states were defined by the HAZUS damage classification (HAZUS 2001). Following with empirical fragility curves presented by HAZUS (2001), O'Rourke and So (2000), and ALA (2001), Berahman and Behnamfar (2007) proposed a Bayesian approach for estimation of the seismic fragility of unanchored on-grade steel liquid storage tanks, which was based on field observations reported by American Lifeline Alliance (ALA 2001). The analytical approaches, which use time history analyses of the structural response along with probabilistic seismic demand model, have also been presented for tanks. A rational procedure for the seismic vulnerability assessment of standard industrial constructions was defined by Iervolino et al. (2004), where the fragility curves were derived by a response surface-based method. Fragility curves for the elephant's foot buckling failure mode were studied and discussed in detail using the cloud analysis (CA) and/or the incremental dynamic analysis (IDA) (e.g., Buratti and Tavano 2014, Bakalis et al. 2016, Cortes and Prinz 2017, Phan et al. 2016a, 2016b, 2016c, and 2017a).

The following subsections detail the current state-of-the-art for the development of fragility curves for tanks. The attention is paid to analytical approaches that currently are widely used.

5.2 Fragility analysis methods

5.2.1 Empirical fragility curves

The study of past earthquakes and the field surveys of actual damage on exposed elements allow compiling extensive statistics on the damage states of various tank typologies under earthquake loading. Unfortunately, there are a few reports based on this approach for tanks. For example, the HAZUS manual (HAZUS 2001) suggested fragility curves for seven classes of liquid storage tanks (buried concrete, elevated steel, etc.). For on-grade steel tanks, HAZUS has one set of curves for anchored tanks and another one for unanchored tanks. The median and standard deviation for HAZUS fragility curves are presented in Table 5.1. Note that the HAZUS medians suggest that anchored tanks perform better (i.e., have higher median values) than unanchored tanks. As indicated previously, of the roughly 40% of tanks in the database for which the base connection was known, the vast majority were unanchored.

Table 5.1. Median and standard deviation for HAZUS fragility curves

Damage state	Unanchored		Anchored	
	Media, μ (g)	Standard deviation, β	Media, μ (g)	Standard deviation, β
Slight/minor	0.15	0.70	0.30	0.60
Moderate	0.35	0.75	0.70	0.60
Extensive	0.68	0.75	1.25	0.65
Complete	0.95	0.70	1.60	0.60

Later, O’Rourke and So (2000) developed fragility curves from the reported performance of over 400 tanks in nine separate earthquakes based on the report by Cooper (NIST 1997). The damage states of the tanks were classified into five categories, as shown in Table 5.2.

Table 5.2. Damage state definitions

Damage state	Description
DS1	No damage to tank or I/O pipes
DS2	Damage to roof, minor loss of contents, minor damage to piping, but no elephant’s foot buckling
DS3	Elephant’s foot buckling with minor loss of content
DS4	Elephant’s foot buckling with major loss of content, severe damage
DS5	Total failure, tank collapse

The influence of the relative amount of stored contents was investigated in their study. Fragility curve estimates for two ranges of a number of stored contents (i.e., $H/D < 0.70$ and $H/D > 0.70$) are listed in Table 5.3. The overall behaviour was as one might expect; fuller tanks performed worse (i.e., lower median values) than comparatively empty tanks.

Table 5.3. Median and standard deviation parameters for fragility curves

Damage state	All tanks		$H/D < 0.70$		$H/D > 0.70$	
	μ (g)	β	μ (g)	β	μ (g)	β
DS ≥ 2	0.70	0.48	0.67	0.50	0.45	0.47
DS ≥ 3	1.10	0.35	1.18	0.34	0.69	0.32
DS ≥ 4	1.29	0.28	1.56	0.35	0.89	0.21
DS = 5	1.35	0.22	1.79	0.29	1.07	0.15

Furthermore, American Lifeline Alliances (ALA 2001) developed seismic fragility curves based on the seismic performance of 532 tanks experienced strong ground motion of at least 0.1 g. Fragility curves were developed considering the effects of filling level and anchorage condition. The ALA fragility curve estimates are reported in Table 5.4 for different three groups of tanks.

Table 5.4. Median and standard deviation for ALA fragility curves

Damage state	All tanks with full ≥ 50%		Anchored with full ≥ 50%		Unanchored with full ≥ 50%	
	μ (g)	β	μ (g)	β	μ (g)	β
DS ≥ 2	0.18	0.8	0.71	0.8	0.15	0.8
DS ≥ 3	0.73	0.8	2.36	0.8	0.62	0.8
DS ≥ 4	1.14	0.8	3.72	0.8	1.06	0.8
DS ≥ 5	1.16	0.8	4.26	0.8	1.13	0.1

Empirical methods have the advantage of being based on real observed data, thus successfully accounting for various effects and the variability in the structural capacity of a group of tanks. However, this may also turn into a drawback, as the empirically-derived fragility curves remain specific to a given site/area, earthquake characteristics, and structural capacities. Available data are often based on low-magnitude events with limited damage, which lead to fragility curves that may be unreliable for greater magnitude events. It has also been noted that undamaged tanks after an event are not properly accounted for in the survey; this leads to a large uncertainty on the actual total number of elements exposed to the event.

5.2.2 Expert judgment-based fragility curves

This procedure, which may be considered out-dated nowadays, entirely relies on the judgment of some experts who are asked to provide an estimate of the mean loss or probability of damage of a given element for different levels of seismic loading. Some of the fragility curves proposed in HAZUS (e.g., road and tunnel) are developed using this approximate method. These techniques have the advantage of not being affected by the lack of extensive damage data (empirical approaches) or the reliability or the structural model used in analytical developments. However, the results rely solely on the individual experience of the experts consulted. The potential bias in the curves can be reduced by extending the number of experts and by assigning appropriate weight to their estimations, based on their expertise level (Porter et al. 2007).

5.2.3 *Analytical fragility curves*

A more general approach relies on analytical fragility curves. A lognormal cumulative distribution function is often used to define a fragility function:

$$P\left[D_{EDP} > LS \mid IM\right] = \Phi\left(\frac{\ln\left(IM / \mu\right)}{\beta}\right) \tag{5.2}$$

where $P[D_{EDP} > LS|IM]$ is the probability that a ground motion with intensity measure IM will cause a demand D_{EDP} exceeding a selected structural limit state LS, $\Phi(\cdot)$ is the standard normal cumulative distribution function, μ is the median of the fragility function (the IM level with 50% probability of collapse), and β is the standard deviation of $\ln(IM)$ (sometimes referred to as the dispersion of IM). Eq. (5.2) implies that the IM values of ground motions causing collapse of a given structure are lognormally distributed.

Differently, from the other methods, an analytical fragility function is commonly obtained from the elastic spectral analysis, nonlinear static analysis, or nonlinear time history analysis. Generating a seismic fragility curve by looking at the elastic spectral response of a structure is perhaps one of the simplest and least time-consuming approaches available. The nonlinear static analysis for the development of fragility curves is an improvement upon the elastic spectral analysis. However, a full nonlinear analysis can be very time-consuming. A simplified methodology, i.e., the capacity-spectrum method, has been developed which benefits from a nonlinear analysis but does not incur the computational cost of a time history analysis. A number of researchers generated seismic fragility curves for bridges using this approach (e.g., Shinozuka et al. 2000), and no contributions are currently available for liquid storage tanks.

Seismic fragility curves can also be generated using a nonlinear time history analysis approach. Although this type of approach tends to be the most computationally expensive, it is also one of the most reliable methodologies available (Shinozuka et al. 2000). For this reason, there have been many researchers that have used a methodology rooted in nonlinear time history analysis to generate fragility curves. The general procedure of this approach is the following:

- The first step is to obtain a suite of ground motions that is appropriate and representative of the target geographic area and captures the uncertainty inherent in ground motions. The characteristics of ground motions are usually based on the magnitude, the source-to-site distance, and the site condition.
- Next, the structural properties (e.g., material strengths and geometric values) are probabilistically sampled from an analytically model. Then, the ground motions are paired with the samples, and the nonlinear time history analysis for each pair is performed. For each simulation, the maximum values of selected engineering demand parameters are collected to generate a probabilistic seismic demand model.
- The capacity or limit state of each component is determined using expert-based, experimental, and/or analytical methods.
- Finally, the seismic demand and the structural capacity models are combined assuming a lognormal distribution as given in Eq. (5.2).

In the literature, different methods that use time history analyses have been proposed. The most commonly used is the CA method. This method implements nonlinear dynamic analyses through a (linear) regression-based probabilistic model (Shome et al. 1998). A second common approach is the IDA method, where a suite of ground motions are repeatedly scaled to find the IM level at which each ground motion causes the exceeding of a certain limit state (Vamvatsikos and Cornell, 2002). In the following, the brief overview of these two methods is provided.

5.2.3.1 Cloud analysis method

The CA method is particularly efficient since it involves the nonlinear analysis of the structure subjected to a set of unscaled ground motion records. Combined with the assumption of a lognormal distribution, the estimate of the median demand can be predicted by a power model (Cornell et al. 2002):

$$D_m = a\left(IM\right)^b \tag{5.3}$$

where a and b are the regression coefficients based on the collection of the demand d_i and intensity measure IM_i from time history analyses of the analysed tank. The methodology using regression analysis to generate the probabilistic seismic demand model was outlined by Cornell et al. (2002), as shown in Figure 5.2.

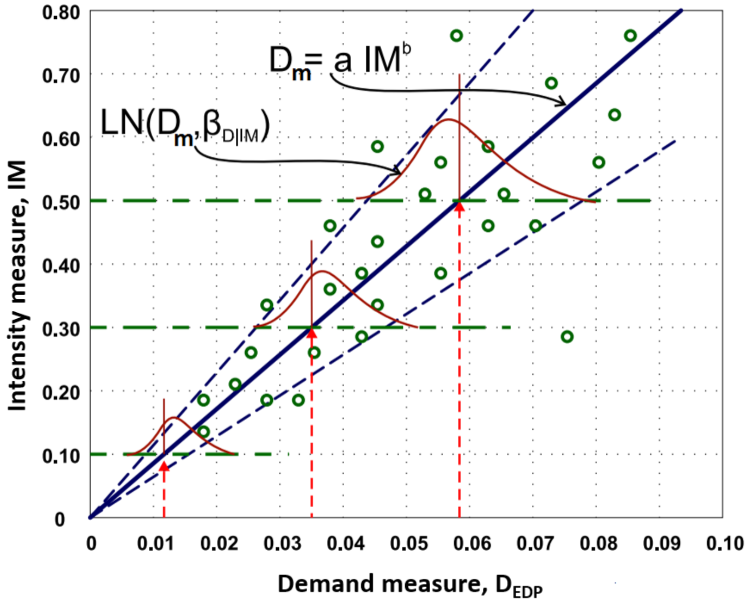

Figure 5.2. An example of probabilistic seismic demand model (Cornell et al. 2002)

The dispersion $\beta_{d|IM}$ of the demand conditioned on the IM can also be estimated from the regression analysis of the demand by using Eq. (5.4):

$$\beta_{d|IM} \cong \sqrt{\frac{\sum_{i=1}^{n}\left[\ln\left(d_i\right)-\ln\left(aIM_i^b\right)\right]^2}{n-2}} \tag{5.4}$$

When both the demand and the limit state are assumed lognormally, the fragility function takes on the following form (Nielson and DesRoches 2007):

$$P\left[D_{EDP} > LS \mid IM\right] = 1-\Phi\left(\frac{\ln\left(LS_m\right)-\ln\left(D_m\right)}{\sqrt{\beta_{d|IM}^2+\beta_{LS}^2}}\right) \tag{5.5}$$

where LS_m is the median estimate of the structural limit state, D_m is the median estimate of the demand, $\beta_{d|IM}$ is the dispersion of the demand conditioned on IM, and β_{LS} is the dispersion of the structural limit state.

The CA method is very attractive because it allows for closed-form solutions of the fragility curves. Nonetheless, the power-law form of the demand is only a good estimate of the behaviour of a structure under earthquake excitations in the interval of values, where the locally linear fit is carried out. In fact, the dispersion is considered as constant, when in reality, there is a clear dependency on the level of IM analysed.

5.2.3.2 Incremental dynamic analysis

The IDA involves performing nonlinear dynamic analyses of the structural model under a suite of ground motion records. The records are scaled to several intensity levels designed to force the structure all the way from elasticity to the onset of failure and/or final global dynamic instability (Vamvatsikos and Cornell 2002). This process produces a set of IM values associated with the onset of exceeding a limit state for each ground motion.

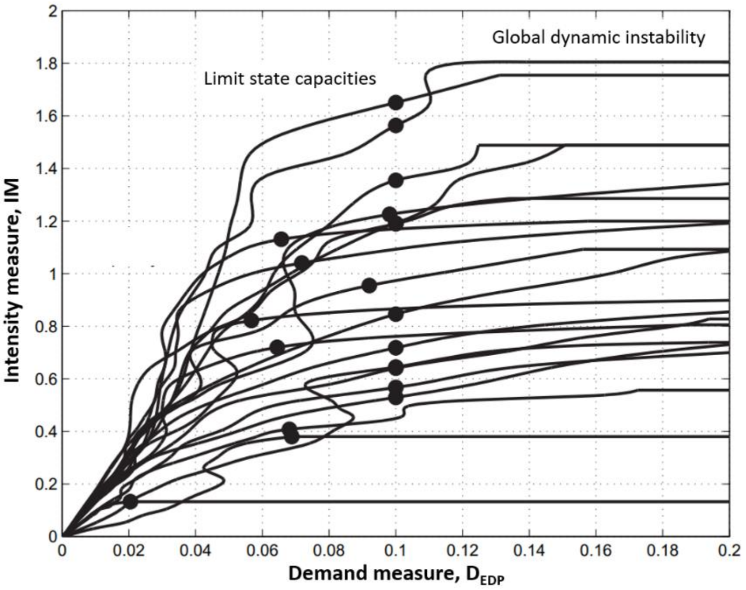

Figure 5.3. An example of IDA curves and their associated limit state capacities (Vamvatsikos and Cornell 2002)

Figure 5.3 shows an example of IDA curves with their associated limit state capacities. The limit state is represented by the dots, while global dynamic instability occurs at the flat lines. This approach can be extended to different levels of the limit state that in many cases, the global dynamic instability does not occur.

The probability of exceeding a limit state at a given IM level can then be estimated as the fraction of records for which the limit state is exceeded, as shown in Figure 5.4. Fragility function parameters including the mean and standard deviation can be estimated by:

$$\ln \mu = \frac{1}{n}\sum_{i=1}^{n} \ln IM_i \tag{5.6}$$

$$\beta = \sqrt{\frac{1}{n-1}\sum_{i=1}^{n} \left(\ln\left(IM_i / \mu\right)\right)^2} \tag{5.7}$$

where IM_i is the IM value associated with the onset of failure for the ith ground motion; this is a method of moments estimator, and $\ln\mu$ and β are the mean and standard deviation, respectively, of a normal distribution representing the $\ln IM$ values. An example of fragility function fitted using this approach is also shown in Figure 5.4.

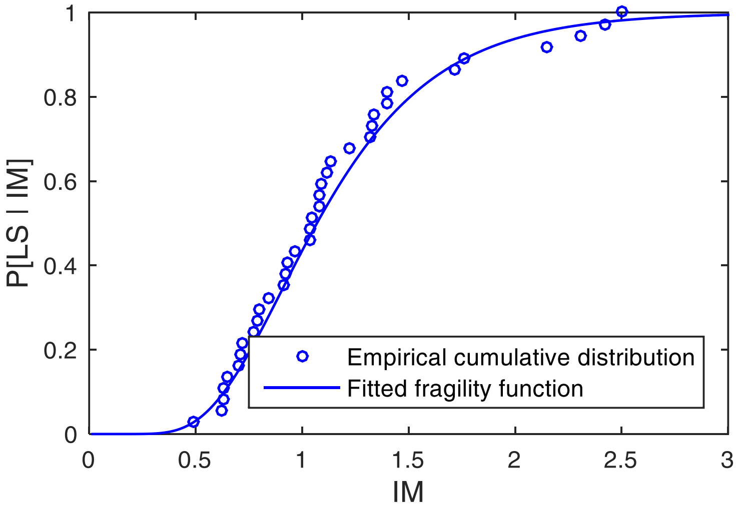

Figure 5.4. An example of observed fractions of collapse and a fragility function estimated using the method of moments estimator (Baker 2014)

5.3 Sensitivity of seismic response to modelling parameters

5.3.1 Uncertainty in modelling parameters

Sources of uncertainty affecting structural performance are often classified as either aleatoric or epistemic. Aleatoric uncertainty refers to that which is inherently random, or stems from the unpredictable nature of events, whereas epistemic uncertainty is due to a lack of knowledge, and stems from incomplete data, ignorance, or modelling assumptions. It is necessary to clarify that the uncertainty of modelling parameters is mainly considered to be epistemic because of the lack of knowledge. Modelling uncertainties involving material or geometric parameters exist in steel liquid storage tanks due to their large-scale configuration. A sensitivity study to identify the influence of various modelling parameters and uncertainties on the seismic response of tanks is commonly conducted before the fragility evaluation. Such a study provides insight into quantifying whether the variation of uncertain parameters should be treated explicitly or to be neglected. The results of the sensitivity analysis could be used to reduce the number of parameters considered in the fragility analysis (Padgett and DesRoches 2007).

There are a number of modelling parameters which are variable in a steel storage tank. These parameters may be attributed to mechanical properties, such as the yield strength and Young's modulus of steel, which are the uncertain parameters that are often considered in vulnerability assessments. The material parameters associated with the steel tank are often assumed to have a normal or lognormal distribution. Another group of uncertain modelling parameters can be attributed to the geometric properties of the tank. These geometric properties include the filling level of the liquid and the thickness of the shell and bottom plate. The filling level of the liquid is one of the most significant parameters that affect the seismic response of the tank. A variation between 80% and 100% of the tank height is often selected for the filling level uncertainty, as suggested by the HAZUS manual (HAZUS 2001). The plate thickness uncertainty is affected by nominal thickness, steel type, measurement technique, presence of a surface coating, and amount of plate deformation. Statistical information on plate thickness can be found from the work of Daidola and Basar (1980) or Hess et al. (2002). The density of the liquid is also considered as variable and assumed to have a uniform distribution.

5.3.2 Screening design

A number of methods are available to assist in the identification of significant parameters or factors. Among them, a design of experiments (DOE) approach is increasing in popularity; this is a statistical approach which investigates the significance of each factor while reducing the computational effort. Two-level designs are sufficient for evaluating many production processes. Factor levels of ± 1 can indicate categorical factors, normalised factor extremes, or simply up and down from current factor settings. However, for experiments with many factors, two-level full factorial designs can lead to large amounts of data, requiring 2^k runs. For example, a two-level full factorial design with 10 factors requires 2^{10} = 1024 runs. Table 5.5 illustrates this concept using four parameters a, b, c, and d. However, individual factors or their interactions often have no distinguishable effects on a response; this is especially true of higher order interactions. As a result, a well-designed experiment can use fewer runs for estimating model parameters.

Table 5.5. Example of two-level full factorial design

Run N.	Parameters			
	a	b	c	d
1	-1	-1	-1	-1
2	-1	-1	-1	1
3	-1	-1	1	-1
4	-1	-1	1	1
5	-1	1	-1	-1
6	-1	1	-1	1
7	-1	1	1	-1
8	-1	1	1	1
9	1	-1	-1	-1
10	1	-1	-1	1
11	1	-1	1	-1
12	1	-1	1	1
13	1	1	-1	-1
14	1	1	-1	1
15	1	1	1	-1
16	1	1	1	1

The experimental setup may be reduced by a fraction 2^{-p}, requiring the total number of runs to be 2^{k-p}. Explicitly, the value of p is the fractional reduction in the number of experiments required. This value of p is determined by the experimenter, balancing the economics of the experiment with the information that is desired (Wu and Hamada 2000). Screening designs are typically of resolution III because resolution III designs permit one to explore the effects of many factors with an efficient number of runs. Sometimes designs of resolution IV are also used for screening designs, in which main effects are confounded with, at worst, three-factor interactions; this is better from the confounding viewpoint, but the designs require more runs than a resolution III design. Back to the above example, a fractional factorial design for four variables can be generated in which the fourth variable is the product of the first three. The more economical design that requires only 8 runs is shown in Table 5.6.

Table 5.6. An example of two-level fractional factorial design

Run N.	Parameters			
	a	b	c	d
1	-1	-1	-1	-1
2	-1	-1	1	1
3	-1	1	-1	1
4	-1	1	1	-1
5	1	-1	-1	1
6	1	-1	1	-1
7	1	1	-1	-1
8	1	1	1	1

After generating the screening design, a static or dynamic analysis of each sample is performed, and various responses of interest are recorded. The analysis of the data to determine the significant factors is performed using an analysis of variance (ANOVA).

5.3.3 Analysis of variance

The ANOVA is a procedure for determining whether variation in the response variable arises within or among different population groups. Therefore, each parameter will be investigated to see its effect on the variance of the measured response. Those parameters that do not affect the variance are designated as insignificant. This task is formalised through the creation of an ANOVA table in which a hypothesis test is performed on each parameter. The null hypothesis states that the given parameter is insignificant, while the alternative hypothesis states otherwise (Hayter 2002). The results of the hypothesis tests are given in terms of a p-value, and a smaller p-value indicates greater evidence that the parameter has a strong influence on the response. A typical significance cutoff value of $\alpha = 0.05$ is usually adopted. Appendix C gives a description of how to calculate the ANOVA table for a fractional factorial design.

5.4 Design of experiments and fragility evaluation

Although the results of the sensitivity study indicate which uncertain parameters affect the seismic response of the tank system, the influence of these sources of uncertainty on the fragility estimates should be determined. The following procedure allows to evaluate the sensitivity of fragility curves to modelling parameters:

- At first, statistically significant samples of the tank system are derived using a DOE method. Latin hypercube sampling (LHS) is used in this work; this is a variance reduction sampling method that stratifies variable marginal distributions in order to fully cover the range of each variable in a more efficient way than pure Monte Carlo sampling (McKay et al. 1979). As a result, a number of tank samples are generated by sampling the significant modelling parameters.
- Each sample is then randomly paired with a set of ground motions. Nonlinear time history analyses are then performed on each pair, and the peak component responses are monitored every each analysis. The fragility curves can be constructed by using either the CA or the IDA that described previously. The IDA curves can be derived for each pair by a number of analyses that are performed with several intensity levels.
- This procedure can be repeated with different sets of tank samples, resulting in different sets of fragility curves of the system considering different levels of uncertainty treatment.

5.5 Closure

Fragility curves constitute one of the key elements of seismic risk assessment studies for industrial plants. Combined with seismic hazard curves, they allow evaluating the failure probability of a component with respect to a predefined failure event. This chapter presents current approaches for evaluating the fragility curves of steel liquid storage tanks, including empirical, expert judgment-based, and analytical approaches.

Expert-based methods have been identified as particularly limited in scope and response, and empirical methods are not an option because sufficient tank damage data is not available. In the absence of adequate empirical data, fragility curves have been developed through a number of analytical methods. The chapter provides the methodology of two well-known methods, namely the CA and the IDA. The procedure of a sensitivity analysis of the seismic response to modelling parameters is also presented in this chapter. The analysis is based on DOE and ANOVA approaches. Finally, a procedure for developing fragility curves considering different levels of uncertainty treatment is presented. An application of this procedure in deriving fragility curves will be presented in Chapter 7.

Chapter 6. Selection of intensity measures for seismic fragility analysis of steel liquid storage tanks

6.1 Introduction

The evaluation of the seismic risk of industrial plants due to the damage of liquid storage tanks strongly depends on the reliability of fragility curves. Nevertheless, they are often empirically rather than analytically evaluated (e.g., HAZUS 2001, ALA 2001, Salzano et al. 2003). However, in modern approaches like the performance-based earthquake engineering, the analytical evaluation is preferred. Probabilistic seismic demand models based on numerical simulations are often used as an essential step for deriving fragility curves. These probabilistic models are traditionally conditioned on selected intensity measures and can be significantly affected by the representation of ground motion uncertainty. Therefore, the main issue is the selection of an appropriate earthquake intensity measure that characterizes the strong ground motion and best correlates with the structural response of each element.

Most of the studies on fragility evaluation have used the peak ground acceleration (PGA) or the 5% damped elastic spectral acceleration at the fundamental period of the structure [$S_a(T_1)$] as an intensity measure. PGA has widely been used to describe the horizontal ground motions owing to its natural relationship to inertial forces, while $S_a(T_1)$ is known as a perfectly efficient and sufficient intensity measure for elastic SDOF systems. Shome et al. (1998) represented a probabilistic seismic demand analysis for structures based on a coupling of probabilistic seismic hazard analysis and time history nonlinear analyses of the structural response. They demonstrated that $S_a(T_1)$ is more efficient than PGA. However, recent studies have also demonstrated that $S_a(T_1)$ may not be particularly efficient nor sufficient for some structures (e.g., tall, long period buildings) or for near-source ground motions (Shome and Cornell 1999, Luco 2002). Therefore, for a specific case study, an optimal intensity measure should be selected. Alternative intensity measures are defined in terms of practicality, effectiveness, efficiency, sufficiency, robustness, and computability (Mackie and Stojadinovich 2003, Luco and Cornell 2007).

Practicality refers to the recognition that the intensity measure has some direct correlation to known engineering quantities. The practicality of an intensity measure may be verified analytically via quantification of the dependence of the structural response on the physical properties of the intensity measure (e.g., energy, response of fundamental and higher modes, etc.). It may also be verified numerically by interpretation of the response of the structure under nonlinear analysis using existing time histories. Sufficiency describes the extent to which the intensity measure is statistically independent of ground motion characteristics such as magnitude and distance. A sufficient intensity measure is one that renders the structural demand measure conditionally independent of the earthquake scenario. This term is more complex and often at odds with the need for computability of the intensity measure. Sufficiency may be quantified via statistical analysis of the response of a structure for a given set of records. The effectiveness of an intensity measure is determined by its ability to evaluate its relationship with an engineering demand parameter in closed form so that the mean annual frequency of a given decision variable exceeding a given limiting value can be determined analytically. The most widely used quantitative measure from which an optimal intensity measure can be obtained is efficiency; this refers to the total variability of an engineering demand parameter for a given intensity measure. Robustness describes the efficiency trends of a $IM - D_{EDP}$ pair across different structures, and therefore, different fundamental period ranges.

The seismic response of tanks is different to the buildings because of the effect of the fluid-structure interaction. The initial forces in the liquid mass, which are produced by the seismic excitation of the tank base, generate hydrodynamic pressure distributions on the tank wall; this results in the overturning moments and the shear forces at the tank base. The probabilistic seismic response of tanks has been widely studied in the past; nevertheless, at present, there is no specific accepted procedure for the efficiency or sufficiency of intensity measures used in assessing the seismic performance of steel liquid storage tanks. A rare example of intensity measure efficiency evaluation for tanks is reported by Buratti and Tavano (2014), where the efficiency and sufficiency of intensity measures were investigated in terms of the maximum lateral displacement of the tank wall. The authors discovered that in this specific case, the peak ground displacement is the most efficient intensity measure. Phan and Paolacci (2016) performed a comparative study for the selection of intensity measures used in the assessment of the seismic vulnerability of anchored steel liquid storage tanks. For a specific case of fix-based tank configurations, the authors suggested $S_a(T_i)$ as the most efficient intensity measure for both slender and broad cases.

This chapter presented herein concerns the probabilistic seismic response analysis for both anchored and unanchored above-ground steel liquid storage tanks. Four bins of ground motion records are selected to investigate the effects of the earthquake magnitude and the source-to-site distance on the selection of intensity measures. Six cases of steel liquid storage tanks, ranging from slender to broad configurations, are examined by using a probabilistic seismic response analysis. Two of them are considered to be unanchored. The main response of the tanks is selected as the compressive meridional stress in the tank wall. The efficiency of each investigated intensity measure is quantified by computing the standard deviation from a proper regression model for the selected engineering demand parameter. The sufficiency is then analysed by evaluating the correlation between the residuals of the above regression model and ground motion parameters. According to the comparative results, the present work suggests the optimal intensity measures with respect to the selected engineering demand parameter for a given portfolio of steel liquid storage tanks.

6.2 Intensity measures and probabilistic seismic demand model

Various well-known intensity measures are used in this study. The most commonly used intensity measure is PGA. The peak ground velocity (PGV) and displacement (PGD) are also used as magnitude-dependent intensity measures. Another widely accepted intensity measure is $S_a(T_1)$. $S_a(T_1)$ is the perfect predictor for the response of elastic SDOF systems, and a good predictor for elastic multi-degree of freedom systems dominated by the first mode of vibration, associated with the T_1 period. Nevertheless, $S_a(T_1)$ does not provide information about the spectral shape in other regions of the spectrum, which may be important for the nonlinear behaviour or for structures dominated by higher modes. In the case of nonlinear shaking, the structure may be sensitive to different spectral values associated with a range of periods. Therefore, other intensity measures, named as S^* and I_{NP}, which account for the spectral shape are considered in this comparative study. Three well-known duration-based intensity measures, including Arias intensity (I_A), cumulative absolute velocity (CAV), and cumulative absolute displacement (CAD) are also selected. The definition of each intensity measure is summarised in Table 6.1.

Table 6.1. Intensity measures used in this study

Intensity measure	Note
$PGA = \max\left\vert \ddot{u}_g\left(t\right)\right\vert$	Peak ground acceleration
$PGV = \max\left\vert \dot{u}_g\left(t\right)\right\vert$	Peak ground velocity
$PGD = \max\left\vert u_g\left(t\right)\right\vert$	Peak ground displacement
$S_a\left(T_1\right)$	Spectral acceleration at fundamental period
$S^* = S_a\left(T_1\right)\left(\frac{S_a\left(2T_1\right)}{S_a\left(T_1\right)}\right)^{0.5}$	Cordova et al. (2001)
$I_{NP} = S_a\left(T_1\right)\left(\frac{S_{aAV}\left(T_1 \ldots 2T_1\right)}{S_a\left(T_1\right)}\right)^{0.4}$	Bojorquez and Iervolino (2011)
$I_A = \frac{\pi}{2g}\int_0^{t_f}\left[\ddot{u}_g\left(t\right)\right]^2 dt$	Arias intensity (Arias 1970)
$CAV = \int_0^{t_f}\left\vert \ddot{u}_g\left(t\right)\right\vert dt$	Cumulative absolute velocity (EPRI 1988)
$CAD = \int_0^{t_f}\left\vert \dot{u}_g\left(t\right)\right\vert dt$	Cumulative absolute displacement

To evaluate the intensity measure efficiency, a probabilistic seismic demand analysis based on the work of Cornell et al. (2002) is presented. Assuming a lognormal distribution, the estimate of the median demand can be predicted by a power model, expressed as:

$$D_m = aIM^b \tag{6.1}$$

This equation can be rearranged as:

$$\ln D_m = \ln a + b \ln IM \tag{6.2}$$

where D_m is the median estimate of the demand, a and b are the regression coefficients. The dispersion of the demand conditioned on the intensity measure can be estimated from the regression analysis of the seismic demand, given as:

$$\beta_{d|IM} \cong \sqrt{\frac{\sum_{i=1}^{n}\left[\ln\left(d_i\right)-\ln\left(aIM_i^b\right)\right]^2}{n-2}} \tag{6.3}$$

The sufficiency of intensity measures is analysed by evaluating the correlation between the residuals of the linear regression model described in Eq. (6.2) with the parameters above involved in hazard calculation, e.g., the moment magnitude, M_W, and the source-to-site distance, R_{jb}. In particular, linear regressions are performed between the regression-residuals of $d_i - IM_i$ and M_W or R_{jb} given in Eq. (6.4):

$$\ln\left(residual_{d_i-IM_i}\right) = c_0 + c_1 M_W \left(\text{or}\, R_{jb}\right) \tag{6.4}$$

where c_0 and c_1 are the linear regression coefficients.

6.3 Numerical model of examined tanks and input signal selection

Different configurations of liquid steel liquid storage tanks, ranging from slender to broad ones, are selected as case studies for the parametric investigation (Table 6.2). The effect of the geometrical configurations, represented by the aspect ratio of the tanks, on the selection of intensity measures is investigated. The water level is filled up 90% of the tank height for all cases (Figure 6.1). The aspect ratios of the tanks range from 0.5 to 3. The mechanical properties of the tanks are shown in Table 6.3.

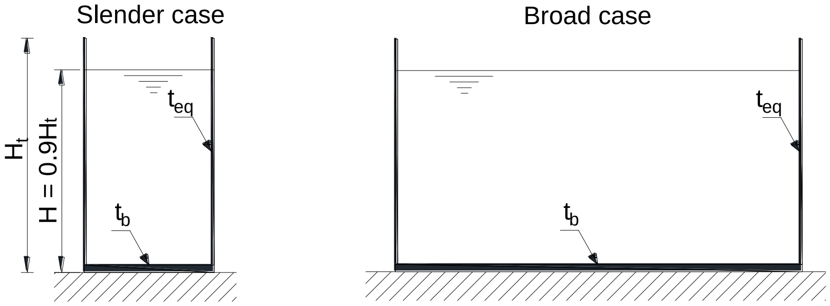

Figure 6.1. Schematic of slender and broad tanks

The spring-mass model of steel liquid storage tanks described in Section 3.3 is used in this study. The numerical models of the anchored and unanchored tanks here adopted are represented in Figure 6.2, where the impulsive and convective motions are simulated by two viscoelastic oscillators.

Table 6.2. Geometrical parameters of the case studies

Type	Name	H_t (m)	H (m)	R (m)	γ	t_{eq} (mm)	t_b (mm)
Anchored	Tank #1	15	13.5	4.5	3	6	8
	Tank #2	15	13.5	5.4	2.5	7	8
	Tank #3	15	13.5	6.8	2	9	8
	Tank #4	15	13.5	9.0	1.5	11	8
Unanchored	Tank #5	15	13.5	13.5	1	15	8
	Tank #6	15	13.5	27.0	0.5	28	8

Table 6.3. Mechanical properties of the tanks

Component	Mechanical property	Value
Steel tank	Young's modulus Yield strength Density	200000 MPa 235 MPa 7850 kg/m^3
Water	Density	1000 kg/m^3

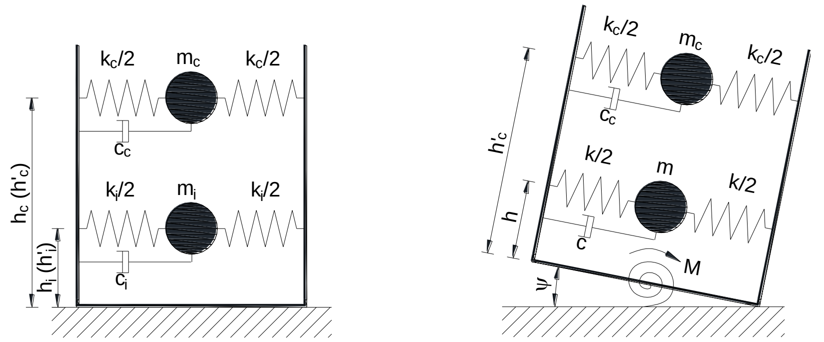

(a) **(b)**

Figure 6.2. Lumped mass model of tanks: (a) anchored and (b) unanchored

In the unanchored tank model, a rotational spring represented the rocking resistance of the bottom plate is added to the tank base, as shown in Figure 6.2(b). The relationship between the base moment, M_{OT}, and the spring rotation, ψ, is established by the simplified method reported by Malhotra and Veletsos (1994a). The $M_{OT} - \psi$ relationships of tanks #5 and #6 are shown in Figure 6.3. The parameters of the spring-mass model for the examined tanks are shown in Table 6.4.

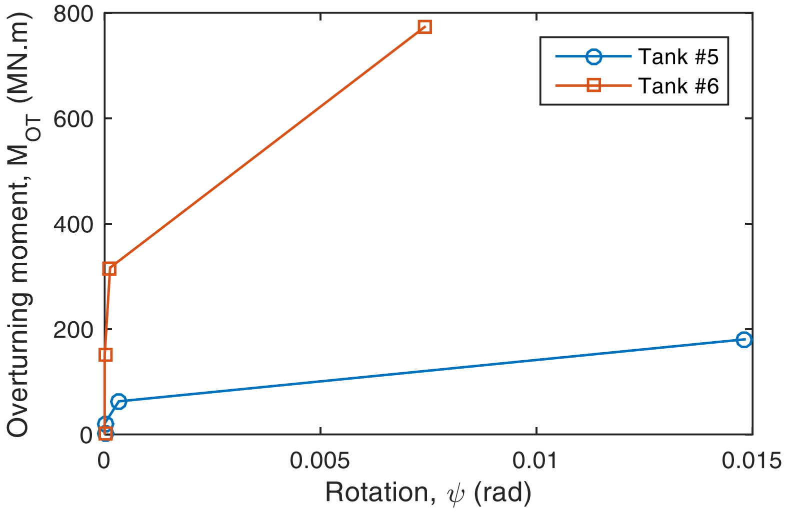

Figure 6.3. Relationships between overturning moment and base rotation of the broad tank

Table 6.4. Parameters of the tank models

Tank	m_i (T)	m_c (T)	T_i (s)	T_c (s)	h_i (m)	h_c (m)
#1	723	136	0.18	3.14	6.12	11.14
#2	1002	235	0.17	3.44	6.10	10.72
#3	1496	465	0.16	3.86	6.05	10.14
#4	2357	1079	0.16	4.44	5.93	9.32
#5	4236	3494	0.18	5.59	5.66	8.32
#6	9275	21643	0.22	9.04	5.40	7.33

The ground motion records used for the numerical simulations have been selected from PEER ground motion database (http://ngawest2.berkeley.edu). The soil of the record stations is characterised by stiff soil conditions (360 m/s ≤ $V_{s,30}$ ≤ 800 m/s), which are in compliance with EN 1998-1 (2004) soil type B. In addition, two magnitude groups are presented including small amplitude ($5.5 \leq M_W \leq 6.5$) and large amplitude ($6.5 < M_W \leq 7.5$). Records are also classified into short distance ($0 \leq R_{jb} \leq 30$) and long-distance ($30 < R_{jb} \leq 100$). The selected 120 records are equally subdivided into four bins, as shown in Table 6.5, where $V_{s,30}$ is the average shear wave velocity. The median response spectrum of each bin are plotted in Table 6.5.

Table 6.5. Selections of ground motion records for four bins

Name	M_W	R_{jb} (km)	$V_{s,30}$ (m/s)	N. records
Bin #1	5.5 6.5	0-30	360-800	30
Bin #2	5.5-6.5	30-100	360-800	30
Bin #3	6.5-7.5	0-30	360-800	30
Bin #4	6.5-7.5	30-100	360-800	30

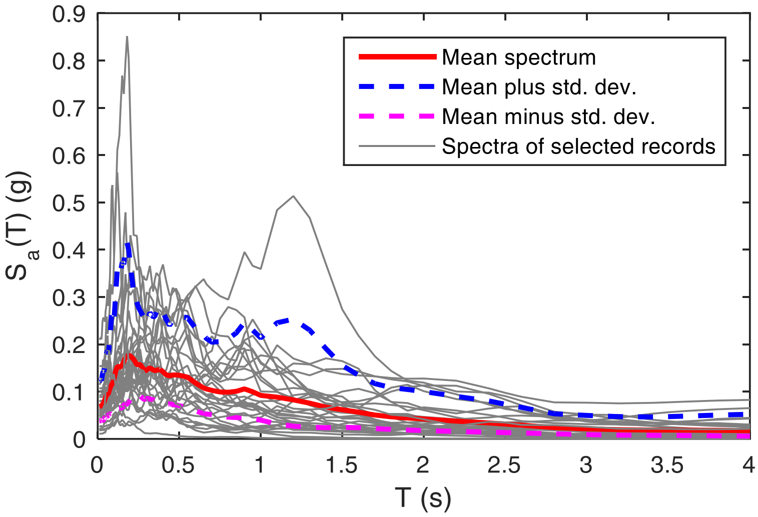

Bin #1

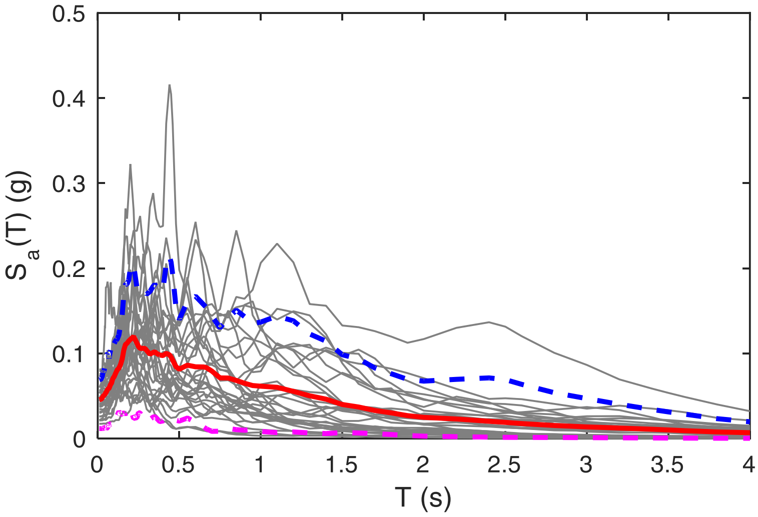

Bin #2

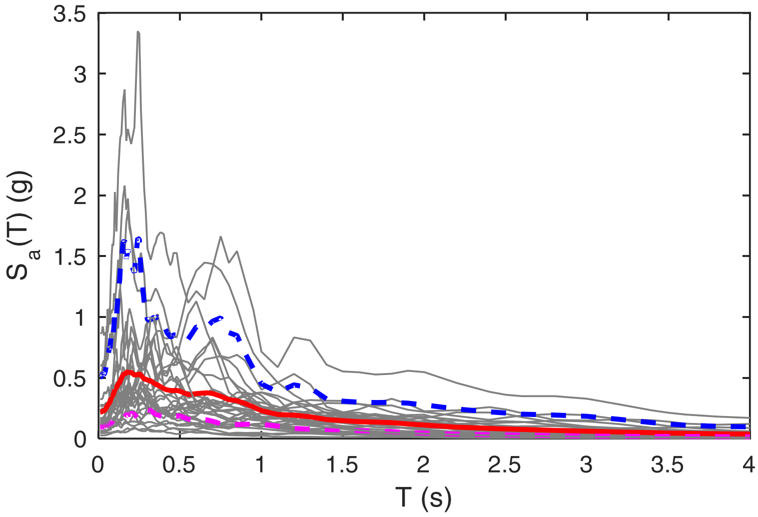

Bin #3

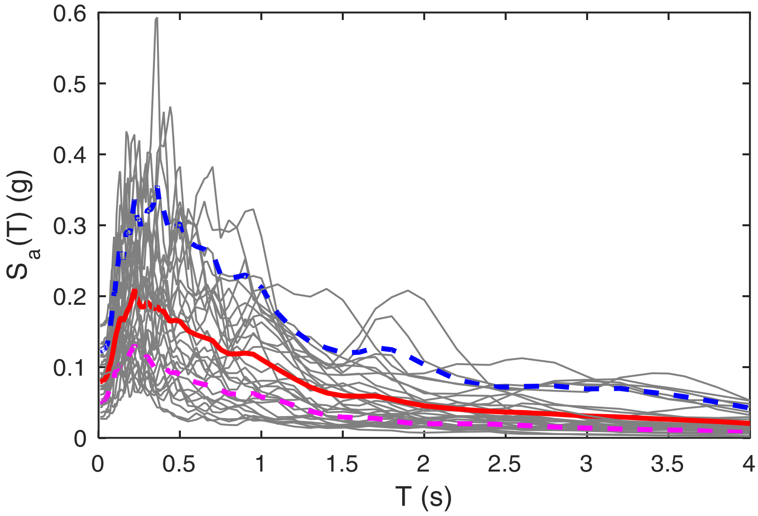

Bin #4

Figure 6.4. Spectra of selected ground motions for four bins

6.4 Comparative results

6.4.1 Intensity measure efficiency

Results of the comparative analysis on the efficiency of intensity measures are presented with respect to the four bins of ground motion records presented in Table 6.5. The intensity measure efficiency is evaluated by computing the standard deviation, $\beta_{d|IM}$, and the coefficient of determination, R^2; the lower standard deviation (or the higher coefficient of determination), the higher intensity measure efficiency. The critical seismic response for both the anchored and unanchored tanks presented herein is the compressive meridional stress in the tank wall, which could lead to a major failure mode, i.e., the elastic-plastic or elephant's foot buckling at the bottom shell course of the tank wall. The calculation of the compressive meridional stress is followed the expressions presented in Section 3.5.

Table 6.6. Bin #1, small amplitude, short distance

Tank	#1		#2		#3	
	$\beta_{d\|IM}$	R^2	$\beta_{d\|IM}$	R^2	$\beta_{d\|IM}$	R^2
PGA	**0.34**	**0.76**	**0.34**	**0.77**	**0.34**	**0.71**
PGV	0.48	0.50	0.51	0.46	0.51	0.35
PGD	0.60	0.23	0.63	0.21	0.59	0.12
$S_a(T_1)$	**0.12**	**0.97**	**0.10**	**0.98**	**0.13**	**0.96**
S^*	0.22	0.90	0.25	0.87	0.28	0.80
I_{NP}	0.15	0.95	0.14	0.96	0.18	0.92
I_A	**0.38**	**0.68**	**0.41**	**0.67**	**0.41**	**0.57**
CAV	0.42	0.61	0.45	0.59	0.45	0.49
CAD	0.52	0.41	0.55	0.38	0.54	0.27
Tank	#4		#5		#6	
	$\beta_{d\|IM}$	R^2	$\beta_{d\|IM}$	R^2	$\beta_{d\|IM}$	R^2
PGA	**0.31**	**0.74**	**0.64**	**0.68**	**0.54**	**0.70**
PGV	0.48	0.39	0.88	0.4	0.76	0.42
PGD	0.57	0.14	1.02	0.19	0.89	0.20
$S_a(T_1)$	**0.11**	**0.97**	0.5	0.81	**0.43**	**0.81**
S^*	0.25	0.83	0.53	0.78	0.57	0.67
I_{NP}	0.16	0.94	**0.46**	**0.84**	0.48	0.76
I_A	**0.38**	**0.61**	**0.69**	**0.63**	**0.61**	**0.63**
CAV	0.42	0.52	0.76	0.55	0.68	0.54
CAD	0.51	0.30	0.94	0.31	0.83	0.32

Due to a large difference of the natural periods of the impulsive and convective components of steel liquid storage tanks, these two motions can be considered uncoupled. The seismic response of tanks is mainly affected by the impulsive component of the liquid motion. The fundamental mode of steel cylindrical tanks subjected to an earthquake excitation is associated with the fundamental mode of a cantilever beam, i.e., the impulsive mode ($T_1 = T_i$). In this respect, the natural impulsive period of the tank models are used as the fundamental periods for calculating the frequency-dependent intensity measures. The comparative results for each intensity measure regarding to the meridional stress response are shown in tables 6.6, 6.7, 6.8, and 6.9. The values highlighted in bold are the most efficient intensity measure for each group.

Table 6.7. Bin #2, small amplitude, long distance

Tank	#1		#2		#3	
	$\beta_{d\|IM}$	R^2	$\beta_{d\|IM}$	R^2	$\beta_{d\|IM}$	R^2
PGA	**0.23**	**0.80**	**0.25**	**0.75**	**0.30**	**0.56**
PGV	0.47	0.17	0.46	0.15	0.43	0.10
PGD	0.50	0.07	0.48	0.06	0.44	0.04
$S_a(T_1)$	**0.12**	**0.94**	**0.11**	**0.95**	**0.10**	**0.95**
S^*	0.29	0.69	0.27	0.70	0.25	0.71
I_{NP}	0.17	0.89	0.15	0.91	0.15	0.89
I_A	0.34	0.57	0.34	0.52	0.34	0.44
CAV	0.38	0.46	0.38	0.42	0.36	0.36
CAD	0.50	0.08	0.47	0.08	0.44	0.07
Tank	#4		#5		#6	
	$\beta_{d\|IM}$	R^2	$\beta_{d\|IM}$	R^2	$\beta_{d\|IM}$	R^2
PGA	**0.28**	**0.62**	**0.53**	**0.74**	**0.32**	**0.68**
PGV	0.43	0.12	0.98	0.11	0.51	0.19
PGD	0.45	0.05	1.02	0.03	0.54	0.11
$S_a(T_1)$	**0.10**	**0.95**	**0.36**	**0.88**	**0.18**	**0.90**
S^*	0.24	0.73	0.64	0.62	0.33	0.66
I_{NP}	0.14	0.90	0.40	0.85	0.22	0.85
I_A	**0.33**	**0.47**	**0.76**	**0.47**	**0.39**	**0.54**
CAV	0.36	0.39	0.83	0.36	0.43	0.43
CAD	0.44	0.07	1.02	0.04	0.54	0.11

The analysis results reported in the tables show that intensity measures exhibiting the highest efficiency are in the structure-specific group (i.e., frequency-dependent intensity measures), where includes information of the fundamental structure period (i.e., the impulsive period). Among this group, the spectral acceleration at the fundamental period $S_a(T_1)$ is the most efficient intensity measure in most of the anchored cases. The use of I_{NP} also leads to a low dispersion as well, especially in the cases of unanchored tanks. Its highest performance can be found in the cases of Tank #5 subjected to Bin #1 and Bin #4 records. In addition, the performance of S^* is lower than that of $S_a(T_1)$ and I_{NP} except the case of Tank #5 subjected to Bin #3 records.

Table 6.8. Bin #3, large amplitude, short distance

Tank	#1		#2		#3	
	$\beta_{d\|IM}$	R^2	$\beta_{d\|IM}$	R^2	$\beta_{d\|IM}$	R^2
PGA	**0.37**	**0.81**	**0.41**	**0.78**	**0.35**	**0.80**
PGV	0.69	0.35	0.70	0.35	0.67	0.29
PGD	0.85	0.01	0.87	0.01	0.80	0.01
$S_a(T_1)$	**0.14**	**0.97**	**0.14**	**0.97**	**0.12**	**0.98**
S^*	0.29	0.88	0.28	0.90	0.26	0.89
I_{NP}	0.18	0.95	0.17	0.96	0.15	0.97
I_A	**0.36**	**0.82**	**0.39**	**0.80**	**0.38**	**0.77**
CAV	0.43	0.74	0.47	0.71	0.46	0.67
CAD	0.78	0.15	0.81	0.14	0.76	0.09
Tank	#4		#5		#6	
	$\beta_{d\|IM}$	R^2	$\beta_{d\|IM}$	R^2	$\beta_{d\|IM}$	R^2
PGA	**0.36**	**0.79**	**0.5**	**0.7**	**0.7**	**0.69**
PGV	0.65	0.30	0.77	0.3	1.11	0.24
PGD	0.78	0.01	0.91	0.01	1.27	0.01
$S_a(T_1)$	**0.13**	**0.97**	0.49	0.71	**0.45**	**0.88**
S^*	0.26	0.89	**0.41**	**0.8**	0.64	0.75
I_{NP}	0.16	0.96	0.46	0.75	0.47	0.86
I_A	**0.37**	**0.78**	**0.47**	**0.73**	**0.62**	**0.76**
CAV	0.44	0.68	0.54	0.66	0.68	0.71
CAD	0.74	0.10	0.86	0.12	1.20	0.10

Among magnitude-dependent intensity measures, PGA shows the best performance for all the cases. In contrast, PGD shows the weakest performance, especially in the cases of large amplitude records. The results also show that the efficiency of this intensity measure group is typically lower than that of the frequency-dependent intensity measures. In the case of duration-dependent intensity measures, I_A appears as the most efficient one. CAV produces instead a slight increase of the standard deviation as compared with I_A, and the use of CAD is not recommended when it shows high dispersions for most of the cases. The preeminence of $S_a(T_1)$ over other intensity measures in the anchored tanks is clearly when the anchored tank is considered as a SDOF system.

Table 6.9. Bin #4, large amplitude, long distance

Tank	#1		#2		#3	
	$\beta_{d\|IM}$	R^2	$\beta_{d\|IM}$	R^2	$\beta_{d\|IM}$	R^2
PGA	**0.31**	**0.57**	**0.32**	**0.57**	**0.30**	**0.61**
PGV	0.41	0.21	0.42	0.24	0.41	0.28
PGD	0.43	0.13	0.45	0.14	0.45	0.13
$S_a(T_1)$	**0.13**	**0.92**	**0.13**	**0.92**	**0.12**	**0.94**
S^*	0.26	0.69	0.23	0.78	0.22	0.79
I_{NP}	0.17	0.86	0.16	0.89	0.14	0.91
I_A	0.30	0.57	0.32	0.56	0.32	0.57
CAV	0.33	0.50	0.35	0.48	0.35	0.48
CAD	0.41	0.22	0.42	0.24	0.42	0.24
Tank	#4		#5		#6	
	$\beta_{d\|IM}$	R^2	$\beta_{d\|IM}$	R^2	$\beta_{d\|IM}$	R^2
PGA	**0.31**	**0.58**	**0.60**	**0.61**	**0.56**	**0.69**
PGV	0.41	0.25	0.84	0.23	0.77	0.40
PGD	0.45	0.11	0.89	0.12	0.88	0.23
$S_a(T_1)$	**0.11**	**0.94**	0.44	0.78	**0.40**	**0.84**
S^*	0.23	0.78	0.54	0.68	0.52	0.73
I_{NP}	0.15	0.90	**0.43**	**0.80**	0.43	0.81
I_A	**0.32**	**0.55**	**0.59**	**0.62**	**0.61**	**0.63**
CAV	0.35	0.47	0.65	0.53	0.70	0.51
CAD	0.42	0.21	0.83	0.24	0.79	0.37

In the case of unanchored tanks, the uplift phenomenon may cause a decrease of the fundamental period of the system, as demonstrated in Section 3.7. Therefore, in some cases, the spectral shape intensity measures S^* and I_{NP} are more efficient than their origin. Figure 6.5 shows examples of the linear regression analysis for Tank #1. The results of the compressive meridional stress demand in the tank wall for each intensity measure are presented by using the data set of small amplitude and long distance records (Bin #1). It is evident that the superiority of $S_a(T_1)$ in terms of the efficiency. The figures also reveal that the long-distance ground motion records produce the intensity measures with higher efficiency. On the other hand, with respect to amplitude, the small amplitude records demonstrate the higher performance of the intensity measures.

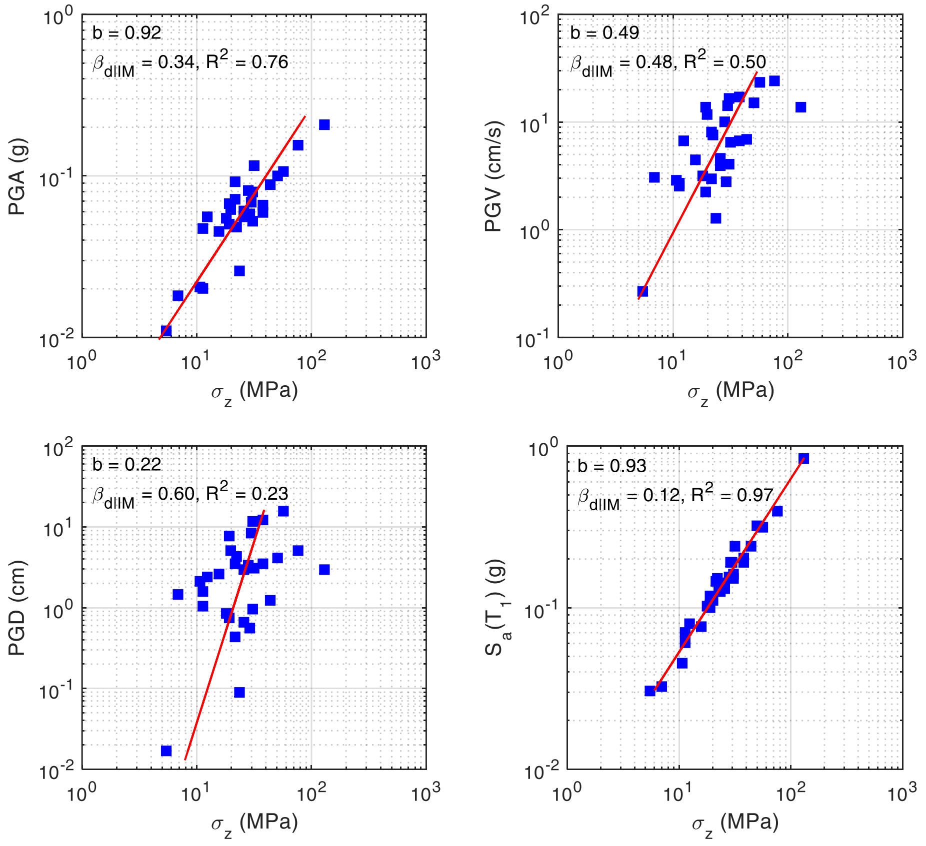

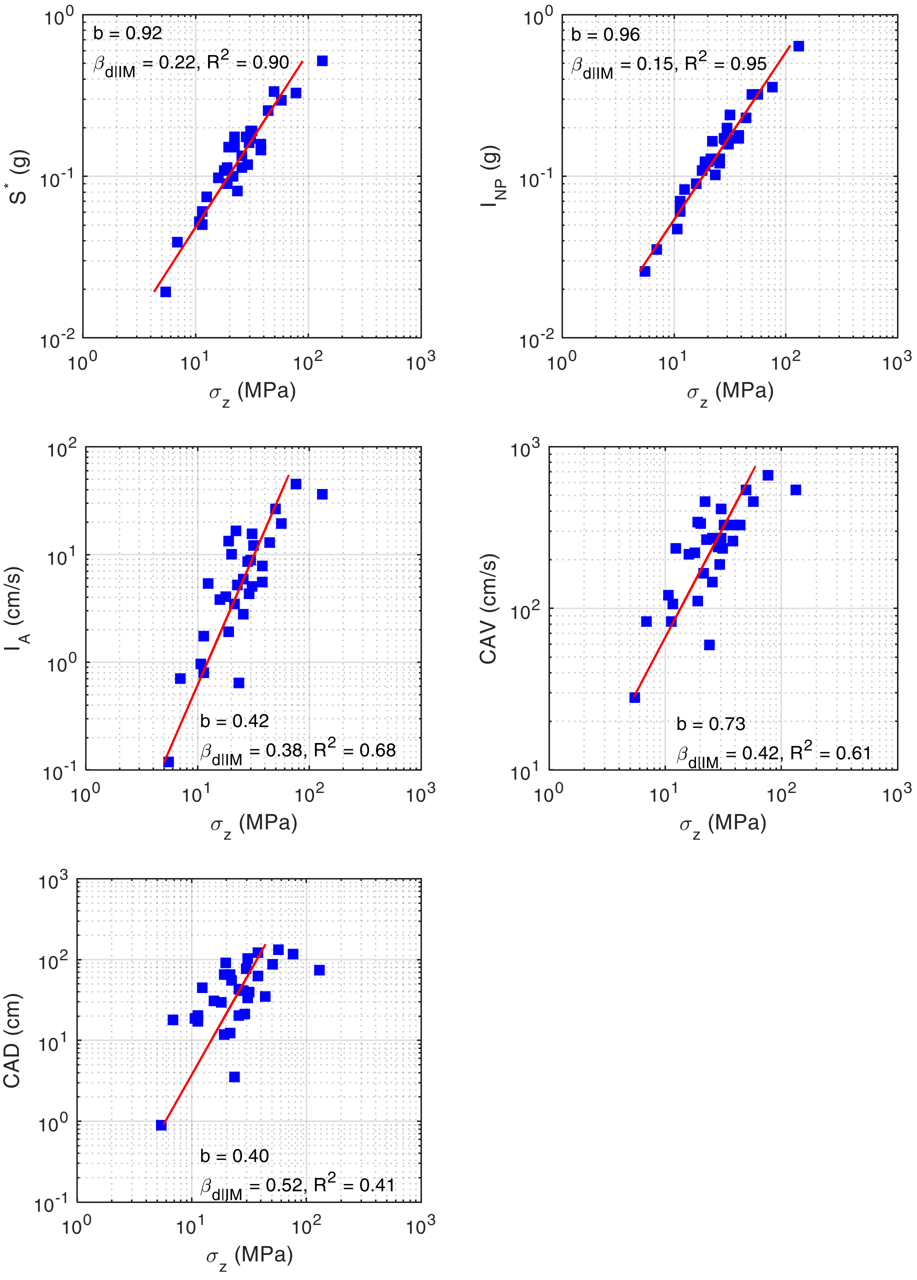

Figure 6.5. Linear regression analysis results for Tank #1 subjected to Bin #1 records

6.4.2 *Intensity measure sufficiency*

The sufficiency of the intensity measures is evaluated by the slope c_1 of the regression line [Eq. (6.4)]. The statistical significance of c_1 on M_W or R_{jb} can be quantified by the p-value for the F statistic of the null hypotheses (c_1 = 0). A small p-value, i.e., less than 0.05, suggests that the estimated coefficient c_1 on M_W or R_{jb} is statistically significant, and therefore, that intensity measure is insufficient (Luco and Cornell 2007). Results of the comparative statistical analysis relative to intensity measure sufficiency are presented in Table 6.10 for the 120 records. The values highlighted in bold are associated with p-values less than 0.05.

Table 6.10. Analysis results of the intensity measure sufficiency

Tank	#1		#2		#3	
	p-val (M_W)	p-val (R_{jb})	p-val (M_W)	p-val (R_{jb})	p-val (M_W)	p-val (R_{jb})
PGA	0.823	0.638	0.574	0.616	0.405	0.607
PGV	0.374	0.258	0.490	0.273	0.525	0.076
PGD	**0.027**	**0.006**	**0.040**	**0.007**	**0.043**	**0.001**
$S_a(T_1)$	0.437	0.823	0.512	0.507	0.159	0.058
S^*	0.778	0.890	0.542	0.746	0.114	0.307
I_{NP}	0.623	0.930	0.356	0.630	0.051	0.110
I_A	0.071	0.358	**0.046**	0.398	**0.047**	0.082
CAV	0.115	0.061	0.089	0.075	0.095	**0.011**
CAD	0.339	0.021	0.435	0.024	0.435	0.004
Tank	#4		#5		#6	
	p-val (M_W)	p-val (R_{jb})	p-val (M_W)	p-val (R_{jb})	p-val (M_W)	p-val (R_{jb})
PGA	0.371	0.634	0.857	0.243	0.274	0.659
PGV	0.567	0.083	0.290	0.645	0.117	0.340
PGD	**0.046**	**0.001**	**0.029**	**0.046**	**0.006**	**0.010**
$S_a(T_1)$	0.174	0.063	0.338	0.455	0.156	0.253
S^*	0.114	0.343	0.841	0.328	0.254	0.823
I_{NP}	**0.036**	0.139	0.742	0.368	0.425	0.636
I_A	**0.033**	0.088	0.283	0.919	0.560	**0.500**
CAV	0.072	**0.012**	0.328	0.444	0.601	0.108
CAD	0.458	**0.005**	0.280	0.127	0.129	**0.036**

In addition, examples of the regression analysis for some representative cases of intensity measures with regard to Tank #1 are shown in Figure 6.6. The analysis results illustrate no significant correlation between the frequency-dependent intensity measures and the ground motion parameters, i.e., M_W or R_{jb}, in most of the cases; this demonstrates the sufficiency of this group.

Among the magnitude-dependent group, PGD shows a significant degree of insufficiency with respect to both the moment magnitude and the source-to-site distance. On the contrary, PGA and PGV display an acceptable sufficiency for all the analysed tanks.

Also of note is that the duration-dependent group shows a considerable degree of insufficiency, especially in terms of R_{jb}.

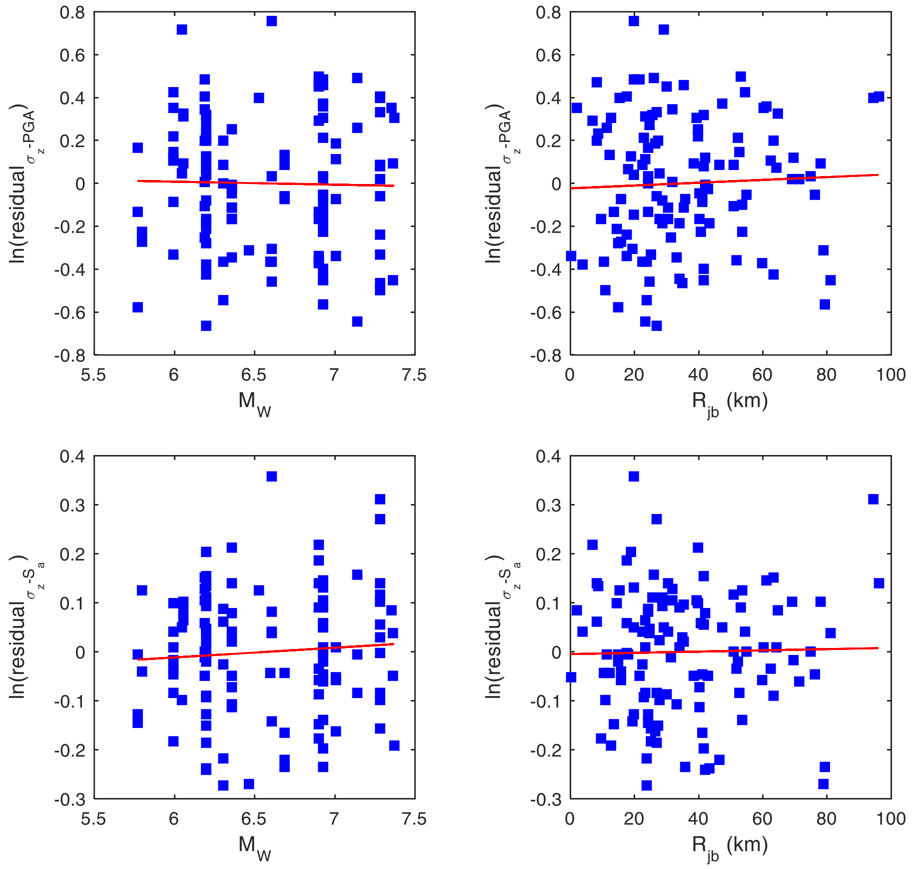

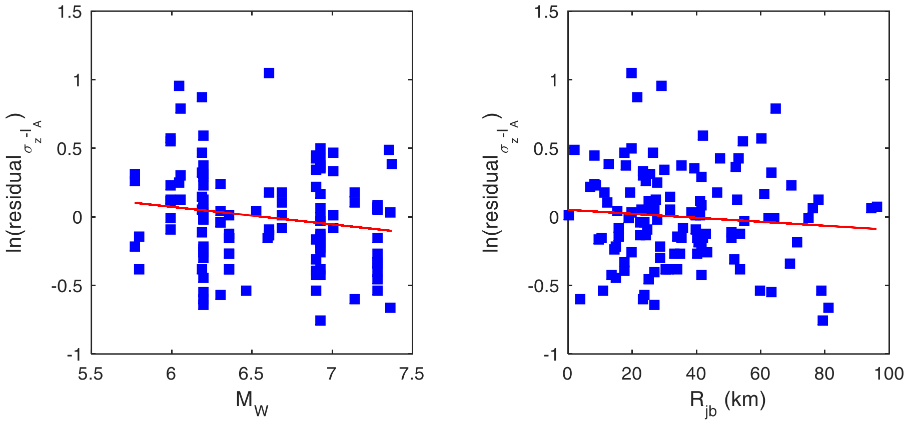

Figure 6.6. Linear regression analysis results of the intensity measure sufficiency for Tank #1

6.5 Closure

In this chapter, a comparative analysis concerning the efficiency and sufficiency of several intensity measures for the probabilistic seismic demand analysis of steel liquid storage tanks is carried out. Sets of magnitude-dependent, frequency-dependent, and duration-dependent intensity measures are investigated. To evaluate the efficiency of the selected intensity measures, a linear regression model between engineering demand parameters and intensity measures is used. In particular, the estimate of the median demand is predicted by using a power model. The sufficiency of each intensity measure is also investigated based on a linear regression, which is performed between the residuals of the above regression analysis and ground motion parameters. Six cases of anchored and unanchored tanks are analysed using four different sets of ground motion records. For this purpose, lumped mass models are used to simulate the seismic behaviour of the storage tanks. A comprehensive comparative analysis leads to the following main conclusions:

- $S_a(T_1)$ is the most efficient intensity measure with respect to the meridional stress demand. In addition, the use of I_{NP} leads to similar values of the dispersion with $S_a(T_1)$, while S^* exhibits a significantly lower performance.
- Among magnitude-dependent intensity measures, PGA shows the best performance. In contrast, PGD shows the weakest performance, especially in the cases of large amplitude records.

- For duration-dependent intensity measures, while I_A provides the higher efficiency, CAV produces an increase of the standard deviation compared with I_A.
- The long-distance ground motion records produce the intensity measures with more efficiency. In contrast, with respect to amplitude, small amplitude records demonstrate the higher performance of the intensity measures.
- Regarding the intensity measure sufficiency, the frequency-dependent intensity measures also show the sufficiency in terms of M_W and R_{jb}. Among the magnitude-dependent group, PGD shows a significantly degree of insufficiency. On the other hand, PGA and PGV display an acceptable sufficiency for all the analysed tanks. The duration-dependent group shows a considerable degree of insufficiency, especially in terms of R_{jb}.

Chapter 7. Seismic vulnerability analysis of unanchored steel liquid storage tanks: Case study #1

7.1 Introduction

Earthquake damage in recent decades (e.g., 1995 Hyogoken-Nanbu Japan, 1999 İzmit Turkey, 2003 Tokachi-oki Japan, 2008 Wenchuan China, 2011 Great East Japan, 2012 Emilia Italy, etc.) has revealed that above ground storage tanks, in particular unanchored tanks, are one of the most vulnerable components in an industrial facility. Damage to tanks can cause significant disruption to the facility operation. In fact, the extensive seismic-induced uncontrolled fires, when flammable materials or hazardous chemicals leak, naturally increase the overall damage to nearby areas. As mentioned in Section 3.1, the seismic response analysis of above ground tanks has been widely studied in the past. The basic idea of the modelling is based mainly on the spring-mounted masses analogy proposed by Housner (1963). This analogy is derived from the solution of the hydrodynamic equations that describe the behaviour of liquid inside a rigid container, fixed to the foundation. Due to practical and economic reasons, many liquid storage tanks have been directly constructed on the compacted soil without anchoring. The dynamic behaviour of unanchored tanks is considerably different from that of rigidly anchored ones. The uplift mechanism of unanchored tanks, developed in response to large overturning moment, is the dominant response under seismic loads. Associated with the bottom plate uplift, significant plastic rotations of the shell-to-bottom plate joint and intensive stresses in the tank wall are developed. As a sequence of work, Malhotra and Veletsos (1994a, 1994b, 1994c) studied the uplift behaviour of the bottom plate of an unanchored tank by idealising the bottom plate as a series of uniformly loaded semi-infinite, prismatic beams that rest on a rigid foundation. However, extensive researches on the uplift behaviour may need a more refined approach, which is based on the nonlinear finite element model of the tank-liquid system.

Prediction and prevention of possible accidental scenarios depend upon the reliability of available tools used to evaluate quantitatively the effects of the seismic action on the equipment. An emerging tool, i.e., seismic fragility curves, provides valuable support for seismic risk assessment of equipment in industrial installations (Salzano et al. 2003, Fabbrocino et al. 2005, Alessandri et al. 2017). These curves are conditional probability statements of potential levels of damage over a range of earthquake intensities and can be used as initial fragility-based damage scenarios in the seismic risk assessment procedure (Alessandri et al. 2017). A number of studies on the fragility evaluation for tanks have been reviewed in Section 5.2, involving empirical, expert judgment-based, and analytical fragility curves. Most of them assume that material and geometric properties are deterministic. However, because of the large scale of above ground tanks, especially broad tanks, the source of uncertainties associated with material and geometry could affect the performance of the tanks. The assessment of which parameters significantly affect the seismic response of tanks appears necessary, which allows finding the most important parameters utilised in the fragility evaluation.

There is a certain number of studies devoted to the sensitivity of the seismic response and fragility of bridges, buildings, and gravity dams (e.g., Nielson and DesRoches 2006, Kwon and Elnashai 2006, Padgett and DesRoches 2007, Bernier et al. 2015). However, limited contributions are available for tanks. A primarily work related to this subject was by Malhotra and Veletsos (1994c), where the sensitivity of the tank response to the ground motion intensity and the plate thickness was investigated by a simplified model. Based on the beam model proposed by Malhotra and Veletsos (1994a), Bakalis et al. (2016) performed static analyses with varying values of modelling parameters to investigate their effect on the uplift response of an unanchored tank. However, these studies were mainly based on the simplified model of tanks and in a deterministic way with discrete values of modelling parameters. Moreover, the sensitivity of seismic fragility curves of tanks to the modelling parameters has not been investigated.

This chapter aims to present an appropriate methodology for the vulnerability analysis of an unanchored cylindrical steel liquid storage tank, named as Case study #1, which is ideally located in a refinery in Sicily (Italy). The significance of a number of modelling parameters associated with material and geometric uncertainties is first examined for the tank based on a screening study, where a nonlinear finite element model of the tank is used. The significant modelling parameters previously defined are then incorporated into the fragility analysis of the tank by a proper sampling approach. Nonlinear time history analyses are performed on a simplified model of the tank, where both nonlinear uplift and sliding mechanisms are included. A suitable probabilistic seismic demand model of the tank, based on the CA method, is presented to derive the fragility curves. The relative importance of ground motion and modelling parameter uncertainties on the fragility curves of the tank is assessed and discussed in detail.

7.2 Description of case study

An existing tank ideally installed in a refinery in Sicily (Italy), which well represents a broad geometry, is selected for this study. The representative tank, named as TK 60, is selected from a group of eleven unanchored tanks, as shown in Figure 7.1; this is a specific case study of the petrochemical plant that is considered within the framework of the INDUSE-2-SAFETY project. The tank is a 54.8-m-diameter cylindrical steel tank and unanchored with respect to the foundation. The tank height is 15.6 m, and the capacity of the tank is 37044 m^3. The tank is provided with a floating roof; however, the effect of the floating roof is neglected in this study. The shell thickness has been designed varying from 8 mm at the top course to 33 mm at the bottom course. The bottom plate has a uniform thickness of 8 mm. The tank is filled with crude oil at a filling level of 14 m (i.e., 90% of the tank height). Both shell and bottom plate are structured by S235 carbon structural steel having a yield strength of 235 MPa. The schematic of the examined tank in front view is shown in Figure 7.2. The detailed shell-to-bottom plate joint and top ring of the tank are also shown in the figure. More detail of nominal material and geometry properties is illustrated Table 7.1.

Table 7.1. Nominal material and geometry properties of the tank

	Property	Design value
Tank	Density (kg/m^3)	7850
	Young’s modulus (MPa)	200000
	Poisson's ratio	0.3
	Yield strength (MPa)	235
	Radius of tank (m)	27.432
	Height of tank (m)	15.6
	Bottom plate thickness (mm)	33, 29.5, 25.5, 21.5, 17.5, 14, 10, 8, 8, 10
	Shell plate thickness (mm)	8
Liquid	Density (kg/m^3)	900
	Liquid level (m)	14

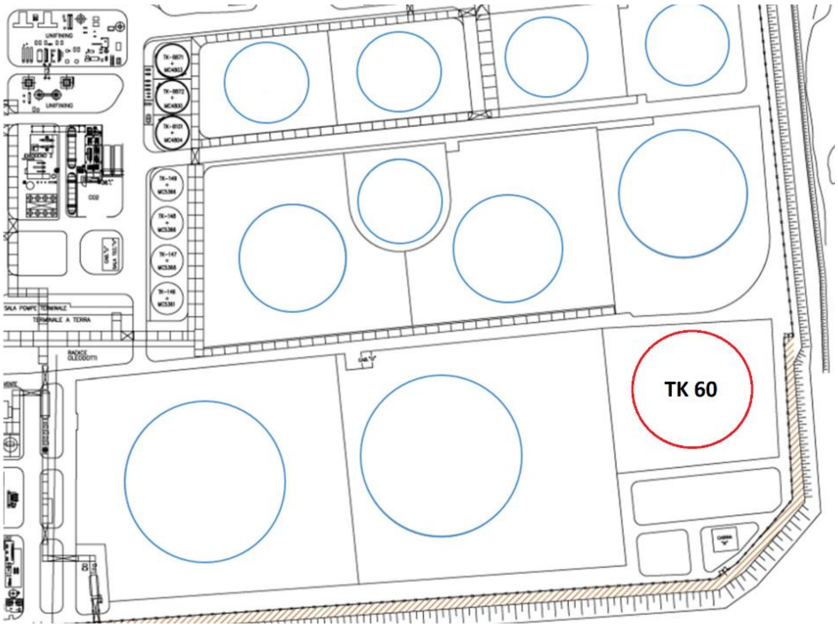

Figure 7.1. Plan view of the group of tanks

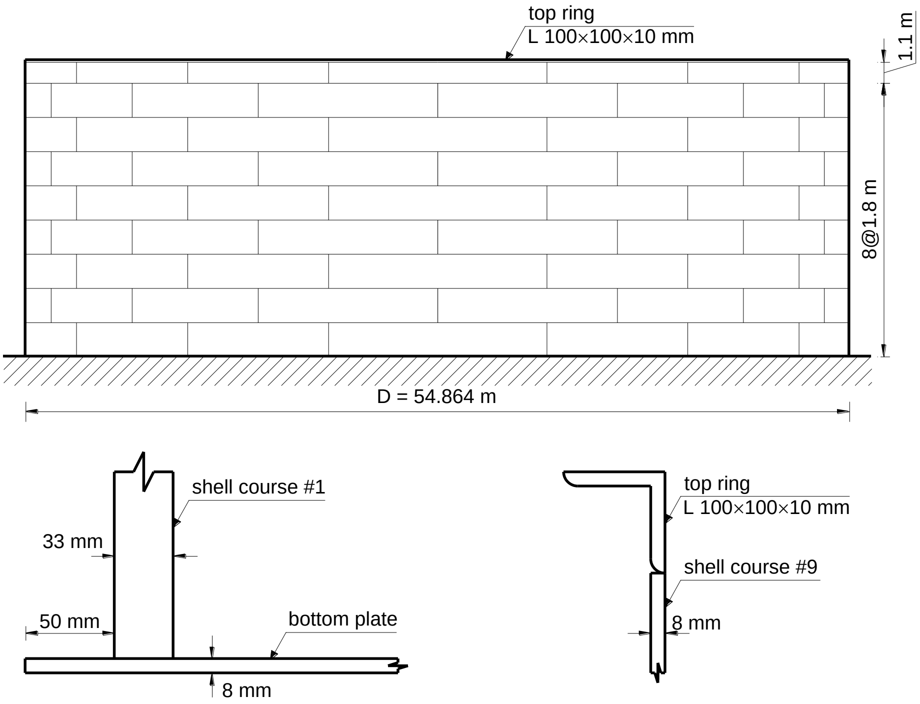

Figure 7.2. Schematic of the tank

7.3 Seismic hazard analysis and ground motion selection

The facility is supposed to be ideally placed in one of the most seismically active zones in Sicily (Italy), characterized by a soil type B. Probabilistic seismic hazard analysis has been conducted with reference to a latitude of 37.17°, a longitude of 15.17°, a radius of 100 km, and a reference time of 1 year (Giannini 2000). Seismogenic zones number 929, 932, 933, 935, and 936 identified by the Italia zonation ZS9 have been selected, as shown in Figure 7.3. The hazard curve $[S_a(T = 0)]$ is shown in Figure 7.4.

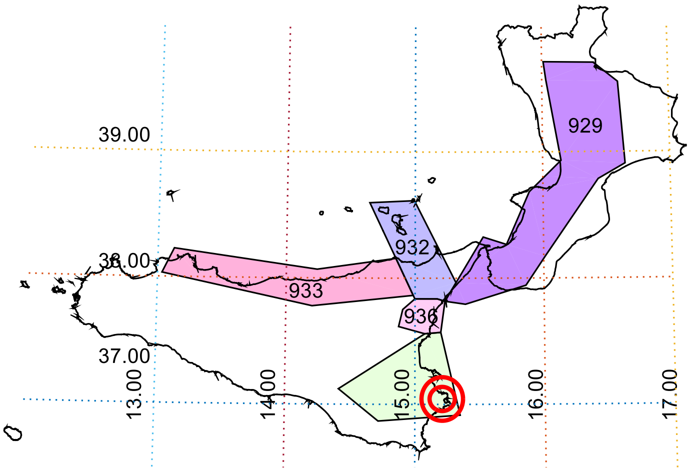

Figure 7.3. Seismogenic zones from the Italian catalogue

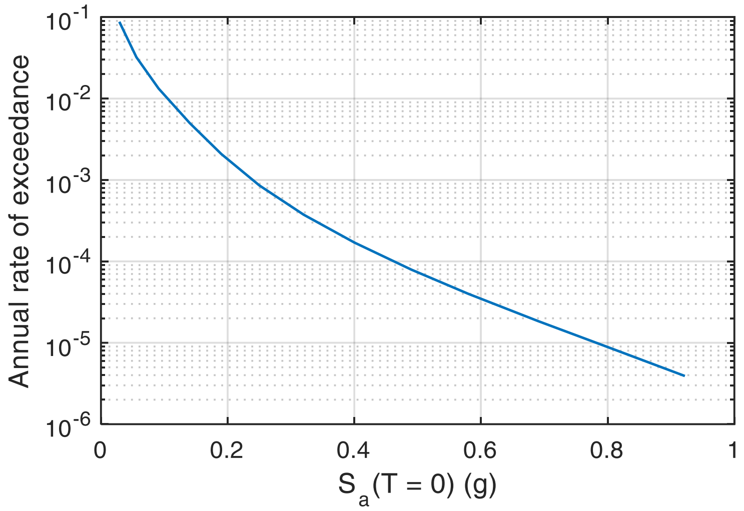

Figure 7.4. Seismic hazard curve for the site

Mean uniform hazard spectra (UHS) for different return periods are calculated. In particular, the UHS are obtained for seven different return periods, i.e., T_r = 75 years, T_r = 130 years, T_r = 240 years, T_r = 430 years, T_r = 780 years, T_r = 1400 years, and T_r = 2500 years. The plot of the UHS is shown in Figure 7.5.

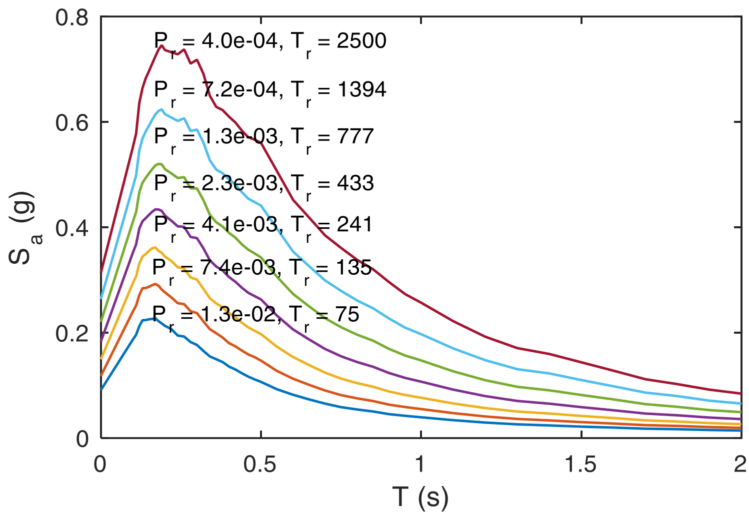

Figure 7.5. Mean UHS for different return periods

A set of 20 compatible accelerograms for each UHS is selected, resulting in a total of 140 accelerograms. The selection is conducted with the following parameters:

- moment magnitude: 4.5-7.5,
- source-to-site distance: 3-80 km,
- soil type: B,
- and period interval: 0.001-4 s.

The records of each set are selected so that the mean response spectrum and its 84% fractile have the best fit to those of the target UHS. Seven sets of selected ground motions are shown in Figure 7.6.

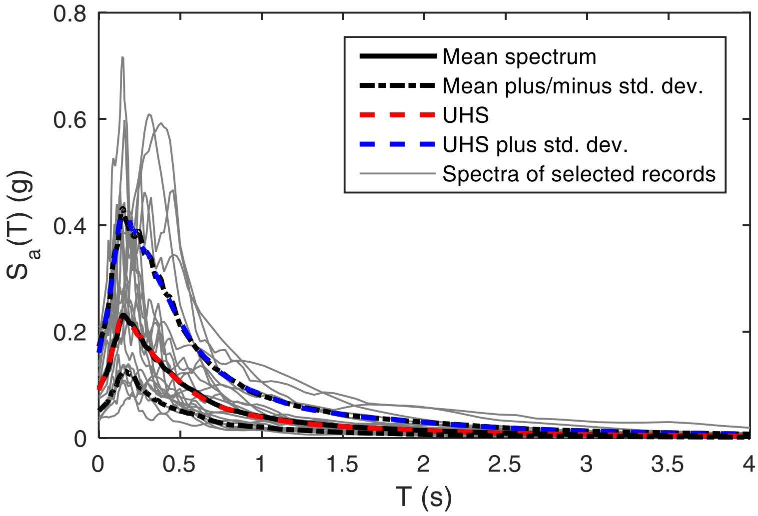

Return period, T_r = 75 years

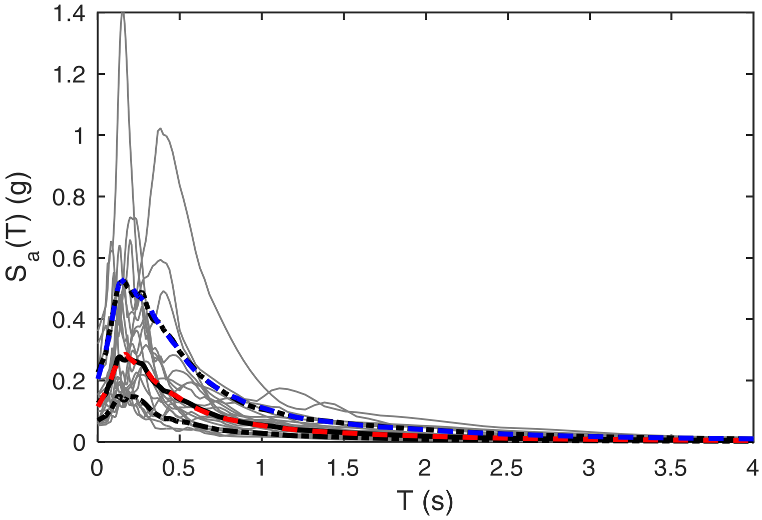

Return period, T_r = 130 years

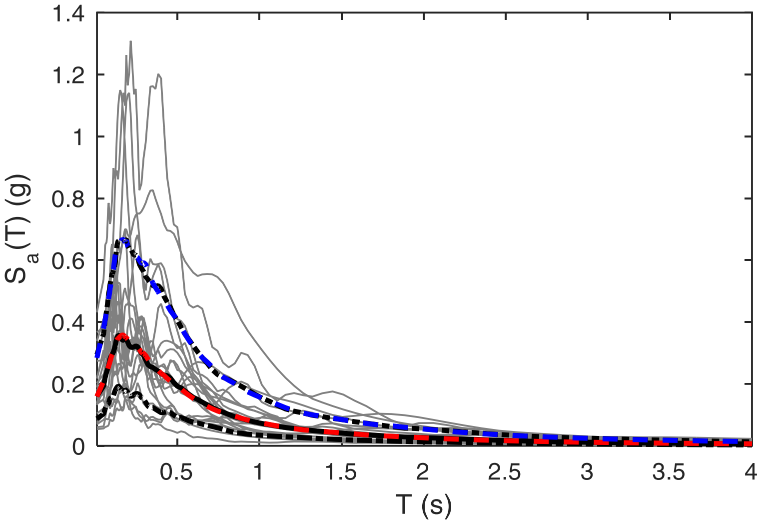

Return period, T_r = 240 years

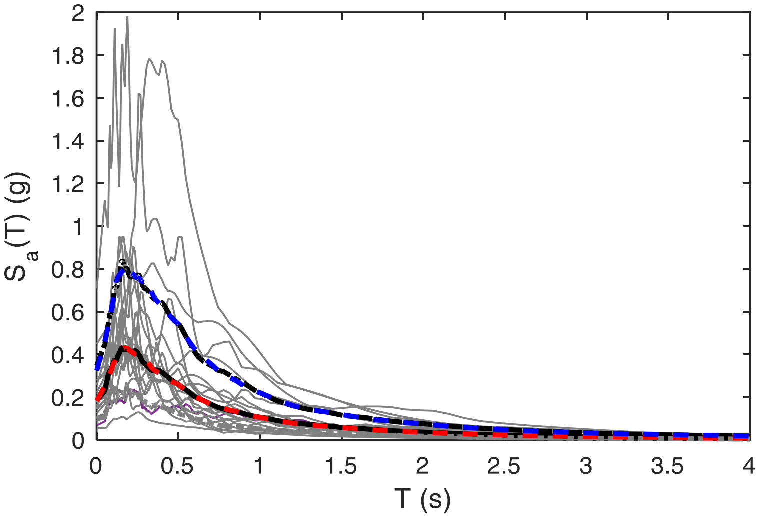

Return period, T_r = 430 years

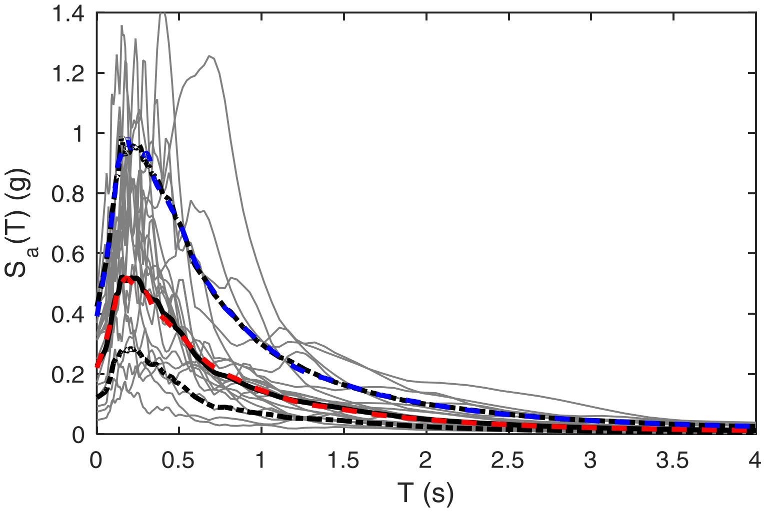

Return period, T_r = 780 years

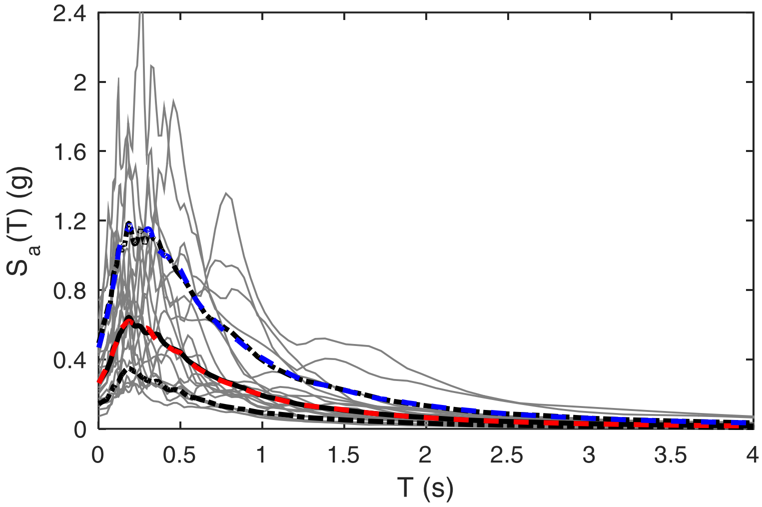

Return period, T_r = 1400 years

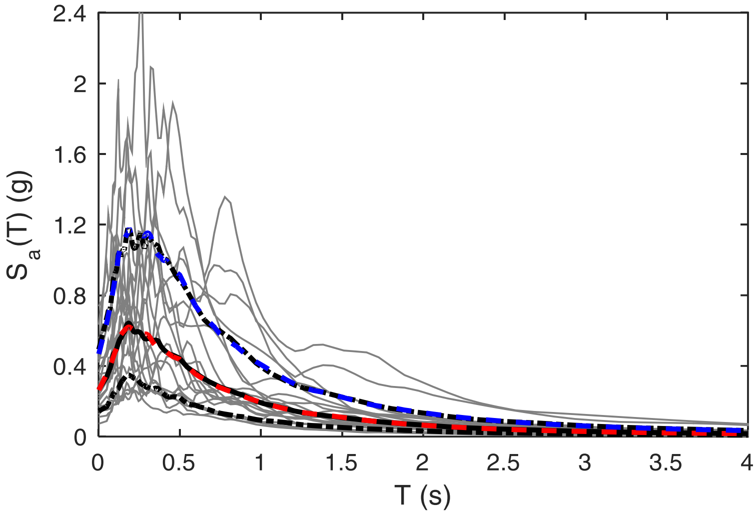

Return period, T_r = 2500 years
Figure 7.6. Selection of 7 sets of ground motions according to UHS

7.4 Numerical model

7.4.1 Nonlinear finite element model

Regarding the objective of the work, two different numerical models of the examined tank are used. The static pushover analysis procedure for the tank described in Chapter 3 is used first for the sensitivity analysis and later for the calibration of the spring-mass model. The procedure is based on a three-dimensional finite element model using the ABAQUS software, where both geometric and material nonlinearities are considered.

The shell and bottom plate are modelled using four-node shell elements with reduced integration. The system is assumed resting on a rigid foundation that is modelled using solid elements. The successive contact and separation between the bottom plate and its rigid foundation are taken into account by a surface-based contact modelling algorithm (SIMULIA 2014). The penalty based method, i.e., a stiff approximation of hard contact, is used for simulating the frictional contact between the bottom plate and the foundation. A friction coefficient of 0.4 is assumed according to the suggestion in API 650 (2007). In order to take into account the variability of yield strength, an elastic-perfectly plastic von Mises type material model is used to present a nonlinear plastic law of the steel tank. Because of the structural symmetry, only half of the tank system is modelled, and symmetry plane boundary conditions are employed to reduce the computational time. A mesh convergence study is first performed leading to an optimal mesh size of 0.4 m in the longitudinal direction and 0.8 m in the circumferential direction. The mesh region near the shell-to-bottom plate joint is more refined with 0.2 m in the longitudinal direction. The three-dimensional finite element mesh of the tank model is illustrated in Figure 7.7.

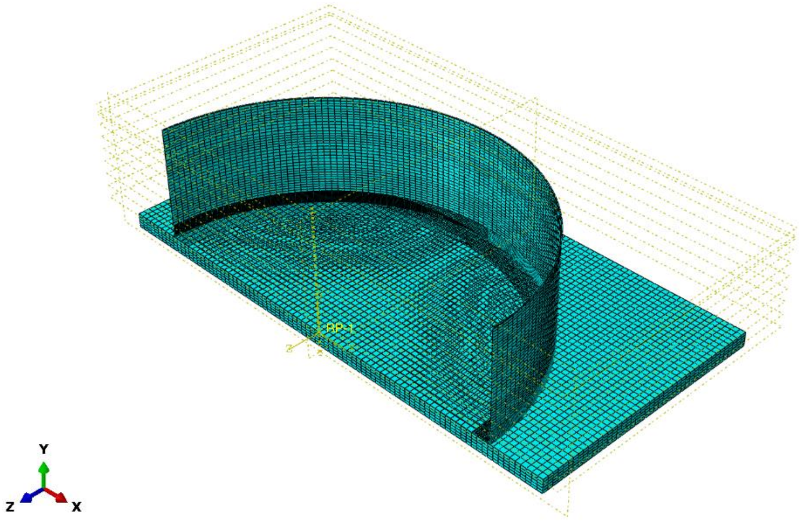

Figure 7.7. Three-dimensional finite element mesh of the tank model

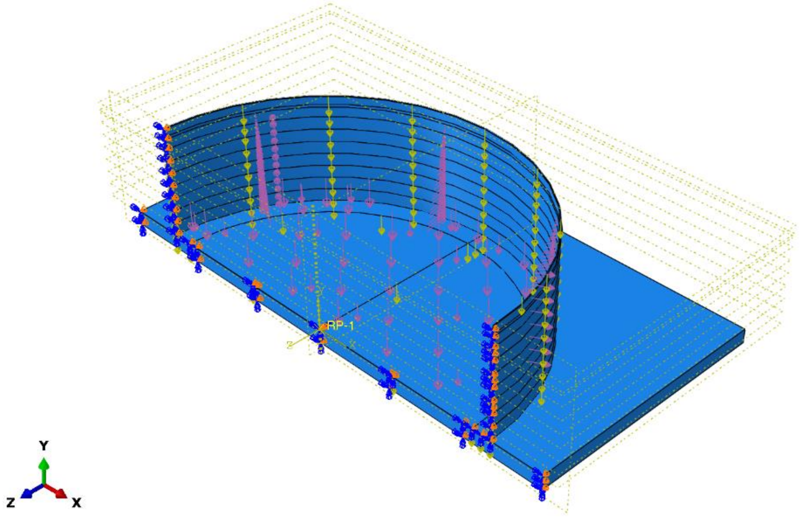

Figure 7.8. Loadings and boundary conditions of the tank model

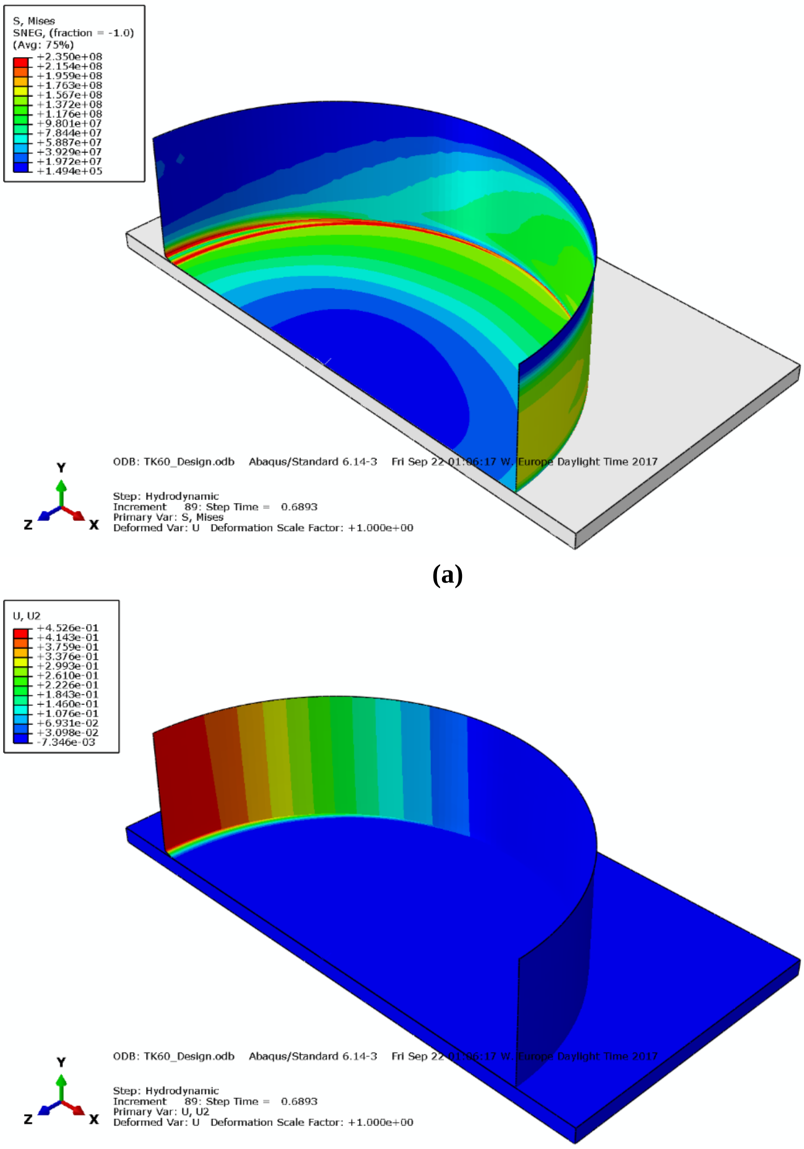

(a)

(b)

Figure 7.9. Contours of the von Mises stress (a) and the vertical displacement (b) of the tank obtained at an acceleration level of 0.69 g

Due to the limited effect of the convective component to the response of the tank, only the impulsive component is considered in the analysis. In the case of broad tanks, the impulsive pressure distributions on the shell and bottom plate due to the liquid motion for rigid and flexible tanks are similar (Veletsos and Yang 1977). It is possible to use an impulsive pressure coefficient that is the solution of a rigid circular cylinder, fixed to a rigid base. Therefore, the impulsive hydrodynamic pressures acting on the shell and bottom plate, which are normalised with the ground acceleration, can be calculated using Eq. (3.26). The loads are applied as a distributed surface load (i.e., pressure) to the shell and bottom plate, as shown in Figure 7.8, using the DLOAD subroutine (SIMULIA 2014).

The pushover analysis is conducted with an increase of the ground acceleration magnitude. The von Mises stress and deformation of the tank obtained at an acceleration level of 0.69 g are shown in Figure 7.9. The maximum uplift of the base plate measured at this magnitude is 0.45 m. Figure 7.10(a) shows two different curves of the $M_{OT} - \psi$ relationship caused by different loadings acting on the bottom plate, with and without hydrodynamic pressure at the bottom plate of the examined tank, and the relationship between the uplift length and uplift $(L - w)$ is presented in Figure 7.10(b). It can be noticed the strong influence of the impulsive pressure at the bottom plate both in terms of overturning moment and rotation demands. Moreover, the uplift length appears to be limited at maximum values of 2.1 m (with impulsive pressure at the bottom plate) and 1.1 m (without impulsive pressure at the bottom plate), which correspond to maximum uplift displacements of about 0.45 m and 0.25 m, respectively.

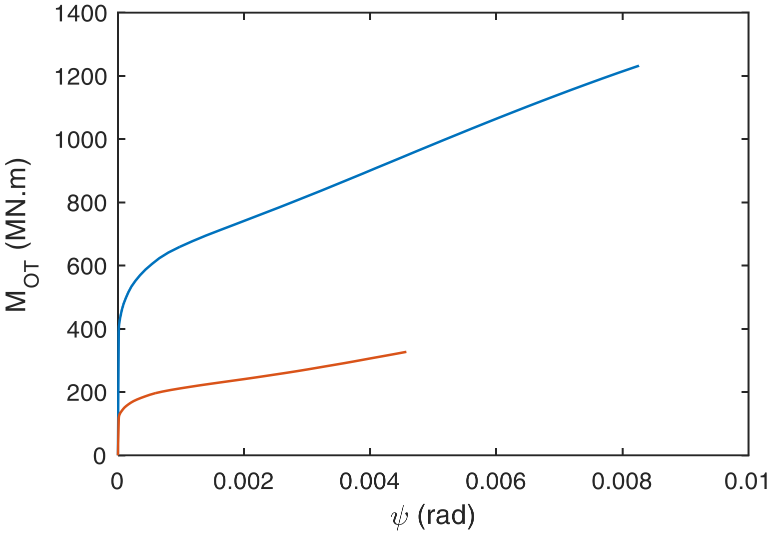

(a)

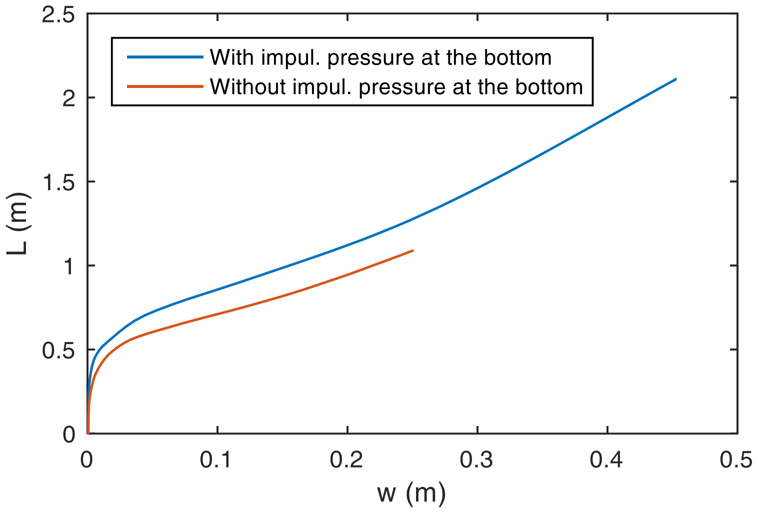

(b)

Figure 7.10. Static pushover analysis results of the tank: (a) overturning moment-rotation curve and (b) uplift length-uplift curve

7.4.2 Calibrated spring-mass model

The calibration procedure that is based on the pushover analysis results of the tank is used. The detailed description of the model is illustrated in Chapter 3. The dynamic parameters of the spring-mass model are calculated from the static pushover analysis results, as shown in Table 7.2. The uplift mechanism of the bottom plate is modelled by adding a rotational spring that represents the rocking resistance of the bottom plate. The $M-\psi$ relationship is obtained from the above static pushover analysis, as shown in Figure 7.10.

Table 7.2. Dynamic parameters of the tank model

Parameter	Calibrated
Total impulsive mass, m (T)	10001
Impulsive natural frequency, ω_i (rad/s)	26.29
Stiffness, k (kN/m)	6906001
Damping coefficient (kN-s/m)	10512
Equivalent height, h (m)	20.325

7.5 Screening study

7.5.1 Modelling parameters

In this study, the two main sources of uncertainty are classified as ground motion and modelling parameters. The uncertainty in earthquake ground motions is previously described in Section 7.3 with a ground motion selection procedure based uniform hazard spectra. The uncertainty in modelling parameters is considered with the selection of six parameters, involving both geometric and material of the examined tank, as shown in Table 7.3.

The uncertainty for geometric parameters of the tank is presented in terms of the filling level of the liquid, the shell plate thickness, and the bottom plate thickness. The liquid level changes approximately from 80% to 100% of the tank height and follows a uniform distribution. This range of filling level is selected according to the suggestion from HAZUS (2001), where fragility curves have been presented for 80-100% filling level of unanchored tanks. The thickness uncertainty is affected by nominal thickness, steel type, measurement technique, presence of a surface coating, amount of plate deformation, etc. According to the suggestion of Daidola and Basar (1980) for various thicknesses of the plate, the coefficient of variance (COV) of the plate thickness t is averaged as $0.06/t$. It is convenient to define that the ratio bias is the ratio between the measured value and the nominal value. Therefore, the ratio bias of the plate thickness has a mean value of 1.0 and a COV of 0.06 and is assumed to follow a normal distribution. The 5th and 95th percentiles of the plate thickness ratio bias are 0.9 and 1.1, respectively.

Table 7.3. Modelling parameters considered in sensitivity analysis

	Modelling parameter	Probability distribution	Distribution parameters	
1	Filling level (m)	Uniform	L = 12.6	U = 15.6
2	Shell plate thickness ratio bias	Normal	μ = 1.0	COV = 0.06
3	Bottom plate thickness ratio bias	Normal	μ = 1.0	COV = 0.06
4	Steel yield strength (MPa)	Normal	μ = 235	COV = 0.09
5	Young’s modulus (MPa)	Normal	μ = 200000	COV = 0.03
6	Liquid density (kg/m^3)	Uniform	L = 870	U = 920

The material strength variable of steel considered in this work is the yield strength of the shell and bottom plate. Mansour et al. (1984) suggested that the weighted average of the COV values for data of more than 60000 samples is 0.09. The 5th and 95th percentiles of a normal distribution of mean 235 MPa and this COV value are 200 MPa and 270 MPa, respectively. The Young's modulus is assumed to be normally distributed with a mean value of 200000 MPa and a COV of 0.03 based on the work by Mansour et al. (1984). The Poisson's ratio is considered non-random with a deterministic value of 0.3. The contained liquid is medium crude oil. The density varies from 870 kg/m^3 to 920 kg/m^3 and follows a uniform distribution. The lower and upper levels for the six modelling parameters are shown in Table 7.4. The lower and upper levels correspond to the lower and upper bounds of the uniform distributions or the 5th and 95th percentiles for the normal distributions.

Table 7.4. Lower and upper levels of the modelling parameters

	Modelling parameter	Lower	Upper
1	Filling level (m)	12.6	15.6
2	Shell plate thickness ratio bias	0.9	1.1
3	Bottom plate thickness ratio bias	0.9	1.1
4	Steel yield strength (MPa)	200	270
5	Young's modulus (MPa)	190000	210000
6	Liquid density (kg/m^3)	870	920

7.5.2 Analysis of variance

The ANOVA is a procedure to assess which modelling parameters have a significant effect on the dominant response of the tank, i.e., the uplift response. The analysis procedure is based on the static pushover model of the tank and a DOE approach. The procedure is as follows:

- A two-level fractional factorial design is generated using the parameters listed in Table 7.3; this is a statistical approach which investigates the significance of each factor while reducing the computational effort as compared to a conventional full factorial experiment. In the two-level design, each parameter is considered at its upper and lower values. For six modelling parameters in Table 7.3, 16 samples of the tank model with various permutations of upper and lower levels of the modelling parameters are required, as shown in Table 7.5. The lower and upper levels correspond to the lower and upper bounds of the uniform distributions or the 5th and 95th percentiles for the normal distributions.

- For each sample, a nonlinear static pushover analysis is performed. The acceleration magnitude is increased from 0.0 g to 0.6 g with a step size of 0.01 g. The response in terms of the uplift displacement of the bottom plate is monitored at three representative levels of the ground acceleration (i.e., 0.2 g, 0.4 g, and 0.6 g).
- For the response at each acceleration level monitored, an ANOVA is conducted. The ANOVA performs hypothesis tests that verify the significance of varying each parameter on the variance of the measured response.

Table 7.5. 16 samples of the tank model with various permutations of upper and lower levels of the modelling parameters

Sample	Modelling parameters					
	(1)	(2)	(3)	(4)	(5)	(6)
1	-1	-1	-1	-1	-1	-1
2	-1	-1	-1	1	1	1
3	-1	-1	1	-1	1	1
4	-1	-1	1	1	-1	-1
5	-1	1	-1	-1	1	-1
6	-1	1	-1	1	-1	1
7	-1	1	1	-1	-1	1
8	-1	1	1	1	1	-1
9	1	-1	-1	-1	-1	1
10	1	-1	-1	1	1	-1
11	1	-1	1	-1	1	-1
12	1	-1	1	1	-1	1
13	1	1	-1	-1	1	1
14	1	1	-1	1	-1	-1
15	1	1	1	-1	-1	-1
16	1	1	1	1	1	1

Note: (1) Filling level, (2) Shell plate thickness, (3) Bottom plate thickness, (4) Steel yield strength, (5) Young’s modulus, and (6) Oil density

The results of the hypothesis tests are given in terms of a p-value, and a smaller p-value indicates greater evidence that the parameter has a strong influence on the tank response. For this study, parameters with a p-value less than a cutoff of 0.05 are considered significant. Results of the ANOVA are shown in Table 7.6, where the boldface parameters are associated with p-values below 0.05 and indicate statistically significant parameters.

Table 7.6. ANOVA results

	Modelling parameter	p-value		
		A_g = 0.2 g	A_g = 0.4 g	A_g = 0.6 g
1	Filling level	**0.001**	**0.000**	**0.000**
2	Shell plate thickness	0.217	**0.001**	**0.000**
3	Bottom plate thickness	**0.022**	**0.000**	**0.000**
4	Steel yield strength	0.808	0.206	**0.000**
5	Young’s modulus	0.795	0.487	**0.003**
6	Liquid density	0.513	0.217	**0.000**

The most important parameters for this tank, which significantly affect the uplift response at all three acceleration levels are the geometry parameters, i.e., the filling level of the tank and the thickness of the bottom plate. Given a deterministic value of the tank radius, the filling level is associated with the aspect ratio of the tank, and thus this results in the significant change of pressure distributions acting on the shell and bottom plate as well as the uplift response of the tank, as illustrated in Figure 7.11.

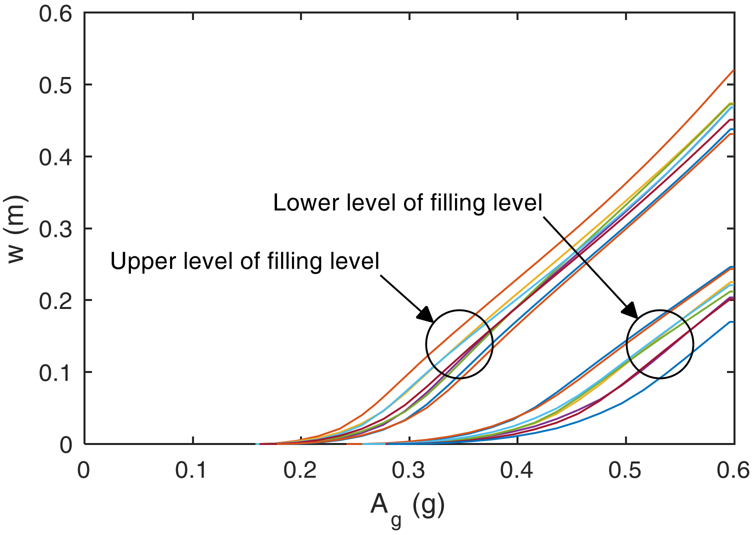

Figure 7.11. Uplift response of the model samples obtained from the static pushover analyses

The bottom plate thickness is also very significant, along with the shell plate thickness. The parameters have a more significant effect when the hydrodynamic pressure increases. In the contract, the material parameters have slight effects at low magnitudes of A_g, e.g., in this case, A_g is less than 0.4 g. The statistical significance of these parameters is found when A_g reaches 0.6 g. Given that in the fragility analysis, a large number of ground motions lead to different levels of the acceleration response. Therefore, the modelling parameters may have a significant effect on the seismic fragility of the tank. It can be suggested that they should be considered in the fragility analysis.

7.6 Fragility curve development

7.6.1 Model sampling

Statistically significant samples of the tank system are derived using Latin Hypercube Sampling (LHS). LHS is a variance reduction sampling method that stratifies variable marginal distributions to fully cover the range of each variable in a more efficient way than pure Monte Carlo sampling (McKay et al. 1979). LHS is used herein to obtain a total of 12 tank samples, as shown in Table 7.7, by sampling the modelling parameters in Table 7.3.

Table 7.7. 12 samples of the tank model generated using LHS

Sample	Modelling parameters					
	(1)	(2)	(3)	(4)	(5)	(6)
1	14.1	0.969	1.115	270.2	201850.0	890
2	15.3	1.057	1.001	214.1	200885.1	913
3	13.4	0.937	1.051	243.0	187831.5	878
4	13.7	0.958	1.024	201.0	197153.3	882
5	15.1	0.911	0.875	215.8	203022.3	920
6	13.3	0.984	1.035	230.5	205447.5	886
7	14.8	0.995	0.971	239.3	193408.1	907
8	15.6	1.158	0.995	225.1	206605.5	898
9	13.0	1.027	0.986	258.1	209083.7	910
10	14.4	1.013	1.079	245.4	195824.5	894
11	12.7	1.069	0.943	232.1	197512.4	902
12	14.2	1.006	0.918	252.5	199023.5	873

7.6.2 Model calibration and probabilistic seismic demand model

The simulation of each sample is first defined by performing the nonlinear pushover analysis in the ABAQUS software.

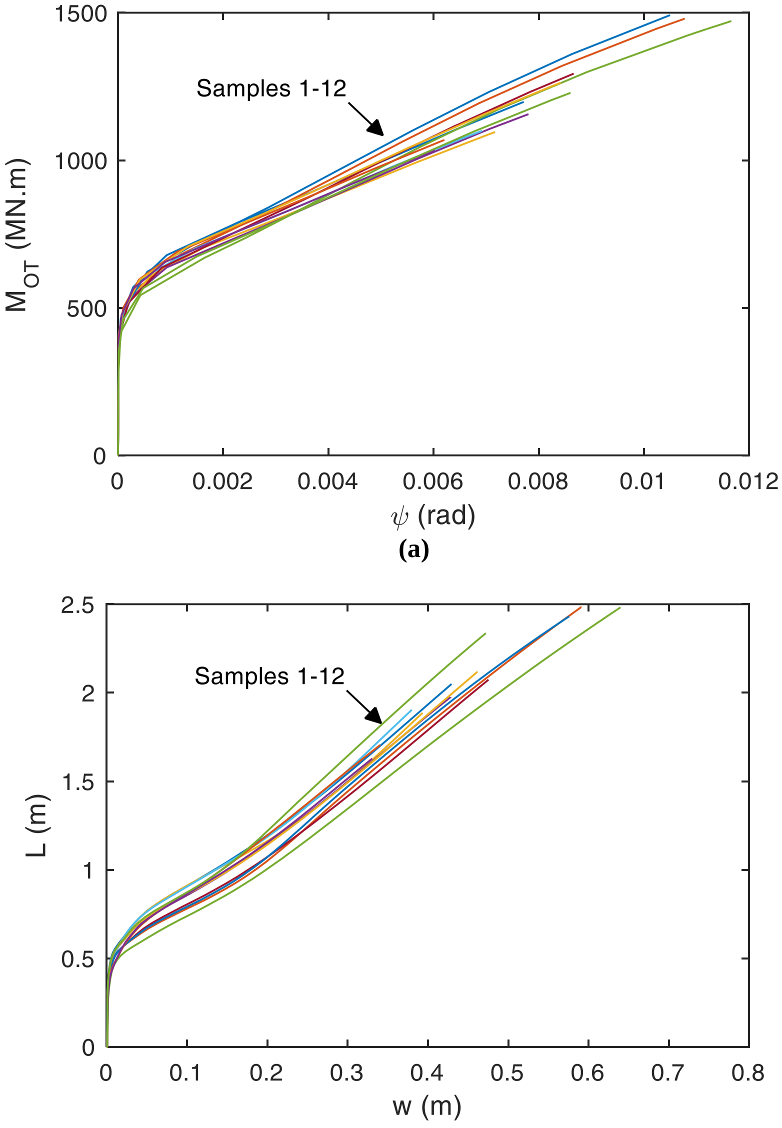

(a)

(b)

Figure 7.12. Variation of uplift and uplift length of the generated samples: (a) overturning moment-rotation curve and (b) uplift length-uplift curve

A spring-mass model of each sample is then calibrated from the pushover analysis results. The variation of uplift and uplift length obtained from the pushover analyses for the generated samples is shown in Figure 7.12. The curves of $M - \psi$ and $L - w$ relationships are presented, and will be used as an input for the calibration of the spring-mass models.

The spring-mass models of the samples are randomly paired with the seven sets of ground motion records. Nonlinear time history analyses are then performed on each ground motion-sample pair. The critical responses of the examined tank are obtained from the nonlinear time history analyses. The response quantities examined include the plastic rotation of the shell-to-bottom plate joint and the maximum compressive stress in the tank wall. The calculations of the responses are described in Section 3.5.

The probabilistic seismic demand model described in Chapter 5, i.e., the CA method, is used in this study. In this model, the estimate of the median demand, as well as the dispersion, are conditioned on an intensity measure, the degree of uncertainty in the model is dependent on the intensity measure used. As proposed in Chapter 6, $S_a(T_i)$ is the most efficient and sufficient intensity measure for both slender and broad tanks, and will be used for the fragility evaluation of this case study.

7.6.3 Determination of damage states and limit state capacities

The commonly observed failure modes of unanchored steel liquid storage tanks during past earthquakes involved elephant's foot buckling of the bottom shell course and plastic rotation of the shell-to-bottom plate joint (Malhotra and Veletsos 1994c, Cortes and Prinz 2017). These failure modes have occasionally resulted in the loss of contents due to the weld or piping fracture (Alessandri et al. 2017).

The elephant's foot buckling is caused by the concentration and high magnitude of the compressive stress developed in the shell when the tank base is uplifted from the ground support. The maximum compressive meridional stress in the shell (σ_z) is calculated using equations (3.48) and (3.52). The critical buckling stress is calculated using the formula developed by Rotter (1985), as presented in Eq. (3.56).

It is noticed that the buckling stress limit is in terms of the maximum pressure response of the seismic analysis. Thus it is conditioned on the IM. The median estimate of the EFB limit can also be predicted by the power function cIM^d, where c and d are the coefficients of the regression analysis. For example, in the case of nominal properties of the tank are considered, the median of the EFB limit is equal to $109.28IM^{-0.05}$.

The second common failure mode developed at the joint of the shell and bottom plate is due to the plastic rotation of the joint caused by the base uplift. The rotation demand of the shell-to-bottom plate joint (θ) associated with an uplift at the edge and a base separation is given in Eq. (3.53), which should be less than the estimated rotation capacity of 0.20 radians.

The probability distributions of the capacity for all damage states are assumed to follow a lognormal distribution. The uncertainty associated with the limit states is given in the form of a lognormal standard deviation or dispersion. A dispersion value of 0.5 is assumed for both the limit states (Nielson and DesRoches 2007, FEMA 2012). The summary of median and dispersion values for the limit states used in this study is shown in Table 7.8.

Table 7.8. Median and dispersion values for the limit states

Damage state	Median	Dispersion
Shell buckling	cIM^d MPa	0.5
Shell-to-bottom plate joint failure	0.2 rad	0.5

7.6.4 Fragility evaluation

The seismic demand placed on each component is assessed against its capacity, or limit state, which is modelled by a lognormal distribution. The regression analysis results for the two demands are shown in Figure 7.13. The fragility curve for each failure mode is then generated using Eq. (5.5). The plot of fragility curves is shown in Figure 7.14. It is observed that the failure of the shell-to-bottom plate joint in the examined unanchored tank is more frequent, with a failure probability of 50% at $S_a(T_i)$ = 1.0 g. The results show a high seismic demand of the shell-to-bottom plate joint rotation when the tank is partially uplifted. The exceeding of the design buckling stress in the tank wall is instead limited. A high seismic demand ($>$ 50%) related to the shell buckling failure mode can be recognised when $S_a(T_i) > 2.0$ g.

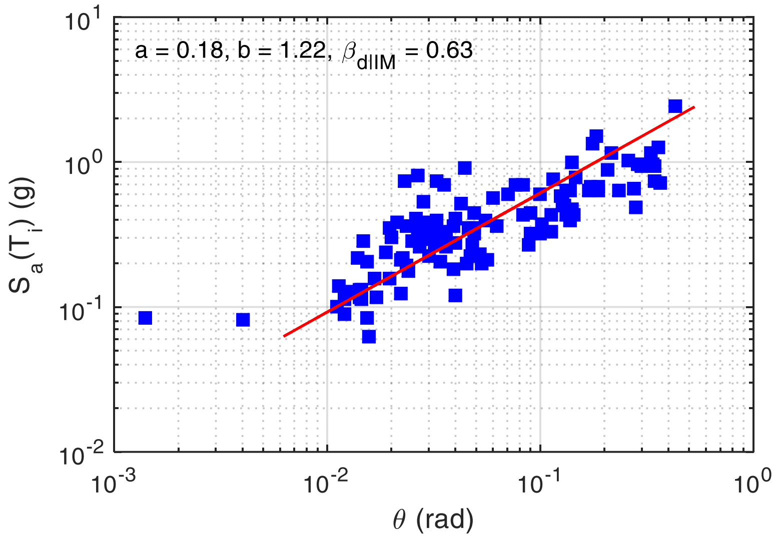

(a)

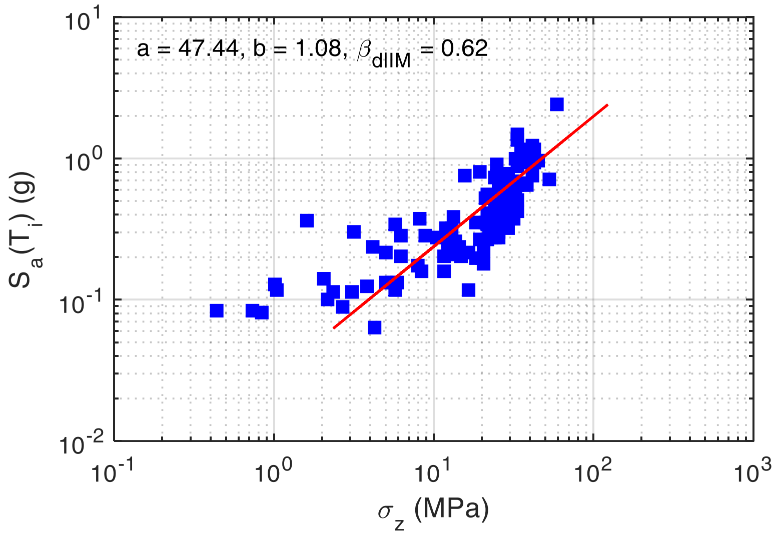

(b)

Figure 7.13. Regression analysis results for the rotation (a) and meridional compressive stress (b) demands

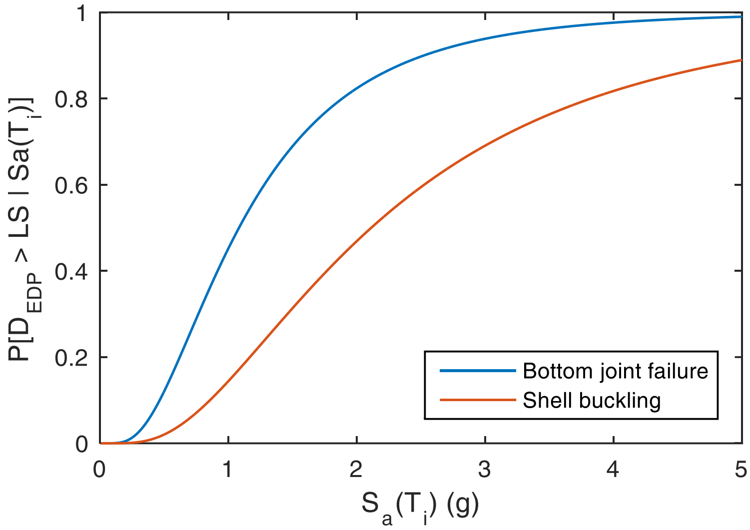

Figure 7.14. Fig. 12 Fragility curves for the shell-to-bottom plate joint failure and shell buckling considering all uncertainties

7.6.5 Sensitivity of fragility curves

The sensitivity study reveals that the seismic responses of the tank are sensitive to a number of different modelling parameters, and the most significant parameters have been identified. The influence of these different sources of uncertainty on the resulting fragility curves is assessed. Three types of fragility curves, with different levels of uncertainty, are considered as follows: (1) the uncertainty in ground motion, material and geometry, (2) the uncertainty in ground motion and geometry, and (3) the uncertainty in ground motion.

The fragility estimates presented in Table 7.9 reveal that the fragility curves developed considering the variation in ground motion and geometry are almost the same as those considering all random variables, as shown in Figure 7.15. The median values differ only 1.9-3.3% and 1.4-1.5% for the dispersion values; this is consistent with the results obtained from the sensitivity analysis, where the geometric parameters, including the filling level and the thickness of the shell and bottom plate, significantly affect the seismic response of the tank. Conversely, the material parameters that comprise steel yielding strength, Young’s modulus, and liquid density have a less effect.

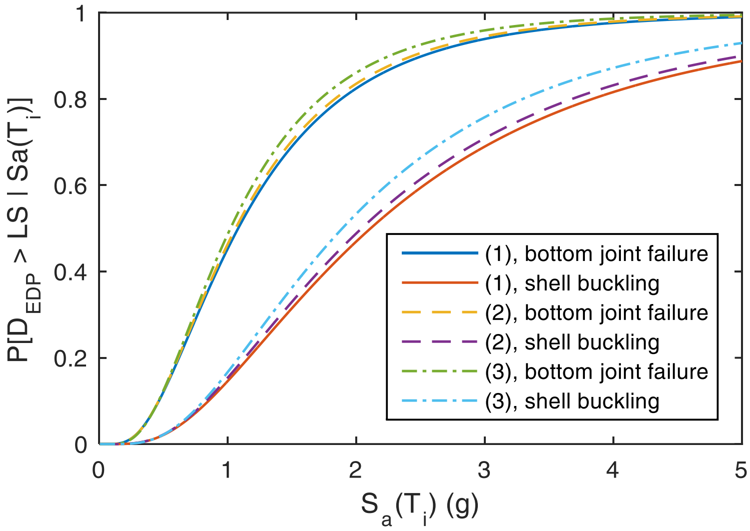

Figure 7.15. A comparison of fragility curves for the shell-to-bottom plate joint failure and shell buckling: (1) all uncertainties, (2) ground motion and geometric uncertainties, and (3) ground motion uncertainty only]

It is worth to note that there is a considerable difference between the fragility curves considering all variable parameters and those developed considering the uncertainty in the ground motion only. A decrease of 5.6-10.4% in the median values and 6.1-7.0% in the dispersion ones are recognised. These results evidence that the computational time and effort can be reduced in the probabilistic seismic demand analysis of the tank by considering only the variability of the significant parameters identified in the sensitivity study.

Table 7.9. Fragility curve estimates for the shell-to-bottom plate joint failure and shell buckling

	Shell-to-bottom plate joint failure		Shell buckling	
	Median (g)	Dispersion	Median (g)	Dispersion
All uncertainties (1)	1.08	0.66	2.11	0.71
Geometric uncertainty (2)	1.06	0.65	2.04	0.70
Ground motion uncertainty (3)	1.02	0.62	1.89	0.66

7.7 Closure

In this chapter, an enhanced seismic fragility analysis of a broad unanchored steel storage tank is proposed, which accounts for both aleatoric (i.e., seismic action) and epistemic (i.e., modelling parameters) uncertainties. The selected case study is ideally placed in Priolo Gargallo (Italy). A screening study, based on a 3D finite element model of the tank and a statistical DOE approach, is first performed to identify the most significant epistemic random variables affecting the uplift response of the tank. The results indicate that those associated with the geometry, i.e., the filling level and the shell and bottom plate thickness, have the strongest effect. Conversely, the material parameters that comprise steel yielding strength, Young’s modulus, and liquid density are recognised to have a limited influence in the case of low seismic actions. However, the statistical significance of these parameters is the highest when the ground shaking reaches 0.6g. The findings of this sensitivity study confirm that all sources of uncertainty should be considered as random variables in the fragility analysis.

The fragility curves considering all random effects are then developed for two critical failure modes, which include the shell buckling and the plastic rotation of the shell-to-bottom plate joint. As a result, the tank failure caused by the plastic rotation of this joint show the higher probability of occurrence compared with those caused by the shell buckling.

The relative importance of the epistemic uncertainty treatments with respect to those associated with the ground motion is also evaluated. The outcomes of the analysis show that the fragility curves associated with all random variables are nearly identical to the fragility curves in which only the geometric parameters and the ground motion vary. A considerable difference is found in comparison with the fragility curves developed considering only the ground motion uncertainty. This finding indicates that in seismic risk assessment of a plant, the random variables of tanks associated with the ground motion and the geometric parameters (i.e., filling level and plate thickness) should be included.

The study presented in this paper uses a single case study to evaluate the sensitivity of the seismic response and fragility to uncertainty parameters. However, this work can be easily extended to a class or portfolio of unanchored tanks.

Chapter 8. Seismic vulnerability analysis of elevated steel liquid storage tanks: Case study #2

8.1 Introduction

Elevated liquid storage tanks were present in the aforementioned industrial plants. These structures traditionally are constructed with a welded steel tank container supported by steel or reinforced concrete columns. The relevant types of damage range from minor cracks to completely collapse of support structures and/or tanks (Sezen and Whittaker 2006). Similar damage and consequences have been found in elevated tanks during more recent earthquakes that struck Japan and China, e.g., the 1995 Kobe earthquake (Suzuki 2006) and the 2008 Wenchuan earthquake (Krausmann et al. 2010). In most cases, the tanks were designed with outdated standards and thus hazards, e.g., seismic-induced fires and seismic-induced tsunamis, were completely ignored (Hatayama 2015).

Various studies have been carried out to investigate both the dynamic responses and the failure mechanisms of existing elevated storage tanks, e.g., Shrimali (2003), Sezen et al. (2008), Moslemi et al. (2011), Brunesi et al. (2015), Paolacci (2015). However, in many cases, conventional procedures and models are not sufficient to accurately predict the nonlinear structural behaviour of tanks. Therefore, a reliable numerical model of both the tank and the support structure with a proper definition of their dynamic properties are needed (Ruiz and Gutiérrez 2015).

The vibration period of the impulsive component generally falls in the maximum amplification field of the response spectrum, whereas the convective period is usually very high and thus associated with a low amplification factor. This finding implies a potential high effectiveness of base isolation systems, which could strongly reduce the base shear due to the impulsive pressure component. In addition, the superficial motion mainly caused by the convective component may produce some negative effects, e.g., the overtopping or the leakage of flammable substances due to the fracture of the roof or the motion of the floating roof. Unfortunately, the base isolation does not control these phenomena, for which alternative solutions should be adopted (De Angelis et al. 2010, Abali and Uckan 2010). The benefit of base isolation systems for tanks has been demonstrated in the last two decades (e.g., Shrimali and Jangid 2002, Abali and Uckan 2010, Paolacci 2015); however, a limited number of practical applications and experimental activities have been performed. Moreover, there is a lack of studies quantifying the benefit of isolation systems through probabilistic approaches.

The seismic vulnerability of an elevated steel storage tank supported by short circular reinforced concrete columns, named as Case study #2, is investigated in this study. The attention is paid to the seismic fragility analysis of the steel tank and the support columns. Fragility curves can be then used to predict failure conditions and thus possible LOC effects in a probabilistic performance-based earthquake engineering framework. A coupling model of the elevated tank using a lumped mass model for the liquid-steel storage tank and a proper nonlinear three-dimensional finite element model stick model for the support structure is presented. The tank model subjected to sets of ground motion records is investigated by means of nonlinear time history analyses. The effects of both far-field and near-source records on the seismic response of the aforementioned elevated tank are assessed and discussed. Two analytical approaches for estimating fragility functions, namely the CA and the IDA, are then used to determine the median relationship between engineering demand parameters and an intensity measure. The resulting probabilistic seismic models have provided seismic fragility curves of the support columns and the steel tank. Subsequently, a seismic isolation system based on a concave sliding bearing (CSB) system is then proposed. In particular, design parameters of the isolation system are evaluated through a vulnerability-based approach by minimizing the failure probability of the support columns.

8.2 Description of case study

The 7.4 magnitude earthquake that struck northwestern Turkey on August 17, 1999 caused extensive damage to residential, commercial, and industrial facilities. Approximately 40% of the heavy industry in Turkey was located in the epicentral region and included oil refineries, pharmaceutical and petrochemical plants, power plants, car assembly and tyre manufacturing facilities, cement production and steel fabrication plants, and other industries. One of those industrial facilities, Habas plant located within 10 km of the fault trace, provides liquefied gases to commercial plants and medical facilities in the region. The major damage at this plant was the collapse of two of the three liquid gas storage tanks, as shown in Figure 8.1. The collapse was mainly due to the support columns.

The two damaged tanks on the left contained liquefied oxygen, while the undamaged tank on the right was filled with liquefied nitrogen. Habas representatives on site reported that the liquefied oxygen tanks were 85% full and the liquefied nitrogen tank was about 25% full immediately before the earthquake. Hence, the tank with 85% liquefied oxygen is considered in this study.

The tank was built in 1995 and consisted of two concentric stainless steel walls, the outer with an outside diameter of 14.6 m and the inner with an outside diameter of 12.8 m. The gap between the walls is filled with insulation. Both walls are supported on a 14.6-m-diameter (1.07-m-thickness) reinforced concrete slab, in turn, supported by sixteen 500-mm-diameter reinforced concrete columns. Each column is 2.5-m-tall, reinforced with sixteen 16-mm-diameter longitudinal bars and 8-mm-diameter ties at 100-mm-centre-to-centre. The main dimensions of the examined elevated tank are illustrated in Figure 8.2.

Figure 8.1. Storage tanks of liquid oxygen at the Habas plant after the 1999 Kocaeli earthquake (Sezen and Whittaker 2006)

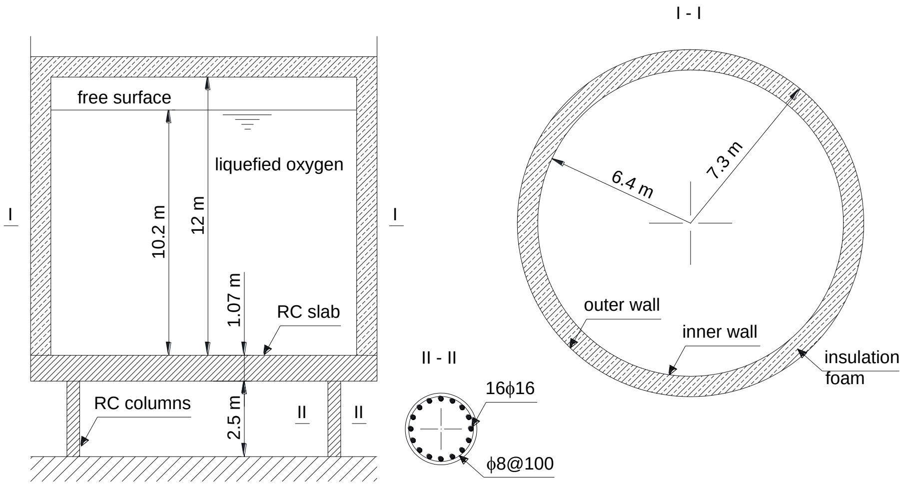

Figure 8.2. Main dimensions of the examined elevated tank

The clear height of the tank between the bottom slab and top stainless cover is about 12 m. The volume of the tank is thus approximately 1500 m^3. According to Sezen and Whittaker (2006), the concrete used for the columns and the bottom slab is of class C30/37, whereas the steel bars have a yielding strength of 420 MPa. The density of the oxygen is 1150 kg/m^3. The details on mechanical properties of the columns and tank are collected in Table 8.1.

Table 8.1. Mechanical properties of the columns and tank components

Component	Mechanical property	Value
Steel tank	Young's modulus Yield strength Density	200000 MPa 205 MPa 7850 kg/m^3
Reinforced concrete columns - Concrete - Longitudinal reinforcement - Transverse reinforcement	 Young's modulus Compressive strength Density Yield strength Yield strength	 32000 MPa 30 MPa 2500 kg/m^3 420 MPa 365 MPa
Liquid oxygen	Density	1150 kg/m^3

8.3 Nonlinear numerical model

Based on the typical details taken from the examined elevated tank, a three-dimensional finite element model stick model is generated by means of the

OpenSEES software (McKenna et al. 2007). The effects of hydrodynamic pressure on the shell and base plate during earthquakes are taken into account by means of the simplified model depicted in Section 3.3. In detail, the liquid mass is lumped and subdivided into two components, named as impulsive mass (m_i) and convective mass (m_c). The impulsive and convective masses, located at heights h_i and h_c, respectively, are connected to the tank base by cantilevers of stiffness k_i and k_c. Table 8.2 reports the dynamic parameters of the tank model, where the calculations of masses, periods, heights are obtained using the method presented by Malhotra et al. (2000), and the relevant damping ratios are set to 2% and 0.5%, respectively. The base slab is assumed to be rigid and is modelled by means of elastic beam-column elements with very high stiffness, i.e., practically rigid links. The support columns are modelled using three-dimensional nonlinear beam-column elements with fiber-based cross-sections.

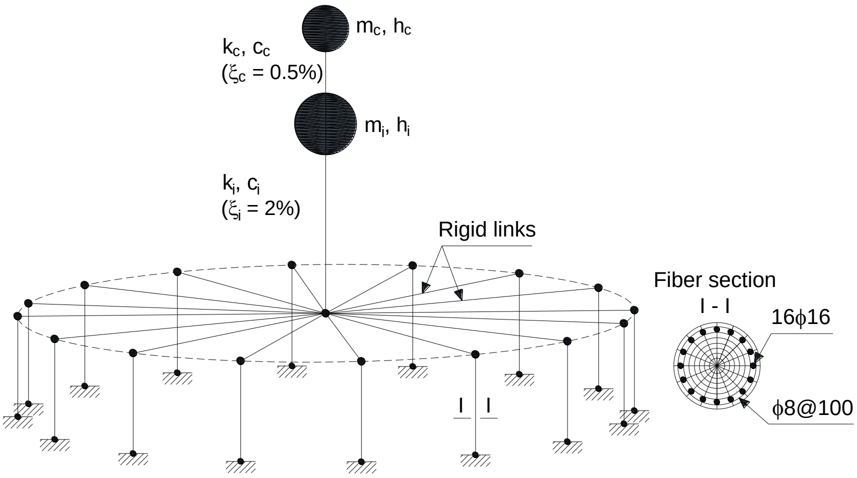

Figure 8.3. Numerical model of the elevated tank

Table 8.2. Dynamic parameters of the tank model

Parameter / Component	Impulsive	Convective
Mass (ton)	1063	447
Damping ratio	2%	0.5%
Period (s)	0.14	3.74
Stiffness (kN/m)	2085108	1260
Height of mass (m)	5.5	7.5

For a typical fix-ended reinforced concrete column, the total lateral deformation is composed of three components: (i) flexural deformation, (ii) reinforcement slip deformation, and (iii) shear deformation. Shear deformation in reinforced concrete columns has commonly been neglected in the design of these structures, due to lack of their complete understanding and being difficult to measure (Sezen 2008). However, for columns with small aspect ratio or without adequate shear-resisting reinforcements, shear deformation governs the total response and, finally, leads to unexpected shear or shear-flexure failure.

According to the classification approach proposed by Sezen and Moehle (2004) and Zhu et al. (2007), the failure modes of a reinforced concrete column can be classified based on three parameters: (i) the plastic shear demand to shear strength ratio, (ii) the aspect ratio of shear span to depth, and (iii) the transverse reinforcement ratio. For the columns of the examined tank, these parameters are gathered in Table 8.3, which entail a pure-shear failure.

Table 8.3. Geometrical and mechanical parameters for the classification of the column failure mode

Column parameter	Value
Plastic shear demand to shear strength ratio, V_p/V_n	1.05
Aspect ratio of shear span to depth, a/d	2.8
Transverse reinforcement ratio, ρ''	0.002

In detail, the force V_n = 300 kN is calculated by the expression developed by Sezen and Moehle (2004) for lightly reinforced concrete columns, whereas V_p = 315 kN is obtained by sectional analysis. The columns have a shear span of 1.25 m and an effective depth of 0.444 m.

The shear force-shear deformation model for the pure-shear failure of the support columns of the tank is obtained by modifying the model developed by Setzler and Sezen (2008); this model is then implemented into the finite element model by employing the section aggregator command of OpenSEES. In this case, a uniaxial hysteretic material is chosen to represent the sectional shear behaviour. It is defined through three points of the envelope curve depicted in Figure 8.4, where the first two points are obtained using the Response 2000 software (Bentz 2000), and the third point is calculated based on the formula of Elwood and Moehle (2005).

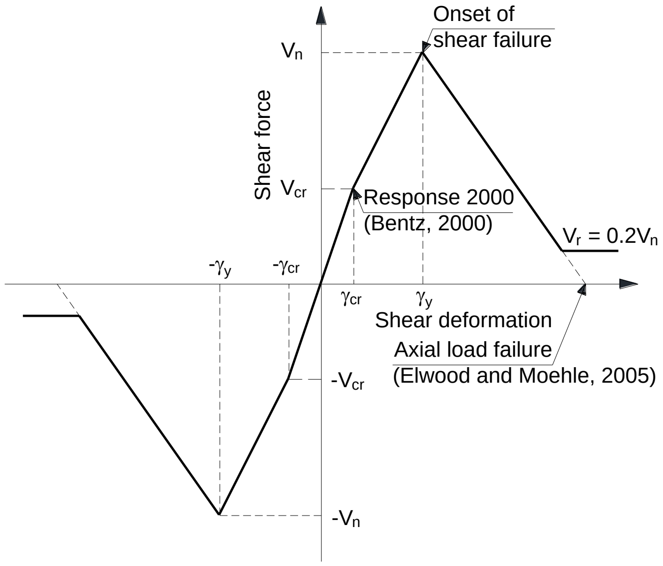

Figure 8.4. Shear force-deformation model for the support columns

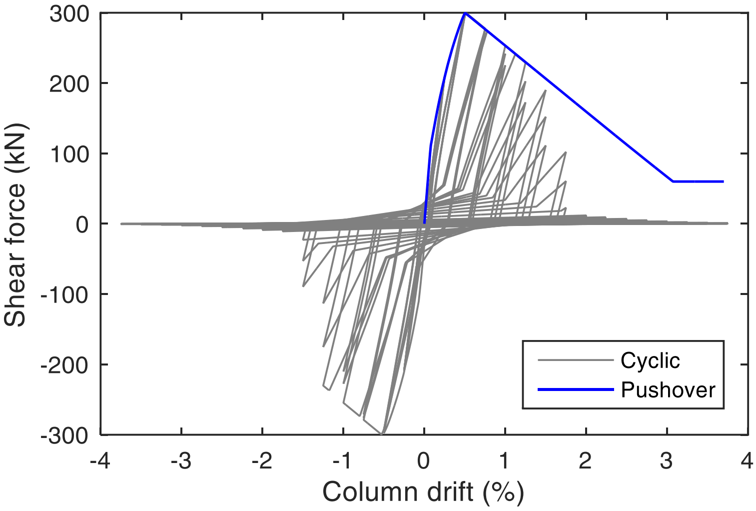

Figure 8.5. Static pushover and cyclic analyses of the examined tank

In order to account for the cyclic lateral load-deformation response of the columns, a hysteresis law is used, which includes pinching, strength, and stiffness degradation effects. A static pushover analysis and a cyclic analysis of the examined tank are performed to gain an understanding of the structural behaviour. The results expressed as the base shear versus the maximum column drift ratio are depicted in Figure 8.5. The pushover and cyclic curves depicted in Figure 8.5 lead also to the evaluation of the maximum column drift that defines the onset of shear failure in the structure, i.e., θ_{sf} = 0.5%.

The vibration periods and modal participating masses (MPM) of the first three modes of the tank model are reported in Table 8.4. These results highlight the practical independence of the convective motion of the fluid (mode 1) from the global motion of the tank model (mode 2 and 3). The motions of the support structure and the impulsive component are mainly involved in the second and third modes, where the modal participating mass equals to 86% of the total system mass. In addition, the period of the second mode (T_2 = 0.29 s) is considerably greater than the impulsive period indicated in Table 8.2 (T_i = 0.14 s); this is due to the influence of the lateral flexibility of the support structure that can give an increase of the fundamental period of the tank.

Table 8.4. Dynamic characteristics of the tank model

Mode	1	2	3
T (s)	3.74	0.29	0.08
MPM (%)	14	51	35

8.4 Seismic vulnerability assessment

8.4.1 Ground motion selection

In order to consider both near-source records -records with Joyner-Boore distance (R_{jb}) less than 15 km, indicated as set A- and far-field records -records with R_{jb} larger than 15 km, indicated as set B-, two sets of 20 natural earthquake records are selected from the PEER ground motion database. The sample records are main-shock free-field recordings, including only the most severe -in terms of PGA- of the two horizontal components of the same registration. The soil property of the record stations is characterised as stiff soil (360 m/s < $V_{s,30}$ < 760 m/s). The set A is endowed with moment magnitudes (M_W) between 6.0 and 6.9 and R_{jb} between 5.18 km and 13.75 km. Conversely, the set B possessed M_W ranging between 6.5 and 7.0 and R_{jb} between 15.19 km and 29.86 km. The response spectra of these records are depicted in Figure 8.6; it also shows the median spectrum for each set of records.

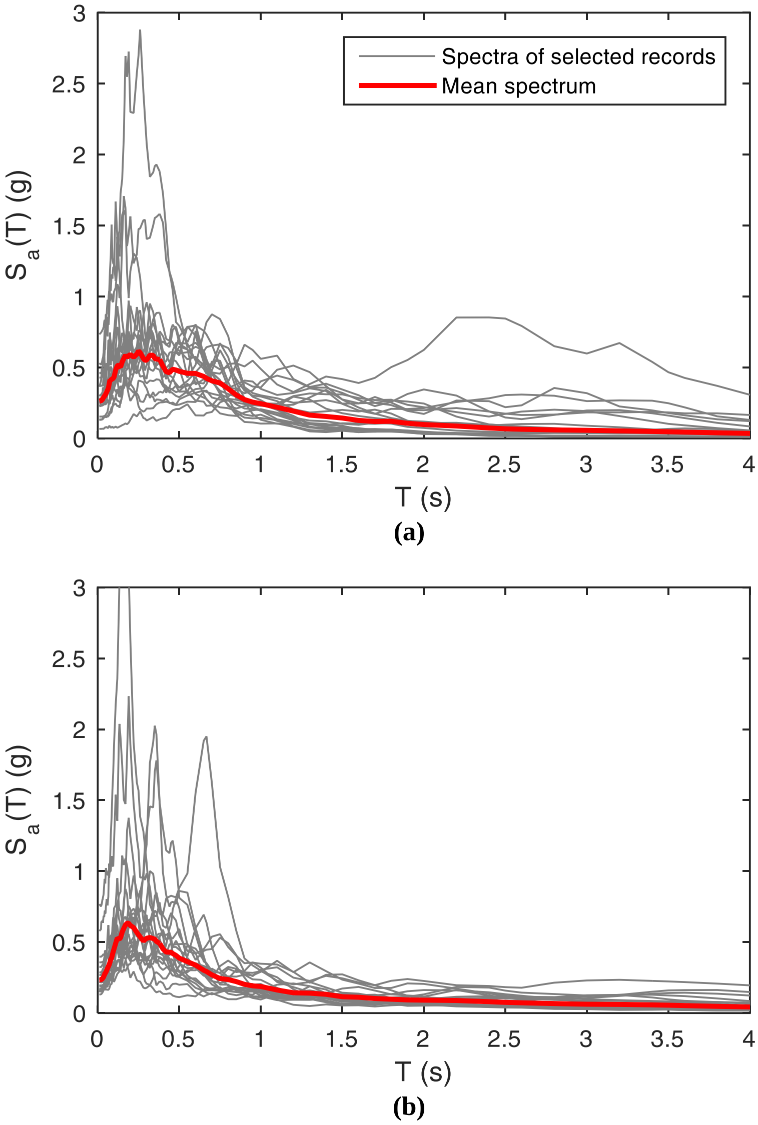

Figure 8.6. Response spectra of the selected accelerograms: (a) set A records and (b) set B records

8.4.2 Seismic response of the examined tank

The seismic response of the tank is preliminarily assessed in terms of peak drift ratio of the support columns, compressive meridional stress in the tank wall, and elevation of the liquid free surface for two sets of ground motion records; the results are shown in figures 8.7, 8.8, and 8.9, respectively.

Given the high axial stiffness of columns, the drift well approximates the chord rotation of the columns. The compressive meridional stress in the tank wall and the maximum sloshing wave height are calculated using the formulas listed in Section 3.5.

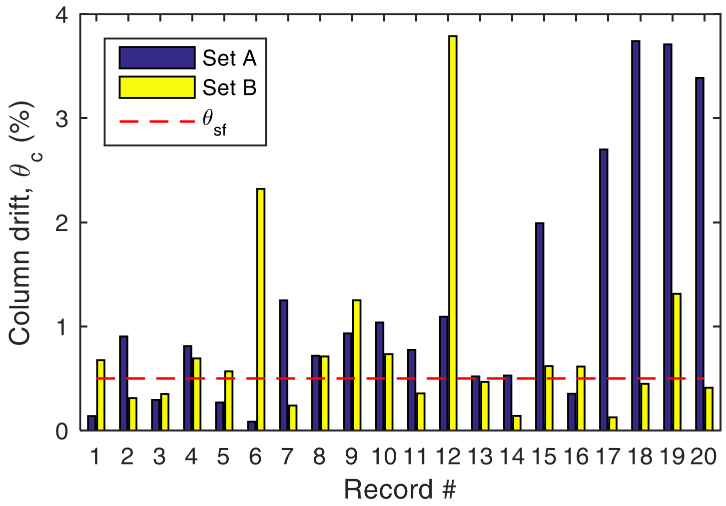

Figure 8.7. Peak drift ratio of the support columns of the tank and corresponding limit state in the shear failure mode for both sets of records

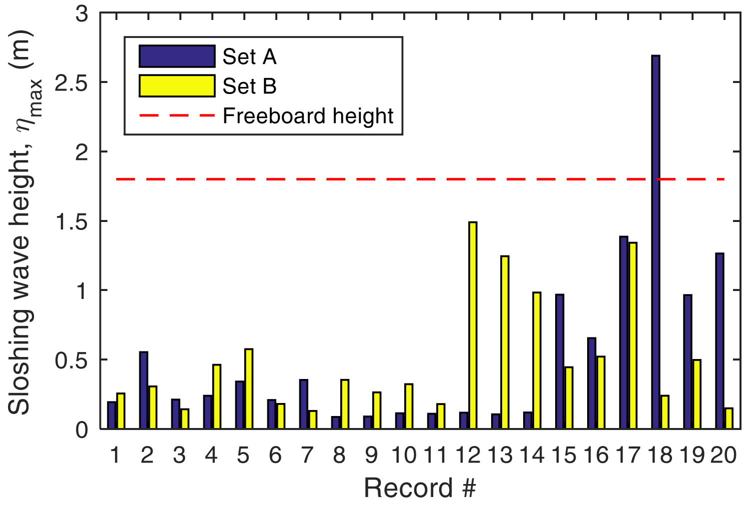

Figure 8.8. Elevation of the liquid free surface corresponding to the limit state of the freeboard height of the tank for both sets of records

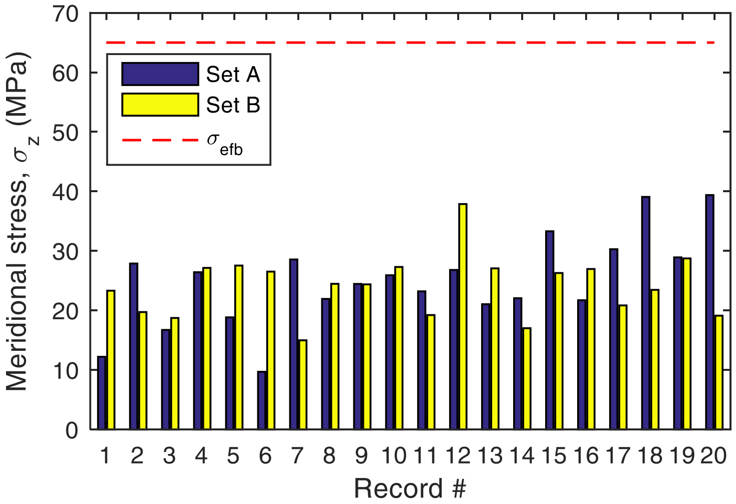

Figure 8.9. Compressive meridional stress of the tank shell wall corresponding to the limit state of the elephant's foot buckling for both sets of records

The corresponding limit states of the tank components are also plotted in figures 8.7, 8.8, and 8.9. The maximum drift ratio of support columns at the onset of pure-shear failure is obtained by the pushover and cyclic analyses presented in Section 8.3, i.e., θ_{sf} = 0.5%. The meridional design buckling stress, σ_{efb} = 65 MPa, is calculated using the formula in Section 3.6. Moreover, in order to avoid damage of the roof, the limit state for the liquid sloshing height is selected as the freeboard height of the tank, i.e., 1.8 m. From the above figures, one can observe that failure of the support structure is the most frequent one. In fact, the shear capacity of the support columns is exceeded in most of the cases, regardless of nature, i.e., near-fault or far-field records, of the seismic action applied. The exceeding of the maximum freeboard of the tank is instead rare, as demonstrated in Figure 8.8. Finally, the occurrence of elephant's foot buckling phenomena is totally hampered by the collapse of columns in shear, as shown in Figure 8.9, where the dashed red line (capacity) stands always above the response.

8.4.3 Efficiency and sufficiency of intensity measures

In this work, a comparative analysis on the efficiency and sufficiency of intensity measures are presented with respect to the drift demand of the columns. Similarly to the work in Chapter 6, the intensity measure efficiency is evaluated by computing the standard deviation $\beta_{d|IM}$, the slope coefficient b, and the determination coefficient R^2 of the linear regression analysis; the lower the standard deviation or the higher the determination coefficient and the higher the intensity measure efficiency. The results obtained for four well-known intensity measures including three magnitude-based intensity measures (PGA, PGV, and PGD) and a structure-specific intensity measure, i.e., the elastic spectral acceleration at the period T_2 of the tank [$S_a(T_2)$], are presented in Table 8.5 for two sets of ground motion records, set A and set B, respectively.

Table 8.5. Linear regression analysis results of the column drift demand

	Set A			Set B		
	$\beta_{d\|IM}$	b	R^2	$\beta_{d\|IM}$	b	R^2
PGA	0.57	1.66	0.72	0.48	1.44	0.68
PGV	0.79	1.58	0.46	0.70	1.14	0.32
PGD	0.98	0.51	0.18	0.82	0.48	0.08
$S_a(T_2)$	0.73	1.25	0.54	0.47	1.31	0.69

From the results shown in Table 8.5, it can be observed that PGA exhibits the best performance for both near-source and far-field records. In contrast, PGD shows lower efficiency among the four intensity measures. In addition, the use of $S_a(T_2)$ leads to a low dispersion as well, especially in the case of far-field records.

The sufficiency of intensity measures has been analysed by evaluating the correlation between the residuals of the linear regression with the aforementioned parameters involved in the hazard calculation. In the present study, the sufficiency of intensity measures has been evaluated with respect to M_W, R_{jb}, and $V_{s,30}$ by fitting linear regression models between regression-residuals obtained from the linear regression model and M_W, R_{jb}, and $V_{s,30}$.

The sufficiency of an intensity measure has been evaluated by means of the slope c_1 of the regression line. The statistical significance of c_1 on M_W or R_{jb} or $V_{s,30}$ can be quantified by the p-value for the F-statistics of the null hypotheses c_1 = 0. A small p-value, i.e., less than 0.05, suggests that the estimated coefficient c_1 on M_W or R_{jb} or $V_{s,30}$ is statistically significant, and therefore, that intensity measure is insufficient (Luco and Cornell 2007).

The results of the comparative statistical analysis relative to intensity measure sufficiency are presented in Table 8.6 for the 40 records composing the two ground motion sets A and B. The values highlighted in bold are associated with p-values less than 0.05.

Table 8.6. Results of the sufficiency analysis

	M_W		R_{jb}		$V_{s,30}$	
	c_1	p-value	c_1	p-value	c_1	p-value
PGA	0.020	0.932	-0.009	0.413	-0.001	0.069
PGV	-0.333	0.316	-0.003	0.840	-0.003	0.011
PGD	-0.491	0.220	-0.026	0.156	-0.004	0.004
$S_a(T_2)$	-0.025	0.933	-0.014	0.277	-0.002	0.041

The statistical analysis results shown in Table 8.6 indicate the sufficiency of PGA with regard to the magnitude, distance, and soil type. A significant degree of insufficiency with respect to the soil type is exposed for PGV, PGA, and $S_a(T_2)$. From the comparative results, it can be concluded that the most efficient intensity measure is PGA, which shows a sufficiency also in general terms. This finding seems to be a good choice when past studies on the vulnerability of storage tanks usually propose PGA as the earthquake descriptor used to define the fragility curves.

8.4.4 Fragility analysis

The CA is applied first to the elevated tank. Both figures 8.10 and 8.11 illustrate the results considering only the record-to-record variability for the column drift, the sloshing wave height of the liquid free surface, and the compressive meridional stress in the tank wall versus PGA. The solid lines represent the regression prediction in logarithmic scale. Table 8.7 reports the associated probabilistic demand parameters. The CA results can be compared with those of the IDA for the same set of records employed earlier. The IDA curves in Figure 8.12 report the change of parameter demand (drift) that is normalised with respect to the shear capacity of the columns (θ_c/θ_{sf}). The failure condition corresponds to θ_c/θ_{sf} = 1 (dashed red vertical line).

Fragility curves of the examined tank are derived for the damage states described above and reported in Figure 8.13. It is evident that the prevalent damage condition is represented by the damage in the support columns for excessive lateral displacement of the tank base. This conclusion is also corroborated by reality, where the collapse of the tank at the Habas plant was uniquely caused by column failure.

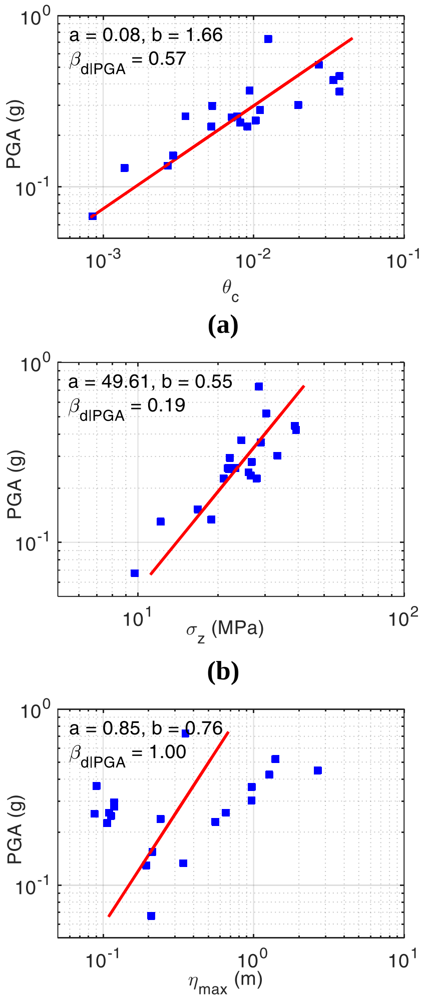

(a)

(b)

(c)

Figure 8.10. Regression analysis with set A records: (a) column drift, (b) meridional stress, and (c) sloshing wave height

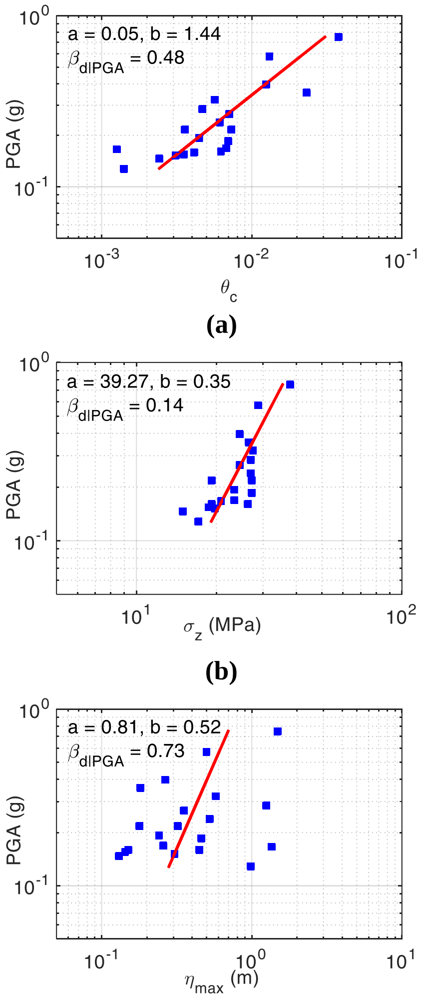

(a)

(b)

(c)

Figure 8.11. Regression analysis with set B records: (a) column drift, (b) meridional stress, and (c) sloshing wave height

Table 8.7. Fragility estimates for the examined tank by the CA

Engineering demand parameter	Set A records			Set B records		
	a	b	$\beta_{d\|PGA}$	a	b	$\beta_{d\|PGA}$
Column drift	0.08	1.66	0.57	0.05	1.44	0.48
Meridional stress	49.61	0.55	0.19	39.27	0.35	0.14
Sloshing wave height	0.85	0.76	1.00	0.81	0.52	0.73

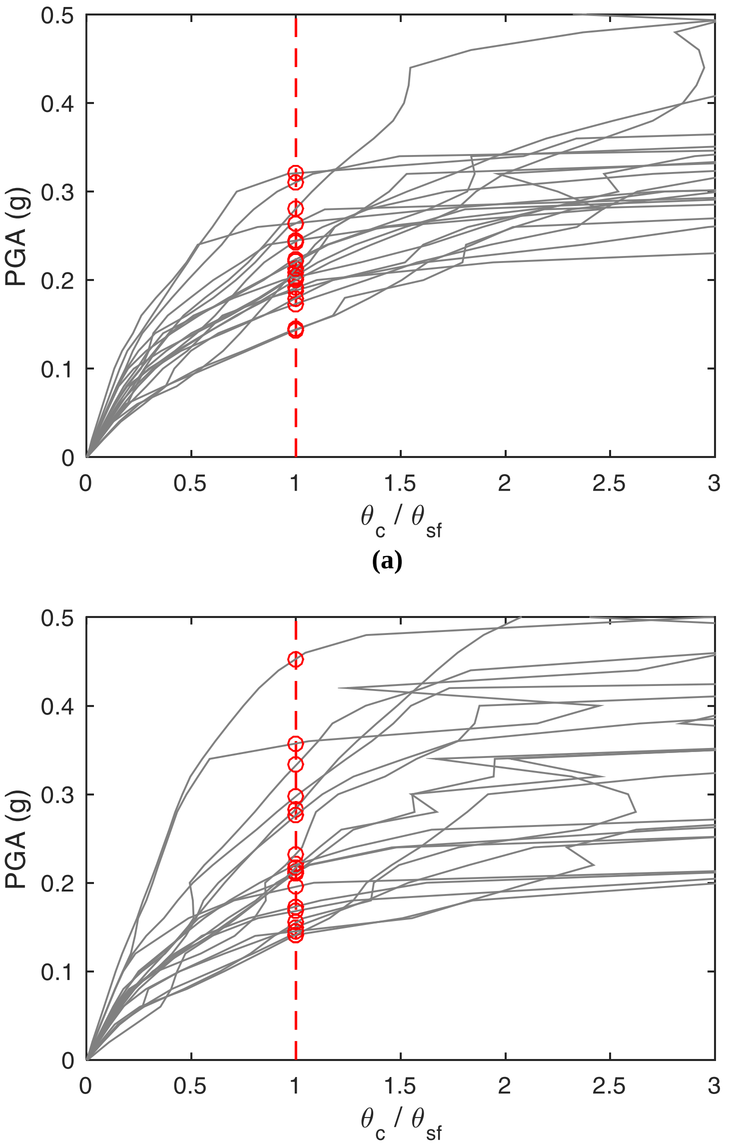

(a)

(b)

Figure 8.12. IDA results for the peak drift ratio of the columns using set A records (a) and set B records (b)

It can also be noticed from Figure 8.13 that for a PGA = 0.3 g, the probability of pure-shear failure reaches 80%, and the 100% probability of failure is recorded as a PGA level of 0.4 g. From the same figure, one can observe that the type of input signal, i.e., near-fault or far-field record, has a rather limited influence on the probabilistic response.

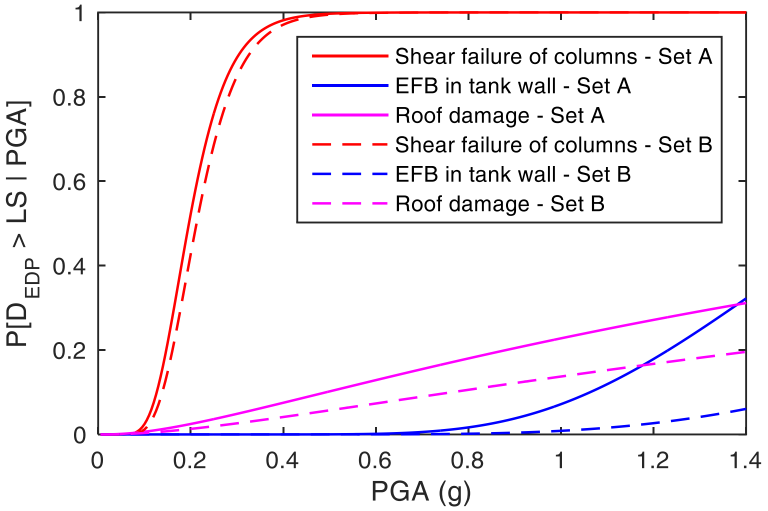

Figure 8.13. A comparison of fragility curves based on the CA for different failure modes of the tank components between set A and set B records

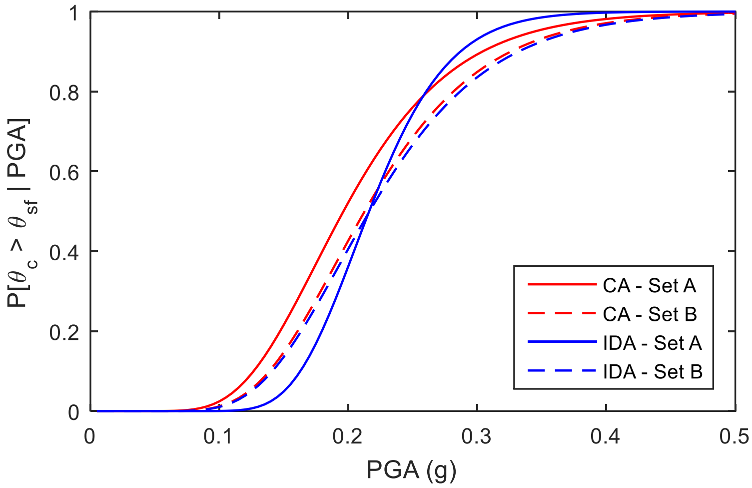

Figure 8.14. A comparison of fragility curves for the shear failure mode of the columns between the CA and the IDA based on two sets of records

A comparison between the CA and the IDA methods in terms of fragility curves of the support columns' damage state is shown in Figure 8.14. A careful reader can observe that the results provided by the two methods for the set B records are very similar. Conversely, for the set A records, the fragility curve derived by the CA are more conservative than those obtained by the IDA; this is generally due to a more accuracy of the IDA with respect to the CA in predicting mean and dispersion.

The implications of using reliable models and methods for the vulnerability assessment of industrial units, e.g., storage tanks, for seismic risk assessment of process plants are evident (Alessandri et al. 2017). For example, a correct evaluation of the leakage conditions in a component is strictly related to the damage prediction reliability. In this respect, the use of an accurate model, like the one adopted in the above example, allows both to decrease the computational effort, necessary for the analysis, and to correctly predict the nonlinear behaviour of the tank and related damage.

The example studied in this chapter also evidenced that the accuracy of the fragility method has a direct repercussion in predicting the correct failure probability and thus the associated LOC effects. In this respect, the use of the IDA is recommended. The above results are a clear demonstration of the high seismic vulnerability of the tank, as dramatically demonstrated during the 1999 Izmit earthquake (Sezen and Whittaker 2006), and the need to adopt a proper seismic mitigation system. Accordingly, in the next section, the design of a CSB system will be presented along with the analysis of its effectiveness evaluated through a fragility analysis.

8.5 Vulnerability-based design of CSBs

In this section, the effectiveness of a CSB system for the seismic protection of the analysed tank is investigated. According to Paolacci (2015), the use of CSBs has been determined as the superiority in protecting elevated storage tanks against earthquakes compared with other isolation systems, e.g., high damping rubber bearings. For structures where the mass corresponds to the entire weight, the typology of these devices represents an attractive solution because of the general independency of the response from the mass (Fenz and Costantinou 2006). The period can be calculated as:

$$T_{iso} = 2\pi\sqrt{\frac{m_{tot}}{k_{iso}}} = 2\pi\sqrt{\frac{m_{tot}}{gm_{tot}\left(\frac{1}{R_{iso}}+\frac{\mu}{X_{iso}}\right)}} = 2\pi\sqrt{\frac{1}{g\left(\frac{1}{R_{iso}}+\frac{\mu}{X_{iso}}\right)}} \tag{8.1}$$

where k_e is the equivalent stiffness of the devices, m_{tot} is the total mass, R_{iso} and μ are respectively the radius and the friction coefficient of the devices, and X_{iso} is the maximum displacement amplitude.

However, when the isolated mass is only a fraction of the total mass, this independency is no longer valid. For example, in the case of storage tanks, the isolation period is calculated as:

$$T_{iso} = 2\pi \sqrt{\frac{m_i + m_b + m_w + m_{iso}}{g m_{tot}\left(\frac{1}{R_{iso}} + \frac{\mu}{X_{iso}}\right)}} \tag{8.2}$$

where m_i is the impulsive part of the liquid mass, m_s is the mass of support structure, and m_w and m_b are the tank wall and base masses, respectively.

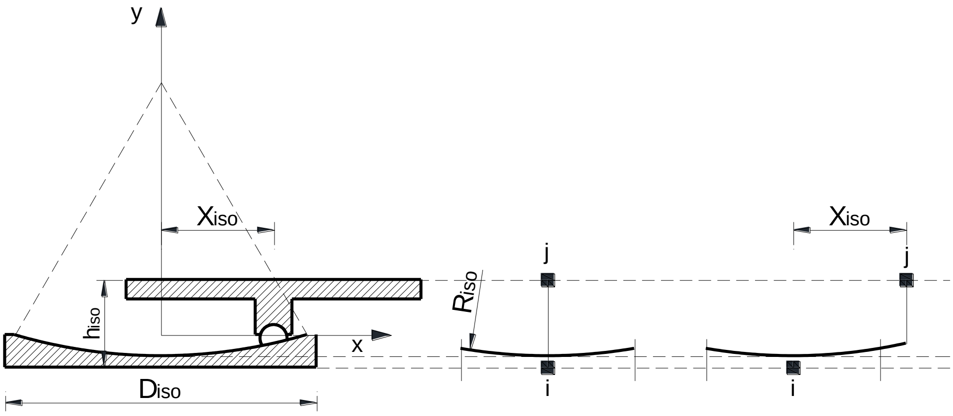

Figure 8.15. Schematic of a CSB system

According to the case study, sixteen CSBs are selected and installed on the top of the columns. The schematic of the CSB is shown in Figure 8.15, which have following characteristics:

- isolator height h_{iso} = 114 mm,
- isolator weight m_{iso} = 110 kg,
- isolator diameter D_{iso} = 490 mm,
- maximum displacement X_{iso} = ±225 mm,
- vertical load carry capacity N_{iso} = 1500 kN.

The numerical model for the isolated tank with the CSBs placed on the top of the columns is shown Figure 8.16. Such devices are modelled in OpenSEES using the singleFPBearing element (Schellenberg 2006), where the initial elastic stiffness of the bearings in local shear direction is selected corresponding to a 0.25-mm-yield deformation and a friction coefficient of 3%. The Coulomb approach is used for the simulation of the devices; the kinetic friction is thus independent of the sliding velocity. Because a little different from the fragility curves obtained using two sets of records, the nonlinear time history analyses of the isolated tank are performed with only the set A records. In this step, the designed parameter of the bearings, i.e., the equivalent period (T_{iso}), is variable. The values of T_{iso} are selected in the range of 0.5 s and 4.5 s for the analysis. An optimised value of T_{iso} will be obtained by evaluating a reduction in the probability of failure.

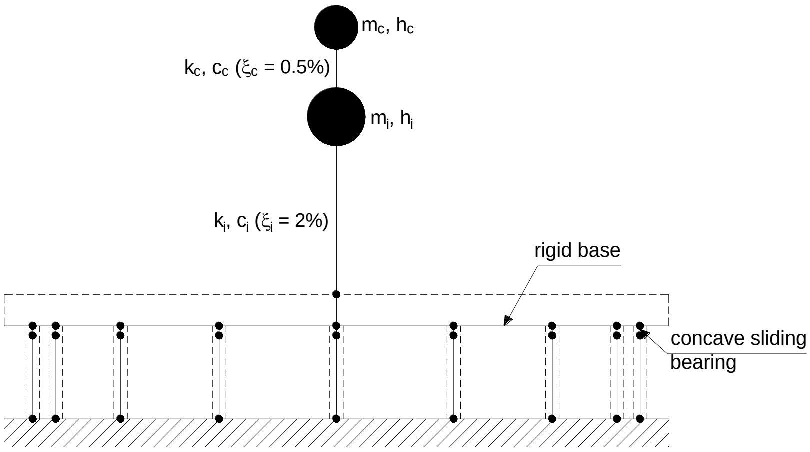

Figure 8.16. Numerical model of the isolated tank in front view

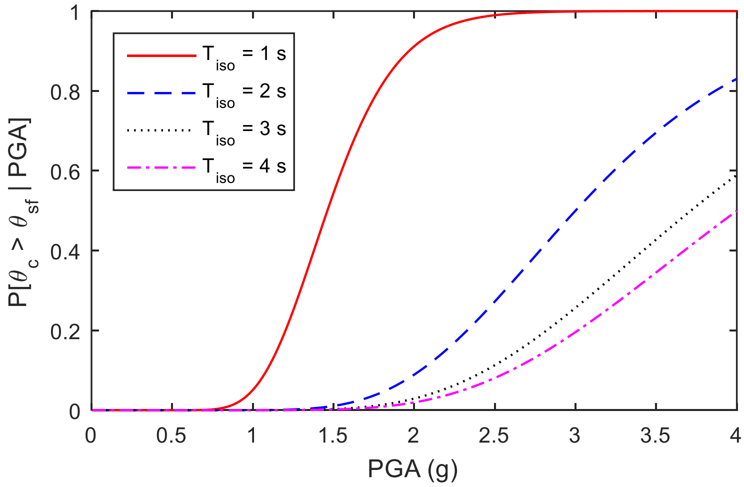

Figure 8.17. Fragility curves for the isolated tank

Subsequently, the fragility curves of the isolated tank are built for the selected isolation periods of the bearings by using the CA method. These curves are derived for the most influencing engineering demand parameter, i.e., the column drift.

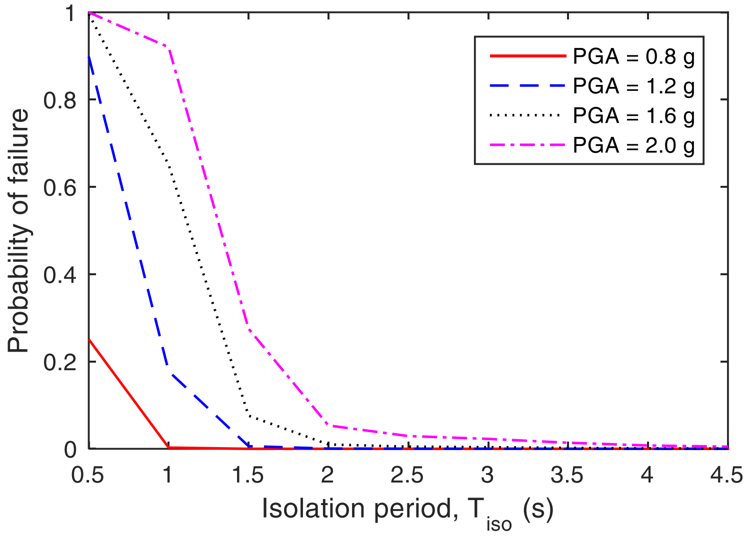

Figure 8.18. Relationship between the isolation period and the probability of failure

Figure 8.17 shows an example of the fragility curves for four cases of T_{iso}, from 1 s to 4 s. It can be seen that the probability of failure in the cases of T_{iso} = 3 s and T_{iso} = 4 s are almost the same, whereas there is a remarkable decrease in the probability recorded for T_{iso} = 2 s as compared with T_{iso} = 1s. In most of the isolated cases, the probability of failure is almost zero up to a PGA level of 0.8 g, where 100% of the collapse occurrence was recognised for the non-isolated one; this demonstrates the usefulness of the CSBs in reducing the seismic response of the tank.

A detailed comparison between T_{iso} and the probability of failure at different PGA levels (e.g., 0.8 g, 1.2 g, 1.6 g, and 2 g) is shown in Figure 8.18. It can be observed from the figure that the probability of failure is close to zero for the isolation periods from 2.5 s. For the design purpose, the selection of T_{iso} = 2.5 s as an optimal period appears a good compromise for both effectiveness and feasibility. In fact, this value of isolation period is associated with the maximum probability reduction for any level of the seismic intensity and an acceptable level of the lateral displacement. The remaining parameters of the bearings are then defined based on the designed isolation period. In detail, the effective radius and the damping coefficient of the bearings are calculated as 1900 mm and 12%, respectively.

8.6 Closure

This chapter addresses the vulnerability assessment of an existing elevated tank supported by circular reinforced concrete columns. Attention has been paid on the formulation of the numerical model, which is based on a three-dimensional finite element model stick model of the shear-failure sensitive support structure combined with a lumped mass dynamic model of the liquid storage steel tank. The important implication is to correctly estimate the damage conditions of elevated tanks that finally result in the correct evaluation of seismic risk assessment for the whole industrial plant and surrounding areas.

The seismic vulnerability of the tank has been assessed in terms of fragility curves, derived using two well-known methods, namely the CA and the IDA. In this respect, a preliminary comprehensive analysis for the evaluation of the most efficient/sufficient intensity measures for elevated tanks has been performed, whose results, given the scarcity of information in the literature, represent a novelty in seismic vulnerability analysis of elevated tanks. It can be concluded that the most efficient intensity measure is PGA, which shows a sufficiency also in general terms. Consequently, the fragility curves in terms of PGA have been derived, revealing that the accuracy of the method for fragility evaluation has a direct implication in predicting failure conditions and thus possible LOC effects.

The obtained results imply a higher probability of occurrence of the damage in the support columns for excessive lateral displacement of the tank base. In particular, relevant values of PGA ranging between 0.3 g and 0.4 g correspond to the failure probabilities of the columns between 80% and 100%. The collapse of the tanks at the Habas plant fully validates these results that demonstrate the high seismic vulnerability of the analysed tank. Subsequently, the design of a CSB system is conducted based on a vulnerability-based approach. In this respect, a lumped mass model, which is properly modified to account for the presence of the isolation system, is used. In particular, the bearings are modelled using a nonlinear model. The design approach is then introduced by evaluating the probability of failure at different PGA levels for a range of isolation periods. In most of the cases, the results of fragility curves present a high effectiveness of the CSBs in reducing the seismic response of the tank. The failure probability of the support columns reduces almost to zero up to a PGA level of 0.8 g. An optimal period for the isolation system is selected as 2.5 s. This value is associated with the maximum probability reduction for any level of the seismic intensity and an acceptable level of the lateral displacement. Finally, the parameters of the CSBs including the effective radius, the damping coefficient, and the maximum displacement are designed based on the optimal isolation period.

Chapter 9. Conclusions and future work

9.1 Conclusions

The main objective of this study was to develop an appropriate methodology with the treatment of uncertainties for the fragility curve evaluation of existing storage tanks in industrial plants, and in particular petrochemical plants, by using analytical approaches. The approaches were based on reliable numerical models proposed for both above ground and elevated steel liquid storage tanks. The results of the study led to the following main conclusions:

1) From an overview of past earthquake damage to steel liquid storage tanks, critical failure modes of the tanks have been identified for the examination in this work. The damage was classified as sloshing damage of the roofs, elastic and elastic-plastic buckling of the shell wall, fracture of the shell and bottom plate, plastic rotation of the shell-to-bottom joint plate in the case of unanchored tanks, failure of the attached piping system, and failure of the support structure in the case of elevated tanks.
2) The possible mechanical models, including spring-mass and refined nonlinear stick models, for both above ground and elevated tanks, have been presented. The attention paid to the modelling of unanchored tanks, whose dynamic behaviour is considerably different from rigidly anchored ones because of uplift and sliding mechanisms. The unanchored tank model, proposed by Malhotra and Veletsos (1994c), was first presented in this work and have applied to some case studies of storage tanks. However, this model that was based on the beam model for the uplift mechanism exhibited some limitations associated with the interaction between the shell deformation and the base uplift. For that reason, an efficient procedure for the model calibration of unanchored tanks has been proposed. The procedure is mainly based on a static pushover analysis, which is performed using a nonlinear finite element modelling of the tank-liquid system.
3) The proposed model has been validated by a shaking table campaign and a full nonlinear finite element model of an unanchored tank. The test was conducted at the CEA EMSI laboratory, Saclay (France) within the framework of the INDUSE-

2-SAFETY European project. A number of tests were carried out with two input signals to obtain significant responses of the tank, e.g., sloshing wave height and uplift displacement. The numerical modelling of the tank has been developed using the ABAQUS software with an implicit dynamic analysis. The time history responses obtained from the numerical analyses in terms of the hydrodynamic pressure acting on the tank wall, the sloshing of the liquid free surface, and the uplift of the base plate were evaluated and compared well with the experimental data. It can be concluded that the proposed spring-mass model is capable of accurately predicting the seismic response of unanchored tanks.

4) An overview of current fragility evaluation approaches for storage tanks has been presented including empirical, expert judgment-based, and analytical approaches. Expert-based methods have been identified as particularly limited in scope and response, and empirical methods are not an option because of the lack of sufficient tank damage data. In the absence of adequate empirical data, fragility curves have been developed through a number of analytical methods. The thesis provided the methodology of two well-known methods, namely the CA and the IDA. A procedure of the screening study of the seismic response to modelling parameters has also been presented. The screening study is useful to have a better understanding of the effect of parameter variations on the structural seismic behaviour and suggests significant parameters that need to be considered as random variables in the fragility modelling. The general procedure of the screening study and the fragility curve evaluation for an examined tank can be summarised as follows:
    a) The modelling parameters associated with material and geometric uncertainties are first presented with their probability distributions.
    b) A two-level fractional factorial design of the modelling parameters is generated. In this design, each parameter is considered at its upper and lower values.
    c) For each sample, a nonlinear static pushover analysis is performed with the increase of the acceleration magnitude, and the responses of the tank sample are monitored at each step of the analysis.
    d) For the response at each acceleration level monitored, an ANOVA is conducted. The ANOVA performs hypothesis

   tests that verify the significance of varying each parameter on the variance of the measured response.
   e) The results of the hypothesis tests are given in terms of a p-value, and a smaller p-value indicates greater evidence that the parameter has a strong influence on the tank response. For this study, parameters with a p-value less than a cutoff of 0.05 are considered significant.
   f) A suite of ground motions that is appropriate and representative of the target geographic area and captures the uncertainty inherent in ground motions is selected.
   g) Statistically significant samples of the tank system are derived using a DOE method, and LHS is used in this work.
   h) Each sample is then randomly paired with a set of ground motions. Nonlinear time history analyses are then performed on each pair, and the peak component responses are monitored every each analysis. The fragility curves can be constructed by using either the CA or the IDA method. The IDA curves can be derived for each pair by a number of analyses that are performed with several intensity levels.
   i) The capacity or limit state of each component is determined using expert based, experimentally based and/or analytically based methods.
   j) Finally, the seismic demand and structural capacity models are combined assuming a lognormal distribution.

5) A comparative analysis concerning the efficiency and sufficiency of several intensity measures for the probabilistic seismic demand analysis of steel liquid storage tanks has been carried out. A comprehensive comparative analysis led to the following main conclusions:
   a) $S_a(T_1)$ is the most efficient intensity measure with respect to the meridional stress demand. In addition, the use of I_{NP} leads to similar values of the dispersion with $S_a(T_1)$, while S^* exhibits a significantly lower performance.
   b) Among magnitude-dependent intensity measures, PGA shows the best performance. In contrast, PGD shows the weakest performance, especially in the cases of large amplitude records.

   c) For duration-dependent intensity measures, while I_A provides the higher efficiency, CAV produces an increase of the standard deviation compared with I_A.
   d) The long-distance ground motion records produce the intensity measures with more efficiency. In contrast, with respect to amplitude, small amplitude records demonstrate the higher performance of the intensity measures.
   e) Regarding the intensity measure sufficiency, the frequency-dependent intensity measures also show the sufficiency in terms of M_W and R_{jb}. Among the magnitude-dependent group, PGD shows a significantly degree of insufficiency. On the other hand, PGA and PGV display an acceptable sufficiency for all the analysed tanks. The duration-dependent group shows a considerable degree of insufficiency, especially in terms of R_{jb}.

6) With the attention paid to the existing steel liquid storage tanks in industrial plants, two case studies of the tanks have been selected. A large unanchored tank ideally located in an oil refinery in Italy, named as Case study #1, and an elevated steel tank that rests on reinforced concrete columns, named as Case study #2, have been investigated. The elevated tank among a group of three tanks in the Habas plant collapsed after 1999 İzmit earthquake in Turkey.
7) In the case study #1, a number of sources of uncertainty associated with the seismic performance of an existing tank in an industrial plant have been identified and evaluated by a sensitivity study. The sensitivity analysis utilised DOE principles to identify which modelling parameters significantly impact the uplift response of the tank. The results of the study provide insight into the potentially uncertain modelling parameters that most significantly affect the seismic response of the tank, which to date has not been thoroughly assessed. Based on a nonlinear finite element pushover model of the tank and a screening design, the most important parameters include those associated with the geometric parameters, i.e., the filling level and the bottom plate thickness have been determined through the sensitivity analysis. The material parameters that include steel yield strength, Young’s modulus, and liquid density have a limited effect. The findings of this sensitivity study have been extended to evaluate which sources of uncertainty have a significant effect on the failure estimates and fragility curves for the

tank. The relative importance of sources of uncertainty with regard to ground motion and modelling parameters has been evaluated in a comparative assessment of fragility curves developed under different uncertainty treatments. Fragility curves considering only those significant parameters identified in the sensitivity study, i.e., geometric parameters, have been nearly identical to those developed with all potential sources treated as variables; this indicates that savings in simulation and computational effort may be achieved through a preliminary screening of modelling parameters.

8) In the Case study #2, the vulnerability assessment of an existing elevated tank supported by circular reinforced concrete columns has been presented. Attention has been paid to the formulation of the numerical model, which was based on a three-dimensional finite element stick model of the shear-failure sensitive support structure combined with a lumped mass dynamic model of the liquid storage steel tank. The seismic vulnerability of the tank has been assessed in terms of fragility curves, derived using two well-known methods, namely the CA and the IDA. In this respect, a preliminary comprehensive analysis for the evaluation of the most efficient/sufficient intensity measures for elevated tanks has been performed. It can be concluded that PGA is the most efficient intensity measure for the evaluation in this case study. Consequently, the fragility curves in terms of PGA have been derived, revealing that the accuracy of the method for fragility evaluation has a direct implication in predicting failure conditions and thus possible LOC effects. The obtained results imply a higher probability of occurrence of the damage in the support columns for excessive lateral displacement of the tank base. The collapse of the tanks at the Habas plant fully validates these results that demonstrate the high seismic vulnerability of the analysed tank. Subsequently, the design of a CSB system has been conducted based on a vulnerability-based approach. In this respect, a nonlinear modelling of the CSB system has been incorporated in the elevated tank model. The design approach has been then introduced by evaluating the probability of failure at different PGA levels for a range of isolation periods. The results of fragility curves present a high effectiveness of the CSBs in reducing the seismic response of the tank. An optimal period for the isolation system is selected as

2.5 s. This value is associated with the maximum probability reduction for any level of the seismic intensity and an acceptable level of the lateral displacement. Finally, the parameters of the CSBs including the effective radius, the damping coefficient, and the maximum displacement have been designed based on the optimal isolation period.

9.2 Impact of research

A primary contribution of the work is the refinement and enhancement of seismic fragility curves for existing steel liquid storage tanks in industrial plants, especially petrochemical plants. Additional benefits and contributions include the following:

1) The critical failure modes of the steel liquid storage tanks observed during past earthquakes are examined and incorporated into the study.
2) The proposed three-dimensional analytical models considering complex mechanisms for both above ground and elevated steel liquid storage tanks provide an enhanced understanding of the seismic response as well as the damage behaviour of the tanks.
3) The comprehensive analysis for the evaluation of the most efficient/sufficient intensity measures is performed for both above ground and elevated tanks, whose results, given the scarcity of information in the literature, represent a novelty in seismic vulnerability analysis of the tanks.
4) The fragility assessment methodology for existing above ground and elevated tanks, which is developed and evaluated in this study, offers a significant contribution to the research community. Moreover, the sensitivity analysis of the uncertain modelling parameters provides an enhanced understanding of which parameters significantly affect the seismic response and fragility of the tank components. The approach proposed in this study could be also helpful for future fragility assessments of the class or portfolio of tanks.
5) Seismic risk assessment and loss estimation tools will benefit from the incorporation of seismic fragility curves. The reliable fragility curves of storage tanks in an industrial site will be a key support to seismic risk assessment, and mitigation activities carried out in later steps for the site and its surrounding areas.

9.3 Recommendations for future work

Areas in which this work can be extended through additional research include the following:

1) The vulnerability was assessed for an existing broad tank; a future study could evaluate for a class or portfolio of tanks with the uncertainty treatment.
2) The effect of the floating roof on the seismic response and seismic vulnerability of tanks will be considered in the future study. A simplified approach for assessing the seismic response of tanks with the presence of the floating roof would be a valuable extension of the research.
3) An optimal ground motion intensity measure for tanks is defined as one that can capture both the impulsive and convective responses. A vector-value intensity measure may be the best solution in this context.

Appendix A. Bessel functions

Bessel functions are the canonical solutions $y(x)$ of Bessel's differential equation:

$$x^2 \frac{d^2 y}{dx^2} + x\frac{dy}{dx} + \left(x^2 - \alpha^2\right) y = 0 \tag{A.1}$$

where α is an arbitrary complex number (i.e., the order of the Bessel function). Bessel functions for integer α are also known as cylinder functions or the cylindrical harmonics because they appear in the solution to Laplace's equation in cylindrical coordinates.

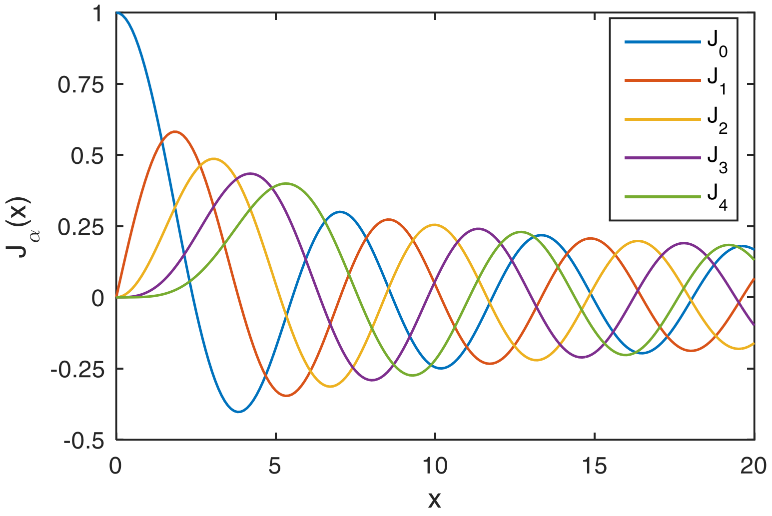

Figure A.1. Bessel functions of the first kind for n = 0, 1, 2, 3, 4

Bessel functions of the first kind, denoted as $J_\alpha(x)$, are solutions of Bessel's differential equation that are finite at the origin ($x = 0$) for integer or positive α, and diverge as x approaches zero for negative non-integer α. It is possible to define the function by its series expansion around $x = 0$, which can be found by applying the Frobenius method to Bessel's equation:

$$J_\alpha(x)=\left(\frac{x}{2}\right)^\alpha\sum_{k=0}^{\infty}\frac{\left(\frac{-x^2}{4}\right)^k}{k!\Gamma(\alpha+k+1)} \tag{A.2}$$

where $\Gamma(z)$ is the gamma function, a shifted generalization of the factorial function to non-integer values. The Bessel function of the first kind is an entire function if α is an integer, otherwise it is a multivalued function with singularity at zero. The graphs of Bessel functions, as shown in Figure A.1, look roughly like oscillating sine or cosine functions that decay proportionally to $1/\sqrt{x}$, although their roots are not generally periodic, except asymptotically for large x.

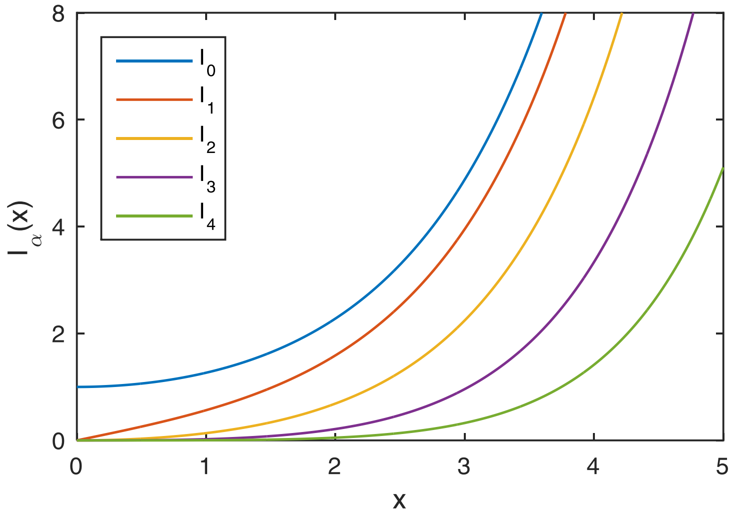

Figure A.2. Modified Bessel functions of the first kind for n = 0, 1, 2, 3, 4

A function $I_\alpha(x)$ which is one of the solutions to the modified Bessel differential equation and is closely related to the Bessel function of the first kind $J_\alpha(x)$. For a real number α, the function can be computed:

$$I_\alpha(x)=\left(\frac{x}{2}\right)^\alpha\sum_{k=0}^{\infty}\frac{\left(x^2/4\right)^k}{k!\Gamma(\alpha+k+1)} \tag{A.3}$$

The series expansion for $I_\alpha(x)$ is thus similar to that for $J_\alpha(x)$, but without the alternating $(-1)^m$ factor. The plots of the modified Bessel functions are shown in Figure A.2.

Appendix B. Similarity requirements for the shaking table test of tanks

The seismic response of tanks is quite complex, in particular in the case of unanchored tanks. One has to take into account sloshing, inertial effects of the fluid, possible buckling of the tank wall, possible uplift and/or sliding of the base. The consequence of this complex behaviour is that seismic tests of reduced scale tanks cannot reproduce a response which is completely similar to that of the prototype. In general, it is not possible to meet all similarity requirements for all relevant parameters.

In the case of small scale, the specimen frequency may be beyond the frequency range of accurate control of the shake table. Therefore, dynamic instability, such as parametric resonance, cannot be reproduced. Actually, for this kind of instability to occur, the excitation signal should have considerable energy in the vicinity of the sum of two eigenfrequencies of the specimen. Clearly, this is not possible when the model frequencies are high, due to small scale, unless high frequency servo valves are used, and accurate shake table control is possible in this frequency range.

B.1 Sloshing

Sloshing is a very low frequency motion. Hence, if one focuses on sloshing waves (i.e., height of sloshing waves, deformation and stresses induced in floating roofs by sloshing), the tank may be considered as rigid and its thickness and material properties do not play any role. The sloshing wave amplitude η at position $\underline{x}$ and time t will be a function of the radius R, the height H, the gravity acceleration g, and of the excitation acceleration α.

$$\eta = f_\eta\left(\underline{x}, t, R, H, g, \alpha\right) \tag{B.1}$$

Using Vachy-Buckingham’s theorem, the dimensionless form is:

$$\frac{\eta}{R} = F_\eta\left(\frac{\underline{x}}{R}, t\sqrt{\frac{g}{R}}, \frac{H}{R}, \frac{\alpha}{g}\right) \tag{B.2}$$

If geometrical scaling is used (i.e., the model is a homothetic copy of the prototype), scaling of the excitation signal according to the classical Froude similitude gives the correct results as far as sloshing waves are of interest. If $\underline{x} = \lambda \underline{x}_0$, where λ denotes the geometrical scaling factor and subscript 0 denotes quantities referred to the prototype, time scaling will be $t/t_0 = \sqrt{\lambda}$ and the excitation amplitude will remain unchanged, α/α_0=1. However, although the above scaling gives the correct sloshing amplitude, it is not possible to obtain a satisfactory pressure similitude. For instance, in the case of a rigid tank the pressure is:

$$p = f_p\left(\underline{x}, t, R, H, g, \alpha, \rho\right) \tag{B.3}$$

The dimensionless form is:

$$\frac{p}{\rho g H} = F_p\left(\frac{\underline{x}}{R}, t\sqrt{\frac{g}{R}}, \frac{H}{R}, \frac{\alpha}{g}\right) \tag{B.4}$$

Hence, if the same fluid is used for the model and the prototype, the above excitation scaling gives the correct ratio of dynamic pressure to hydrostatic pressure; this means that the dynamic pressure will be $p = \lambda p_0$. Nevertheless, since on the fluid-structure interface $\underline{\sigma} \cdot n = -p$, the stresses in the structure will be smaller than in the prototype, $\underline{\sigma} = \lambda \underline{\sigma}_0$; this is because the proposed similitude is not a real Froude similitude for the structure. In fact, since ρ remains unchanged, the ratio of elastic forces to gravity forces cannot be the same for the prototype and the model.

B.2 Buckling

An approximate estimate of buckling occurrence of the tank wall can be obtained by comparing the earthquake induced stresses in the tank wall to the critical buckling stress which depends on the particular type of buckling considered. Of course, the actual situation is more complicated since (i) buckling is not governed by only one component of the stress tensor at a particular point, and (ii) in the nonlinear case, the superposition of static and dynamic stresses is no longer valid.

Since sloshing frequencies lie, in general, much below the frequency range of spectral amplification of the excitation signal and if base uplift and/or sliding does not occur, earthquake induced stresses are due, mainly, to pure inertial fluid effects (the so called impulsive response). Under this assumption and neglecting the mass of the shell itself, the stress in the shell reads:

$$\underline{\sigma} = f_\sigma\left(\underline{x}, t, R, H, \rho, \alpha, E, t_s\right) \tag{B.5}$$

The dimensionless form is:

$$\frac{\sigma}{E} = F_{\sigma}\left(\frac{\underline{x}}{R}, \frac{t}{R}\sqrt{\frac{E}{\rho}}, \frac{H}{R}, \frac{\alpha\rho R}{E}, \frac{t_s}{R}\right) \tag{B.6}$$

It may be observed that the excitation time scaling corresponding to velocity similarity will give the same dynamic stresses in the model and the prototype. Time will be contracted, $t/t_0 = \lambda$, and the excitation amplitude will be increased, $\alpha/\alpha_0 = 1/\lambda$.

Nevertheless, the above scaling does not meet all similarity requirements regarding the critical buckling stress. Actually, critical buckling stress depends on the hydrostatic pressure also, to a lesser (diamond buckling) or higher (elephant's foot buckling) extent:

$$\sigma_{cr} = f_{cr}(E, t_s, R, \rho g H, \sigma_y) \tag{B.7}$$

The dimensionless form is:

$$\frac{\sigma_{cr}}{E} = F_{cr}\left(\frac{\sigma_y}{E}, \frac{t_s}{R}, \frac{\rho g H}{E}\right) \tag{B.8}$$

Consequently, a distortion of the critical buckling stress will occur since the last dimensionless product cannot be the same in the model and the prototype.

B.3 Uplift

Base uplift and sliding depend, amongst others, on the ratio of seismic forces to elastic forces (and/or to yield stress, e.g., $\alpha\rho R/E$ or $\alpha\rho R/\sigma_y$) and on the ratio of seismic forces to gravity forces, α/g. Once again, it is not possible to apply an excitation signal scaling meeting both requirements. Another problem, regarding uplift, is that the base plate is, usually, much thinner than the wall. Hence, applying the same thickness scaling for the base and the wall is not always feasible, because it would lead to an extremely thin base plate.

B.4 Conclusions

The above discussion points out the difficulties related to the similitude law to be used for seismic tests of scaled tanks. Actually, it is not possible to respect all relevant dimensionless parameters. A complete geometrical scaling is assumed ($\underline{x} = \lambda \underline{x}_0$) and the same fluid will be used. Therefore, differences concern only the excitation time and amplitude scaling. As a compromise, it is suggested that depending on the phenomenon of interest two different scaling laws of the excitation signal are used.

- If the main concern is sloshing wave height of the liquid free surface: $t/t_0 = \sqrt{\lambda}$ and $\alpha/\alpha_0 = 1$.
- If the main concern is buckling of the tank: $t/t_0 = \lambda$, and $\alpha/\alpha_0 = 1/\lambda$.

If base uplift and/or sliding occur and if the same thickness scaling for the base plate as for the wall is applied, it may be expected that their dimensionless amplitudes will be higher than those of the prototype. Since sloshing and impulsive components' contributions correspond to quite different frequency ranges, it may be of interest to investigate the possibility of combining the two above excitation scaling laws. One could use Froude excitation scaling in the low frequency range and velocity excitation scaling for higher frequencies. Of course, filtering and amplitude modulation will modify slightly the original signal. Such a signal scaling could be a means to obtain simultaneously good representative responses, in the gross, for both sloshing waves and stresses in the tank. However, in any case, since ρ does not change, the influence of hydrostatic pressure, base uplift and/or sliding on the tank response will be distorted.

Appendix C. ANOVA table calculations

The general form of the ANOVA table for a fractional factorial design is given in Table C.1 (Hayter 2002):

Table C.1. ANOVA for fractional factorial design

Source	DOF	Sums of squares	Mean squares	F-stat
Factor 1	1	SSF_1	MSF_1	F_1
$\vdots$	$\vdots$	$\vdots$	$\vdots$	$\vdots$
Factor k	1	SSF_k	MSF_k	F_k
Block	$n_b(n) - 1$	SSb	MSb	F_b
Error	$n_T - (n_b(n) - 1) - k - 1$	SSE	MSE	
Total	$n_T - 1$	SST		

where n_b is the number of blocks per replicate, n_{bb} is the number of trials per interaction, n is the number of replicates, and k is the number of parameters.

The sums of squares are calculated as:

$$SSF_i = (n)2^{k-p-1}\sum_{j=1}^{2}\left(\bar{y}_{j\ldots\ldots} - \bar{y}_{\ldots\ldots}\right)^2$$

$$SSb = n_{bb}\sum_{b=1}^{n_T/n_{bb}}\left(\bar{y}_{\ldots\ldots b} - \bar{y}_{\ldots\ldots}\right)^2 \tag{C.1}$$

$$SST = \sum_{j=1}^{n_T}\left(y_j - \bar{y}_{\ldots\ldots}\right)^2$$

$$SSE = SST - \sum_{i=1}^{k} SSF_i - SSb$$

where $\bar{y}_{j=1\ldots\ldots}$ is the mean of all response values where parameter i is $(+)$, $\bar{y}_{j=2\ldots\ldots}$ is the mean of all response values where parameter i is $(-)$, $\bar{y}_{\ldots\ldots}$ is the mean of all response values, $\bar{y}_{\ldots\ldots b}$ is the mean of all response values for block number b, and y_j is the response of jth trial.

The mean squares are given as:

$$MSF_1 = \frac{SSF_1}{1} \tag{C.2}$$

$$MSF_k = \frac{SSF_k}{1}$$

$$MSb = \frac{SSb}{n_b(n)-1}$$

$$MSE = \frac{SSb}{n_T - (n_b(n)-1) - k - 1}$$

The values of F-stat are given as:

$$F_1 = \frac{MSF_1}{MSE}$$

$$F_k = \frac{MSF_k}{MSE} \tag{C.3}$$

$$F_b = \frac{MSF_b}{MSE}$$

References

Abali, E., Uckan, E., 2010, “Parametric analysis of liquid storage tanks base isolated by curved surface sliding bearings,” Soil Dynamics and Earthquake Engineering, Vol. 30, No. 1-2, pp. 21-31.

ALA, 2001, “Seismic fragility formulation for water system: Part 1-Guideline,” ASCE.

Alessandri, S., Caputo, A.C., Corritore, D., Renato, G., Paolacci, F., Phan, H., 2017, “On the use of proper fragility models for quantitative seismic risk assessment of process plants in seismic prone areas,” ASME Pressure Vessels and Piping Conference, Vol. 8, No. V008T08A022.

API 650, 2007, “Seismic design of storage tanks-Appendix E. Welded steel tanks for oil storage,” 11th Edition, Washington, DC.

Arias, A., 1970, “A measure of earthquake intensity,” Final chapter in collection: Seismic Design for Nuclear Power Plants, MIT Press, Cambridge, MA, pp. 438-469.

Bakalis, K., Fragiadakis, M., Vamvatsikos, D., 2016, “Surrogate modeling for the seismic performance assessment of liquid storage tanks,” Journal of Structural Engineering, Vol. 143, No. 4.

Baker, J.W., 2015, “Efficient analytical fragility function fitting using dynamic structural analysis,” Earthquake Spectra, Vol. 31, No. 1, pp. 579-599.

Barton, D.C., Parker, J.V., 1987, “Finite element analysis of the seismic response of anchored and unanchored liquid storage tanks,” Earthquake Engineering & Structural Dynamics, Vol. 15, No. 3, pp. 299-322.

Bayraktar, A., Sevim, B., Altunışık, A.C., Türker, T., 2010, “Effect of the model updating on the earthquake behavior of steel storage tanks,” Journal of Constructional Steel Research, Vol. 66, No. 3, pp. 462-469.

Bentz, E.C., 2000, “Sectional analysis of reinforced concrete members,” PhD Thesis, Department of Civil Engineering, University of Toronto.

Berahman, F., Behnamfar, F., 2007, “Seismic fragility curves for un-anchored on-grade steel storage tanks: Bayesian approach,” Journal of Earthquake Engineering, Vol. 11, No. 2, pp. 166-192.

Bernier, C., Padgett, J.E., Proulx, J., Paultre, P., 2015, "Seismic fragility of concrete gravity dams with spatial variation of angle of friction: Case study," Journal of Structural Engineering, Vol. 142, No. 5.

Berahman, F., Behnamfar, F., 2007, "Seismic fragility curves for un-anchored on-grade steel storage tanks: Bayesian Approach," Journal of Earthquake Engineering, Vol. 11, No. 2.

Bojorquez, E., Iervolino, I., 2011, "Spectral shape proxies and nonlinear structural response," Soil Dynamics and Earthquake Engineering, Vol. 31, pp. 996-1008.

Brunesi, E., Nascimbene, R., Pagani, M., Beilic, D., 2014, "Seismic performance of storage steel tanks during the May 2012 Emilia, Italy, Earthquakes," Journal of Performance of Constructed Facilities, Vol. 29, No. 5.

Buratti, N., Tavano, M., 2014, "Dynamic buckling and seismic fragility of anchored steel tanks by the added mass method," Earthquake Engineering & Structural Dynamics, Vol. 43, No. 1, pp. 1-21.

Cambra, F.J., 1982, "Earthquake response considerations of broad liquid storage tanks," Earthquake Engineering Research Center, Rep. UCBIEERC-82125.

Cambra, F.J., 1983, "A study of liquid storage tank seismic uplift behaviour," Proceedings of Pressure Vessels and Piping Technology Conference.

Clough D.P., 1977, "Experimental evaluation of seismic design methods for broad cylindrical tanks," Earthquake Engineering Research Center, Report UCB/EERC.

Cordova, P.P., Deierlein, G.G., Mehanny, S.S.F., Cornell, C.A., 2001, "Development of a two-parameter seismic intensity measure and probabilistic assessment procedure," 2nd U.S.-Japan Workshop on PBEE Methodology for Reinforced Concrete Building Structures.

Cornell, C., Jalayer, F., Hamburger, R., Foutch, D., 2002, "Probabilistic basis for 2000 SAC Federal Emergency Management Agency steel moment frame guidelines," Journal of Structural Engineering, Vol. 128, No. 4, pp. 526-533.

Cortés, G., Nussbaumer, A., Berger, C., Lattion, E., 2011, "Experimental determination of the rotational capacity of wall-to-base connections in storage tanks," Journal of Constructional Steel Research, Vol. 67, No. 7, July 2011, pp. 1174-1184.

Cortes, G., Prinz, G.S., 2017, "Seismic fragility analysis of large unanchored steel tanks considering local instability and fatigue damage," Bulletin of Earthquake Engineering, Vol. 15, No. 3, pp. 1279-1295.

Daidola, J.C., Basar, N.S., 1980, "Probability design for ship hull structural strength," Spring Meeting/STAR Symposium, SNAME, California, pp. 105-124.

De Angelis, M., Giannini, R., Paolacci, F., 2010, "Experimental investigation on the seismic response of a steel liquid storage tank equipped with floating roof by shaking table tests," Earthquake Engineering & Structural Dynamics, Vol. 39, pp. 377-396.

EN 1998-1, 2004, "Eurocode 8: Design of structures for earthquake resistance - Part 1: General rules, seismic actions and rules for buildings," Brussels, Belgium.

EN 1998-4, 2006, "Eurocode 8: Design of structures for earthquake resistance - Part 4: Silos, tanks and pipeline," Brussels, Belgium.

EPRI, 1988, "A criterion for determining exceedance of the operating basis earthquake," EPRI NP-5930, Palo Alto, CA.

Elwood K.J., Moehle J.P., 2005, "Axial capacity model for shear-damaged columns," ACI Structural Journal, Vol. 102, No. 4, pp. 578-87.

Fabbrocino, G., Iervolino, I., Orlando, F., Salzano, E., 2005, "Quantitative risk analysis of oil storage facilities in seismic areas," In Journal of Hazardous Materials, Vol. 123, No. 1-3, pp. 61-69.

FEMA P-58-1, 2012, "Seismic performance assessment of buildings - Volume 1: Methodology," Prepared by Applied Technology Council, California, US.

Fenz, D.M., Constantinou, M.C., 2006, "Behaviour of the double concave friction pendulum bearing," Earthquake Engineering and Structural Dynamics, Vol. 35, pp. 1403-1424.

Fischer, F.D., Rammerstorfer, F.G., 1999, "A refined analysis of sloshing effects in seismically excited tanks," International Journal of Pressure Vessels and Piping," Vol. 76, No. 10, pp. 693-709.

Fischer, E.C., Liu, J., Varma, A.H., 2016, “Investigation of cylindrical steel tank damage at wineries during earthquakes: Lessons learned and mitigation opportunities,” Practice Periodical on Structural Design and Construction, Vol. 21, No. 3.

Giannini, R., 2000, “Mathazard: A program for seismic hazard analysis,” University of Roma Tre, Rome, Italy (in Italian).

Gonzáleza, E., Almazána, J., Beltrán, J., Herrera, R., Sandoval, V., 2013, “Performance of stainless steel winery tanks during the 02/27/2010 Maule Earthquake,” Engineering Structures, Vol. 56, pp. 1402-1418.

Hayter, A., 2002, “Probability and statistics for engineers and scientists,” Duxbury, Pacific Grove, second edition.

Haroun, M.A., Housner, G.W., 1981, “Earthquake response of deformable liquid storage tanks,” Journal of Applied Mechanics, Vol. 48, pp. 411-418.

Hatayama, K., 2008, “Lessons from the 2003 Tokachi-oki, Japan, earthquake for prediction of long-period strong ground motions and sloshing damage to oil storage tanks,” Journal of Seismology, Vol. 12, No. 2, pp. 255-263.

HAZUS, 2001, “Earthquake loss estimation methodology,” National Institute of Building Science, Risk Management Solution, Menlo Park, CA, USA.

Hess, P., Bruchman, D., Assakkaf, I., Ayyub, M., 2002, “Uncertainties in material strength, geometric, and load variables,” Naval Engineers Journal, Vol. 114, No. 2, pp.167-180.

Hines, W.W., Montgomery, D.C., Goldsman, D.M., Borror, C.M., 2003, “Probability and statistics in engineering, 4th Ed., Wiley, Hoboken, N.J.

Housner, G.W., 1963, “The dynamic behaviour of water tanks,” Bulletin of the Seismological Society of America, Vol. 53, pp. 381-387.

Ibata, T., Isho, N., Kazuo, I., 2013, “Damage to storage tanks caused by the 2011 Tohoku earthquake and tsunami and proposal for structural assessment method for cylindrical storage tanks,” Proceedings of 7th International Conference and Exhibition on Liquefied Natural Gas, Houston, USA.

Iervolino, I., Fabbrocino, G., Manfredi, G., 2004, “Fragility of standard industrial structures by a response surface based method,” Journal of Earthquake Engineering, Vol. 8, No. 6, pp. 927-945.

Jacobsen, L.S., 1949, “Impulsive hydrodynamics of fluid inside a cylindrical tank and of fluid surrounding a cylindrical pier,” Bulletin of the Seismological Society of America, Vol. 39, No. 3, pp. 189-203.

Kana, D.D., 1979, “Seismic response of flexible cylindrical liquid storage tanks,” In Nuclear Engineering and Design, Vol. 52, No. 1, pp. 185-199.

Karamanos, S.A., Patkas, L.A., Platyrrachos, M.A., 2006, “Sloshing effects on the seismic design of horizontal cylindrical and spherical industrial vessels,” Journal of Pressure Vessel Technology, Vol. 128, No. 3, pp. 328-340.

Krausmann, E., Cruz, A., Affeltranger, B., 2010, “The impact of the 12 May 2008 Wenchuan earthquake on industrial facilities,” Journal of Loss Prevention in the Process Industries, Vol. 23, No. 2, pp. 242-248.

Kwon, O.S., Elnashai, A., 2006, “The effect of material and ground motion uncertainty on the seismic vulnerability curves of RC structure,” Engineering Structure, Vol. 28, No. 2, 289-303.

Lau, D.T., Clough, R.W., 1989, “Static tilt behavior of unanchored cylindrical tanks,” Berkeley: Earthquake Engineering Research Center, University of California.

Luco, N., 2002, “Probabilistic seismic demand analysis, SMRF connection fractures, and near-source effects,” Ph.D. thesis, Dept. of Civil and Environmental Engineering, Stanford University, California.

Luco, N., Cornell, C.A., 2007, “Structure-specific scalar intensity measures for near-source and ordinary earthquake ground motions,” Earthquake Spectra, Vol. 23, No. 2, pp. 357-392.

Mackie K., Stojadinovic B., 2003, “Seismic demands for performance-based design of bridges,” PEER Report 2003/16, Pacific Earthquake Engineering Research Center, University of California, Berkeley, CA.

Malhotra, P.K., 1995, “Base uplifting analysis of flexibly supported liquid-storage tanks,” Earthquake Engineering & Structural Dynamics, Vol. 24, No. 12, pp. 1591-1607.

Malhotra, P.K., Veletsos, A.S., 1994a, “Beam model for base-uplifting analysis of cylindrical tanks,” Journal of Structural Engineering, Vol. 120, No. 12, pp. 3471-3488.

Malhotra, P.K., Veletsos, A.S., 1994b, “Uplifting analysis of base plates in cylindrical tanks,” Journal of Structural Engineering, Vol. 120, No. 12, pp. 3489-3505.

Malhotra, P.K., Veletsos, A.S., 1994c, “Uplifting response of unanchored liquid-storage tanks,” Journal of Structural Engineering, Vol. 120, No. 12, pp. 3524-3546.

Malhotra, P.K. Wenk, T., Wieland, M., 2000, “Simple procedure for seismic analysis of liquid storage tanks,” Structural Engineering International, 3/2000.

Manos G.C., Clough R.W., 1982, “Further study of the earthquake response of a broad cylindrical liquid storage tank,” Earthquake Engineering Research Center, Report UCB/EERC 82-07.

Mansour, A.E., Jan, H.Y., Zigelman, C.I., Chen, Y.N., Harding, S.J., 1984, “Implementation of reliability methods to marine structures,” Transactions of the Society of Naval Architects and Marine Engineers, Vol. 92, pp. 11-20.

McKay, M.D., Conover, W. J., Beckman, R. J., 1979, “A comparison of three methods for selecting values of input variables in the analysis of output from a computer code,” Technometrics, Vol. 21, No. 2, pp. 239-245.

McKenna, F., Fenves, G.L., Scott, M.H., 2007, “OpenSees: Open system for earthquake engineering simulation,” Berkeley (CA): PEER, University of California.

Moslemi M., Kianoush M.R., Pogorzelski W., 2011, “Seismic response of liquid-filled elevated tanks,” Engineering Structures, Vol. 33, No. 6, pp. 2074-84.

NIST GCR 97-720, 1997, “A study of performance of petroleum tanks during earthquakes,” authored by T. Cooper, prepared for the U.S Department of Commerce, Washington, D.C.

Nielson, B.G., DesRoches, R., 2007, “Analytical seismic fragility curves for typical bridges in the central and southeastern United States,” Earthquake Spectra, Vol. 23, No. 3, pp. 615-633.

NZSEE, 2009, “Seismic design of storage tanks,” Wellington (New Zealand): New Zealand National Society for Earthquake Engineering.

O’Rourke, M.J., So, P., 2000, “Seismic fragility curves for on-grade steel tanks,” Earthquake Spectra, Vol. 16, No. 4, pp. 801-814.

Ormeño, M., Larkin, T., Chouw, N., 2015, “The effect of seismic uplift on the shell stresses of liquid-storage tanks,” Earthquake Engineering & Structural Dynamics, Vol. 44, No. 12.

Ozdemir, Z., Souli, M., Fahjan, Y.M., 2010, “Application of nonlinear fluid-structure interaction methods to seismic analysis of anchored and unanchored tanks,” Engineering Structures, Vol. 32, No. 2, pp 409-423.

Padgett, J.E., DesRoches, R., 2007, “Sensitivity of seismic response and fragility to parameter uncertainty,” Journal of Structural Engineering, Vol. 133, No. 12.

Peek, R., Jennings, P.C., 1988, “Simplified analysis of unanchored tanks,” Earthquake Engineering and Structural Dynamics, Vol. 16, No. 7, pp. 1073-85.

Porter, K., Kennedy, R., Bachman, R., 2007, “Creating fragility functions for performance-based earthquake engineering,” Earthquake Spectra, Vol. 23, No. 2, pp. 471-489.

Paolacci, F., 2015, “On the effectiveness of two isolation systems for the seismic protection of elevated tanks,” Journal of Pressure Vessels and Technology, Vol. 137, No. 3, pp. 031801-031801-8.

Phan, H.N., Paolacci, F., 2016, “Efficient intensity measures for probabilistic seismic response analysis of anchored above-ground liquid steel storage tanks,” ASME Pressure Vessels and Piping Conference, Vol. 5, No. V005T09A010.

Phan, H.N., Paolacci, F., Alessandri, S., Hoang, P.H., 2016a, “Vulnerability-based design of sliding concave bearings for the seismic isolation of steel storage tanks,” ASME Pressure Vessels and Piping Conference, Vol. 8, No. V008T08A002.

Phan, H.N., Paolacci, F., Alessandri, S., 2016b, “Fragility analysis methods for steel storage tanks in seismic prone areas,” ASME Pressure Vessels and Piping Conference, Vol. 8, No. V008T08A023.

Phan, H.N., Paolacci, F., Corritore, D., Akbas, B., Uckan, E., Shen, J.J., 2016c, “Seismic vulnerability mitigation of liquefied gas tanks using concave sliding bearings,” Bulletin of Earthquake Engineering, Vol. 14, No. 11, pp. 3283-3299.

Phan, H.N., Paolacci, F., Bursi, O.S., Tondini, N., 2017a, “Seismic fragility analysis of elevated steel storage tanks supported by reinforced concrete columns,” Journal of Loss Prevention in the Process Industries, Vol. 47, pp. 57-65.

Phan, H.N., Paolacci, F., Mongabure, P., 2017b, “Nonlinear finite element analysis of unanchored steel liquid storage tanks subjected to seismic loadings,” ASME Pressure Vessels and Piping Conference, Vol. 8, No. V008T08A040.

Rotter, J.M., 1985, “Buckling of ground supported cylindrical steel bins under vertical compressive wall loads,” Proceedings of Metal Structures Conference, Institution of Engineers, Australia, Melbourne, pp.112-127.

Rotter, J.M., 1985, “Local inelastic collapse of pressurised thin cylindrical steel shells under axial compression,” Research Report, School of Civil and Mining Engineering, University of Sydney.

Ruiz, D.P., Gutiérrez, S.G., 2015, “Finite element methodology for the evaluation of soil damping in LNG tanks supported on homogeneous elastic halfspace,” Bulletin of Earthquake Engineering, Vol. 13, No. 3, pp. 755-75.

Saha, S.K., Matsagar, V.A., Jain, A.K., 2016, “Seismic fragility of base-isolated water storage tanks under non-stationary earthquakes,” Bulletin of Earthquake Engineering, Vol. 14, No. 4, pp. 1153- 1175.

Salzano, E., Iervolino, I., Fabbrocino, G., 2003, “Seismic risk of atmospheric storage tanks in the framework of quantitative risk analysis,” Journal of Loss Prevention in the Process Industries, Vol. 16, No. 5, pp. 403-409.

Schellenberg, A., 2006, “Computer program singleFPBearing element for analysis of single FP bearings in OpenSees,” Pacific Earthquake Engineering Research Center, Berkeley, California.

Setzler, E.J., Sezen, H., 2008, “Model for the lateral behavior of reinforced concrete columns including shear deformations,” Earthquake Spectra, Vol. 24, No. 2, pp. 493-511.

Sezen, H, 2008, “Shear deformation model for reinforced concrete columns,” Structural Engineering & Mechanics, Vol. 28, No. 1, pp. 39-52.

Sezen, H., Lıvaoğlu, R., Doğangün, A., 2008, “Dynamic analysis and seismic performance evaluation of above-ground liquid-containing tanks,” Engineering Structures, Vol. 30, No. 3, pp. 794- 803.

Sezen, H., Moehle, J.P., 2004, “Shear strength model for lightly reinforced concrete columns,” Journal of Structural Engineering, Vol. 130, No. 11, pp. 1692-703.

Sezen, H., Whittaker, A.S., 2006, “Seismic performance of industrial facilities affected by the 1999 Turkey earthquake,” Journal of Performance of Constructed Facilities, Vol. 20, No. 1.

Shinozuka, M., Feng, M.Q., Lee, J., Naganuma, T., 2000, “Statistical analysis of fragility curves,” Journal of Engineering Mechanics, Vol. 126, pp. 1224-1231.

Shrimali, M.K., 2003, “Seismic response of elevated liquid storage steel tanks under bi-direction excitation,” Steel Structures, Vol. 7, pp. 239-251.

Shrimali, M.K., Jangid, R.S., 2002, “Non-linear seismic response of base-isolated liquid storage tanks to bi-directional excitation,” Nuclear Engineering and Design, Vol. 217, No. 1-2, pp. 1-20.

Shome, N., Cornell, C.A., 1999, “Probabilistic seismic demand analysis of nonlinear structures,” Reliability of Marine Structures Program Report No. RMS-35, Dept. of Civil and Environmental Engineering, Stanford University, California.

Shome, N., Cornell, C.A., Bazzurro, P., Carballo, J.E., 1998, “Earthquakes, records, and nonlinear responses,” Earthquake Spectra, Vol. 14, No. 3, pp. 469-500.

SIMULIA, 2014, “Abaqus 6.14 Documentation,” Dassault Systèmes Simulia Corp., Providence, RI, USA.

Suzuki, K., 2008, “Earthquake damage to industrial facilities and development of seismic and vibration control technology-based on experience from the 1995 Kobe (Hanshin-Awaji) earthquake,” Journal of System Design and Dynamics, pp. 1-11.

Tanaka, M., Sakurai, T., Ishida, K., Tazuke, H., Akiyama, H., Kobayashi, N., Chiba, T., 2000, “Proving test of analysis method on nonlinear response of cylindrical storage tank under severe earthquakes," Proceedings of 12th World Conference on Earthquake Engineering (12 WCEE), Auckland, New Zealand.

Tippmann, J., Prasad, S., Shah, P., 2009, "2-D tank sloshing using the coupled Eulerian-Lagrangian (CEL) capability of ABAQUS®/Explicit," 2009 SIMULIA Customer Conference, Dassault Systemes Simulia Corp.

Vamvatsikos, D., Cornell, C.A., 2002, "Incremental dynamic analysis," Earthquake Engineering & Structural Dynamics, Vol. 31, No. 3, pp. 491-514.

Vathi, M., Karamanos, S.A., 2015, "Simplified model for the seismic performance of unanchored liquid storage tanks," ASME Pressure Vessels and Piping Conference, Vol. 5, No. V005T09A014.

Veletsos, A.S., 1984, "Seismic response and design of liquid storage tanks," Guidelines for seismic design of oil & gas pipelines system, ASCE, NY, pp. 255-370.

Veletsos, A., Tang, Y., 1987, "Rocking response of liquid storage tanks," Journal of Engineering Mechanics, Vol. 113, No. 11, pp. 1774-1792.

Veletsos, A.S., Yang, J.Y., 1977, "Earthquake response of liquid storage tanks advances in civil engineering through mechanics," Proceedings of 2nd Engineering Mechanics Specialty Conference, Raleigh(NC):ASCE, pp. 1-24.

Veletsos, A.S., Yang, J.Y., Tang, Y., 1992, "Dynamic response of flexibly supported liquid-storage tanks," Journal of Structural Engineering, Vol. 118, No. 1.

Virella, J.C., Godoy, L.A., Suárez, L.E., 2006, "Dynamic buckling of anchored steel tanks subjected to horizontal earthquake excitation," Journal of Constructional Steel Research, Vol., No. 6, pp. 521-531.

Whittaker, D., Jury, R.D., 2000, "Seismic design loads for storage tanks," Proceedings of 12th World Conference on Earthquake Engineering.

Wozniak, R.S., Mitchell, W.W., 1978, "Basis of seismic design provisions for welded steel oil storage tanks," American Petroleum Institute 43rd midyear meeting, session on Advances in Storage Tank Design, Toronto, Canada.

Wu, C.F.J., Hamada, M., 2000, “Experiments: Planning, analysis, and parameter design optimization,” John Wiley & Sons, Inc., New York.

Yang, J.Y, 1976, “Dynamic behavior of fluid-tank systems,” Ph.D. Dissertation, Rice University, Houston, Texas, 1976.

Young, S., Balluz, L., Malilay, J., 2004, “Natural and technologic hazardous material releases during and after natural disasters: A review,” In Science of The Total Environment, Vol. 322, No. 1-3, pp. 3-20.

Zhu, L., Elwood, K., Haukaas, T., 2007, “Classification and seismic safety evaluation of existing reinforced concrete columns,” Journal of Structural Engineering, Vol. 133, No. 9, pp. 1316-1330.